KU LEUVEN

FACULTY OF SCIENCE

The role of Sch9 in the vacuolar function in *Saccharomyces cerevisiae*

Alice UWINEZA

Promotor: Prof. Dr. J. Winderickx

Co-promotor: Dr. E. Swinnen

Dissertation presented in
fulfillment of the requirements
for the degree of Master of Science
in Biochemistry and Biotechnology

Academic year 2012 -2013

Acknowledgements

*I would like to express my gratitude to **Prof. Dr. Winderick**, thanks for giving me the opportunity to do research in your laboratory. Everything I learned in your lab, intellectually and socially, will help me to keep on growing as a scientist.*

***Erwin**, well I think we can both say it was quite a year. Thanks for your guidance, your continued patience and ongoing motivation. I enjoyed every critical discussion we had about my data. You challenged me to put all my scientific knowledge, practical skills and my writing abilities together to investigate a very exciting scientific project. Although I will never be able to express how much gratitude I owe you, Urakoze cane for being my supervisor!*

*To all the members of the laboratory of functional biology, I thank each and one of you. **Hanne** and **Tine**, thanks for being so optimistic all the time. It really got me through the hard moments. **Ruben**, your ability to see things and put everything in perspective is indispensable. **Tobias**, "brother form another mother", next to being very helpful during my experiments, you always tried to cheer me up, thank you.*

***Mammie** et **Pappie**, Turahageze! Je dis souvent chaque' un ses problèmes, mais vous vous êtes toujours assuré que mes problèmes sont les vôtres. Même si pendant tous ses années passées vous ne pouviez pas m'aider beaucoup avec mon travail scolaire, vous m'avez toujours motivé et soutenu. Je peux vous dire merci d'être mes parents ou d'avoir me donner cette vie magnifique, mais au lieu de cela je choisisse de vous dire que je vous aime.*

***Aline**, **Noëla**, **Aurore**, **Brenda**, **Florent** and **Flavier**, one for all and all for one. There is no need to write more because we do not talk, we act. **Olivier**, welcome to the family.*

***An**, my study mate, thanks for the many talks! Our endless chocolate, wine and shopping moments brought a perfect balance to my academic career. **Marina**, you are a friend for life. Thanks for being you.*

***Bart**, **Maxim**, **Steven** and **Marie**, the Guido Gezelle third floor gang. The past five years, I have lived in this residence were amazing because of your presence. We arrived as strangers but studied together, had many laughs and even cried together. We will carry on together.*

***Cecilia** and **Ileana**, the party squad, each night out together was memorable. Hilarious to me are all the great moments we had in kitchens. I remember exchanging cultural dishes, gossiping about our boyfriends, studying, dancing and spending the morning afters in the kitchen. Those moments I will cherish forever.*

***Glenn**, **Lien** en **Ward**, dank je voor al die jaren vol vriendschap. Van Giesbergen naar Gent, Leuven, Polen, Engeland,... waar we ook zitten, we steunen elkaar.*

Table of Contents

Acknowledgements i

List of abbreviations v

Introduction 1

1. Analysis of ageing processes using yeast as model 1

1.1. Life cycle of *S. cerevisiae* 1

1.2. Extended life span of S. cerevisiae and other model organisms 2

2. The protein kinase Sch9 3

2.1. Upstream regulation of Sch9 3

2.2. Targets of Sch9 7

2.3. The human orthologue of Sch9 12

3. Vacuolar proton-translocating ATPase 13

3.1. V-ATPase assembly 13

3.2. Regulation of V-ATPase activity 14

3.3. Functions of V-ATPase 15

Objectives 18

Materials and Methods 19

4. Media 19

5. Yeast strains used in this study 19

6. Tetrad analysis 20

7. Growth assays 20

7.1. Growth curve analysis 20

7.2. Spot tests 20

8. Yeast two-hybrid (Y2H) screening 21

9. *In silico* research: phosphorylation sites 22

10. Western blots 22

11. Co-immunoprecipitation (Co-IP) 23

12. Fluorescence study 23

13. Longevity 24

Results 25

14. Interaction between *SCH9* and *VMA*s 25

14.1. Confirmation of the interaction between *SCH9* and *VMA*s 25

14.2. Growth assay of *vmaΔ* and *vmaΔsch9Δ* in liquid media 27

14.3. Phenotypic overlap of the *sch9Δ* and *vmaΔ* strains 30
15. Screening for physical interaction between Sch9 and Vma proteins: Sch9 interacts with Vma6. 37
16. Confirmation of the interaction between Vma6 and Sch9 41
17. The vacuolar morphology is independent of the activity of the Sch9 protein 43
18. V-ATPase activity do not mediate Sch9 localization 46
19. Phosphorylation of the Vma proteins 48
20. The involvement of the V-ATPase activity in life span 55
20.1. Longevity 55
20.2. Superoxide levels 56
Discussion 61
21. Genetic interaction 61
22. Physical interaction 62
23. Functional interaction 62
24. Chronological Life Span 63
Summary 64
Samenvatting 65
References 66
Addendum 71
Materials and Methods 71
25. Media 71
25.1. YP medium 71
25.2. Sporulation medium 72
25.3. Synthetic (S) medium 72
26. Tetrad analysis 73
26.1. Crossing 73
26.2. Sporulation 73
26.3. Separation of tetrads 73
26.4. Genotyping 73
27. Gap repair cloning of Yeast two-hybrid (Y2H) vectors 73
27.1. Generating the Y2H-*VMA* vectors 74
28. Genomic tagging of *VMA* genes and Western blot 76
28.1. Creating chromosomal VMA-Myc fusions 76
28.2. Genomic transformation 77

28.3. Determination of successful genomic transformation 77
28.4. Protein extraction 78
28.5. Protein quantification 78
28.6. Western blotting 78
29. Co-immunoprecipitation (Co-IP) 80
29.1. Yeast transformation with plamids 81
29.2. Preparation of yeast protein extracts for Co-IP 81
29.3. Protein quantification 82
29.4. Immunoprecipitation 82
29.5. Western blot 82
30. Fluorescence study 82
30.1. Generating strains with Vph1-GFP and GFP-Sch9 plasmids 83
30.2. FM4-64 staining 83
31. Longevity 83
31.1. Cultivation of the cells 83
31.2. DHE measurements 83
31.3. Survival – Colony formation units (CFUs) 84
Supplementary tables 85
Risk-analysis 91

List of abbreviations

3-AT: 3-aminotriazole

AC: Adenylate cyclase

AMPK: adenosine monophosphate-activated protein kinase

cAMP: 3'-5'-cyclic adenosine monophosphate

CFU: Colony forming unit

CLS: Chronological life span

Co-IP: Co-immunoprecipitation

CRE: cAMP response element

CSM: Complete supplement mixture

DHE: Dihydroethidium

ER: Endoplasmic reticulum

EtOH: Ethanol

FM4-64: N-(3-triethylammoniumpropyl)-4-(ρ-diethylaminophenylhexatrienyl)- pyridinium dibromide

Gal: Galactose

Gly: Glycerol

HEPES: 4-(2-hydroxyethyl)-1-piperazineethanesulfonic acid

HM: Hydrophobic motif

Millipore : Immobilon-P membrane

MnSOD: Mitochondrial superoxide dismutase

MOPS: 3-(N-morpholino)propanesulfonic acid

mTORC2: Mammalian TORC2

Mw: Molecular weight

OD: optical density

OXPHOS: Oxidative phosphorylation subunits

PAC: Polymerase A and C

PDK-1: phosphoinositide-dependent protein kinase 1

PDS: Post diauxic-shift

Phos-tag gels: Phosphate-affinity gels

PHS: Phytosphingosine

PKA: Protein kinase A

PKB: Protein kinase B

rDNA: Ribosomal deoxyribonucleic acids

ribi: Ribosome biogenesis

RLS: Replicative life span

RNA Pol II: Ribonucleic acid polymerase II

RNA Pol III: Ribonucleic acid polymerase III

ROS: Reactive oxygen species

RP: Ribosomal protein

rpm: rounds per minute

rRNA: Ribosomal ribonucleic acid

RRPE: rRNA processing element

RT: room temperature

SD: Synthetic complete

SDS-PAGE: Sodium dodecyl sulfate polyacrylamide gel electrophoresis

SGA: Synthetic genetic array

SPT: Palmitoyltransferase

STDEV: Standard deviations

STRE: Stress response element

T-loop: Activation loop

TM: Turn motif

TOR: Target Of Rapamycin

TORC2: Target of rapamycin complex 2

V-ATPase: Vacuolar proton-translocating ATPase

*vma*Δ: Vacuolar membrane ATPase deletion

WT: wild type

Y2H: Yeast two-hybrid

YNB: Yeast nitrogen base

YPD: Yeast Peptone Dextrose

Introduction

1. Analysis of ageing processes using yeast as model

All over the world, a fast growing population of elderly people is observed. In this extent, it is to be expected that diseases related to ageing e.g. neurodegenerative diseases, cancer, type 2 diabetes, etc. will increase over the following years. *Saccharomyces cerevisiae (S. cerevisiae)*, also called budding yeast, is one of the major model organisms used in gerontology, the study of ageing. As a unicellular, eukaryotic fungi, *S. cerevisiae* is a good model to study ageing because many cellular processes, including life span regulation, are well conserved between yeast and mammals (Longo & Fabrizio, 2012).

1.1. Life cycle of *S. cerevisiae*

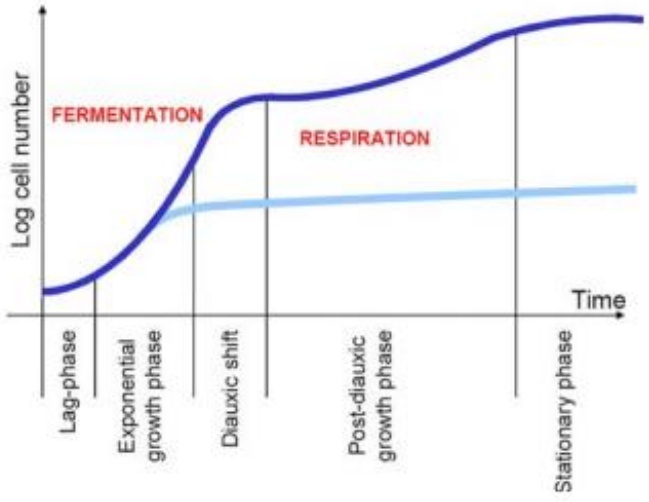

Figure 1: Growth curve of S. cerevisiae. The dark blue line represents growth of cells in complete growth medium and presence of fermentable carbon sources. The light blue line illustrates growth of yeast when transferred to medium lacking essential nutrients. (Smets et al., 2010).

Depending on the available carbon sources, *S. cerevisiae* can grow via fermentation or respiration (Smets et al, 2010). In complete growth medium and presence of fermentable sugars, the yeast cells will grow exponentially, after acclimatization during the lag-phase. During the exponential growth phase, sugars like glucose are fermented to ethanol and acetate. Once most of the fermentable sugars are metabolized, the cells undergo a diauxic shift. This means that the cells switch from fermentation to respiration. Throughout the post-diauxic phase, ethanol and acetate, which were accumulated during fermentation, are used as carbon sources. Using oxygen and these non-fermentable sugars, the cells are able to continue growing, but at a lower rate compared to the exponential growth phase. When all carbon sources are consumed, the cells enter the stationary phase. In this phase the cells do not grow or divide anymore and prepare themselves for surviving the starvation condition (Fig. 1). Cells can also enter the stationary phase when they are cultured in glucose-containing medium lacking other essential nutrients, such as phosphate, nitrogen, sulfur, etc. .

1.2. Extended life span of S. cerevisiae and other model organisms

Ageing can be defined as the progressive changes that take place throughout time in a living organism and lead to an increased probability of death of that organism. In yeast, life span is studied by measuring two different ageing models: Chronological life span (CLS), the time non-dividing yeast cells can survive during a nutrient starvation period and replicative life span (RLS), the amount of daughter cells a single mother cell is able to produce. While yeast CLS studies are model for ageing of human post-mitotic cells, which have entered the resting phase and do not proliferate anymore, RLS is comparable to asymmetric division in human stem cells (Breitenbach et al, 2012).

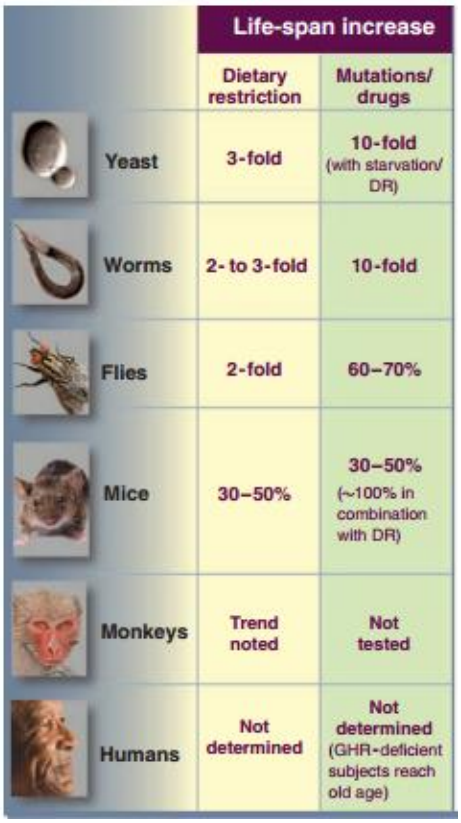

Figure 2: Results of dietary restriction experiments and mutations in genes or inhibition of proteins involved in nutrient sensing pathways (Fontana et al, 2010).

Many independent research groups found that ageing could be delayed by dietary restriction or mutations that reduce the activity of nutrient- sensing pathways (Fabrizio et al, 2010; Fontana et al, 2010; Kaeberlein et al, 2007; Smets et al, 2008; Smets et al, 2010; Wei et al, 2008; Wei et al, 2009). Dietary restriction experiments, in which the food intake of organisms is diminished, were performed on several model organisms. In all of these species, chronological life span extension, compared to the same kind of organisms with a normal diet, was noted. Mutations in genes encoding for proteins involved in nutrient sensing pathways or inhibition of those proteins using chemical components also led to an increased life span (Fig. 2). Conservation studies of the nutrient sensing pathways showed that the TOR and PKA pathways, which couple cell growth to available nutrients, are conserved from yeast to worms, flies and mammals (Fontana et al, 2010; Longo & Fabrizio, 2012).

A major factor in nutrient sensing pathways of yeast is the Sch9 protein kinase. Deletion of the *SCH9* gene prolonged yeast life span (Fabrizio et al, 2010; Fabrizio et al, 2001; Kaeberlein & Kennedy, 2005). The molecular mechanisms by which this life span regulator controls ageing, is currently under extensive investigation.

2. The protein kinase Sch9

The protein kinase Sch9 is a member of the eukaryotic AGC kinase group (Jacinto & Lorberg, 2008). Proteins belonging to this family are located in the cytoplasm and have protein sequences homologous to protein kinases A, G and C. Like other AGC proteins, Sch9 has several conserved functional regions: A central catalytic domain, an activation loop, a turn motif (TM) and C-terminal regulatory domain which contains a hydrophobic motif (HM) (Fig. 3). At the N-terminal side of the activation loop, Sch9 has a calcium-dependent C2 domain with unknown function. Sch9 acts as a signaling mediator, relaying upstream signals from intracellular and extracellular cues, to downstream targets by phosphorylating them on their serine and/or threonine residues (Roelants et al, 2004; Smets et al, 2010; Stichternoth et al, 2011; Urban et al, 2007). We will elaborate on some important functions of Sch9 in the next paragraph. As these functions need tight control, the activity of Sch9 itself is also highly regulated. Therefore we will first discuss the known mechanism by which Sch9 activity is mediated.

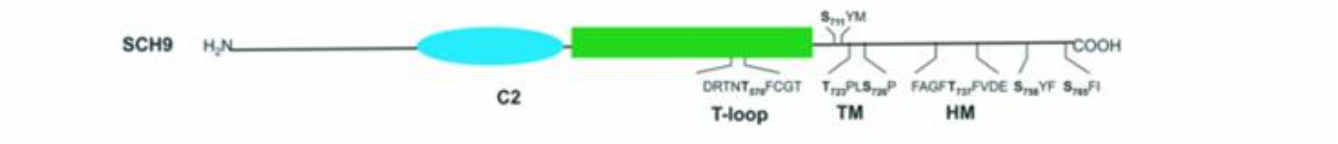

Figure 3: Budding yeast AGC kinase Sch9 conserved regions and phosphorylation sites. Sch9 has a central catalytic domain (green) with an activation loop (T-loop), and a C-terminal domain containing a turn motif (TM) and a hydrophobic motif (HM) like other AGC kinases. In addition Sch9 contains a C2 domain (blue) of which the function is unidentified. The T-loop is phosphorylated by Pkh1/2, and the TM and the HM are phosphorylated by TORC1 (Jacinto & Lorberg, 2008).

2.1. Upstream regulation of Sch9

The activity of AGC kinase Sch9 is regulated through phosphorylation at the T-loop and at the C-terminal region (Jacinto & Lorberg, 2008). Different factors have been found to control Sch9 phosphorylation and will be reviewed below.

2.1.1. TORC1

The Target Of Rapamycin (TOR) is a serine/threonine kinase of the phosphatidylinositol kinase family (Martin & Hall, 2005). *S. cerevisiae* has two TOR homologues, Tor1 and Tor2 (Wullschleger et al, 2006). These proteins are part of TOR complexes which control cell growth. Tor interacting proteins Avo1/2/3, Lst8 and Bit61 associate with the catalytic subunit Tor2 for the formation of target of rapamycin complex 2 (TORC2) (Fig. 4). This complex

mediates cell growth through regulating the polarization of actin cytoskeleton. Unlike TORC2, the catalytic subunit of target of rapamycin complex 1 (TORC1) can consist of Tor1 or Tor2. One of the two Tor homologues binds to Lst8, Kog1 and Tco89 to form the multiprotein complex TORC1 (Fig. 4). Although both complexes are named target of rapamycin, only TORC1 is sensitive to rapamycin. Rapamycin-treated yeast cells and cells with loss-of-function mutations in TORC1 show the same phenotype as nutrient-deprived cells e.g. inhibition of protein synthesis, upregulation of stress response genes and cell cycle arrest, which led to the general conclusion that TORC1 couples nutrient availability to the cell growth machinery (Smets et al, 2010; Urban et al, 2007).

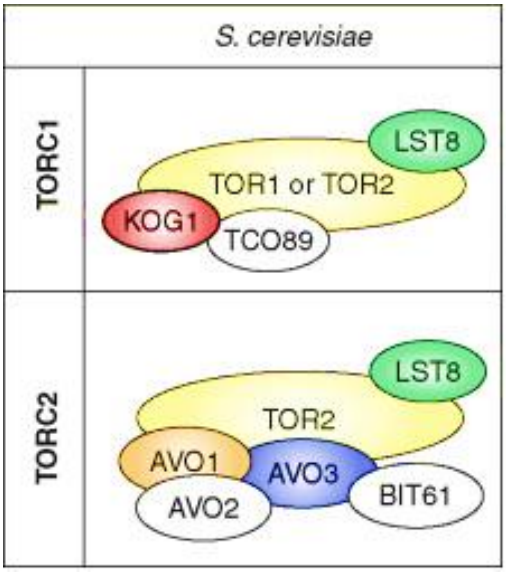

Figure 4: Composition of TOR complexes. TORC1 consists of Kog1, Tco89, Lst8 and a catalytic domain which is composed of Tor1 or Tor2. In TORC2, only Tor2 can be found, together with Bit61, Lst8 and Avo1/2/3 (modified from Zinzalla V., Strugill T.W. and Hall M.N., 2010).

TORCs are generally known to phosphorylate AGC kinases and research whether Sch9 is also a target, elucidated Sch9 to be a major substrate of TORC1 (Fig. 5). With mutational analysis of serine and threonine residues in the C-terminal domain of Sch9, five sites phosphorylated by TORC1 were identified, of which two in the TM and three in the HM (Fig. 3) (Jacinto & Lorberg, 2008; Urban et al, 2007).

The extent of Sch9 phosphorylation by TORC1 was proven to be dependent on the quality of nutrients the cells were subjected to (Powers, 2007; Urban et al, 2007). Environmental stress e.g. poor-quality carbon and nitrogen conditions, or carbon and nitrogen starvation, decreases TORC1 phosphorylation of Sch9.

Intriguingly, recent research indicated that mitochondrial dysfunction caused by mitochondrial genomic defects or by treatment with a protonophore, but not respiratory incompetence

caused in *pet* mutants (lacking nuclear genes required for respiratory competence), specifically causes dephosphorylation of Sch9 at its TORC1 target sites, while leaving the Pkh1/2 site unaffected (see below) (Kawai et al, 2011). Whether this mitochondrial dysfunction signal is transduced via reduced TORC1 signaling and/or an as-yet-undescribed Sch9 phosphatase is presently still unclear.

2.1.2. Pkh1 and Pkh2

Phosphorylation in the HM and TM is not enough to activate Sch9. Phosphorylation by the 3-phosphoinositide-dependent protein kinase 1 (PDK-1) homologues, Pkh1 and Pkh2 (Pkh1/2), in the activation loop is also required (Fig. 3) (Jacinto & Lorberg, 2008; Powers, 2007; Roelants et al, 2004; Urban et al, 2007). T570 of Sch9, located in the activation loop, is the residue phosphorylated by Phk1/2 kinases (Liu et al, 2005b).

Lui *et al.*, demonstrated *in vitro* phosphorylation of Sch9 by Pkh1/2 to be dependent on phytosphingosine (PHS), a building block of sphingolipids (Liu et al, 2005a). In addition to having a structural role, building blocks of plasma membranes, sphingolipids act as signaling molecules for cell growth, apoptosis and differentiation. Next to stimulating Sch9 activity through Pkh1/2, PHS also stimulates autophosphorylation of Sch9.

Later, Huang *et al*., confirmed phosphorylation of Sch9 by Pkh1/2 to be dependent of sphingolipid synthesis pathway *in vivo* (Fig. 5) (Huang et al, 2012). The first step of sphingolipids synthesis is catalyzed by serine palmitoyltransferase (SPT). Comparison of cells in which SPT activity is down-regulated to cells with wild type SPT activity, showed that the amount of Sch9 phosphorylated on T570 was decreased in SPT down-regulated cells.

2.1.3. Snf1

A recent study concerning Sch9 phosphorylation indicated that Sch9 is also phosphorylated by Snf1, a conserved adenosine monophosphate-activated protein kinase (AMPK), and this phosphorylation is regulated by replicative aging (Lu et al, 2011; Smets et al, 2010).

Research indicated that the histone acetyltransferase complex, NuA4, controls the phosphorylation of Sch9 by Snf1 through Sip2, one of the regulatory subunits of Snf1 (Fig. 5) (Lu et al, 2011). During replicative aging, NuA4 complex activity rises and acetylates Sip2, which then binds to and inhibits Snf1 activity, resulting in down-regulation of Sch9 phosphorylation and subsequently extension of RLS.

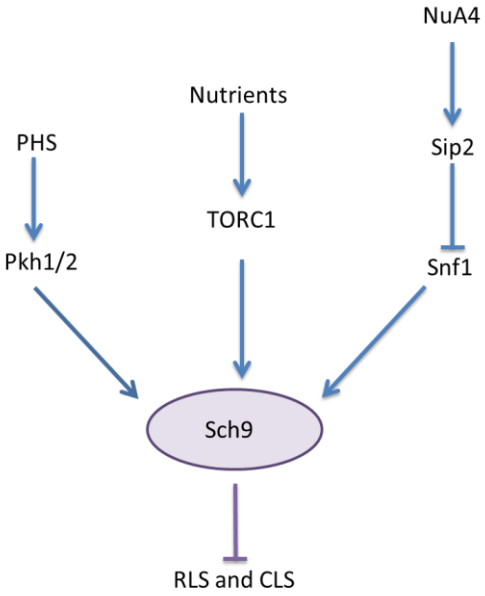

Figure 5: Pkh1/2, TORC1 and Snf1 phosphorylate Sch9. These phosphorylations stimulate Sch9 to inhibit RLS and CLS processes. Arrows indicate positive regulation and flat arrows represent negative regulation.

As such, at least three pathways have been elucidated which, independently of each other, regulate Sch9 activity through its phosphorylation. Each of these pathways serves to adjust Sch9 activity in response to different extrinsic and intrinsic signals (Fig. 5). In addition, Sch9 has other potential phosphorylation sites and *in vitro* studies identified two other kinases , Tos3 (Kim et al, 2005) and Pho85 (Ptacek et al, 2005), which phosphorylate Sch9. But these kinases have never been reported to phosphorylate Sch9 *in vivo*.

2.1.4. Sch9 localization

An additional regulation mechanism of Sch9 function is presumably via protein localization. GFP tagged Sch9 has been detected throughout the whole cell, but enriched at the vacuolar membrane (Jorgensen et al, 2004). When cells were subjected to acute glucose starvation, this vacuolar enrichment disappeared, while it remained unaltered when cells are growing in steady state on different carbon sources or when treated with rapamycin.

Besides vacuolar membrane localization, nuclear localization of Sch9 has been detected too, and proven to be essential for defense against osmotic stress (Pascual-Ahuir & Proft, 2007b).

Mechanisms of Sch9 localization regulation remain elusive. C2 domains are capable of binding phospholipids. Possibly, the C2-domain at the N-terminal end of Sch9 is used to target Sch9 at the vacuolar membrane (Smets et al, 2010).

2.2. Targets of Sch9

Sch9 is a major signaling mediator in nutrient sensing and functions mainly as a downstream effector of TORC1. Using genome-wide expression analysis, Smets et al. proved that next to TORC1-dependent functions, Sch9 has several roles in the cell independent of TORC1 (Smets et al, 2008).

2.2.1. Protein synthesis regulation

For protein synthesis, expression of ribosomal protein (RP) genes and ribosome biogenesis (ribi) are essential. During ribosome biogenesis, ribosomal subunits are synthetized in the cytoplasm and transported into the nucleus. Ribosomal ribonucleic acid (rRNA) binds with these proteins to form functional ribosomes. Expression of RP genes and ribi genes is regulated by TORC1, mainly through Sch9. Ribonucleic acid polymerase II (RNA Pol II) is responsible for transcription of ribi and RP genes. Fhl1, Ifh1 HmoI, Sfp1 are transcription factors known to regulate expression of RP genes and Sfp1 mediates transcription of ribi genes. Sch9 acts in parallel with these transcription factors to regulate the expression of the RP and ribi genes (Huber et al, 2011; Jorgensen et al, 2004). Ribi genes have two regions in their promoter, Polymerase A and C (PAC) element and rRNA processing element (RRPE), known to be bound by transcription repressors Dot6, Tod6 and Stb3 (Fig. 6). Although RP genes have no PAC element or RRPE element in their promoter, RP genes transcription is regulated through Stb3. Sch9 regulates ribosome biogenesis and expression of RP by phosphorylating Dot6, Tod6 and Stb3, which results in inhibiting these transcription repressors to bind to the promoters of ribi and RP genes, rendering it possible for RNA Pol II to perform transcription.

Maf1 is a transcription inhibitor, this protein associates with ribonucleic acid polymerase III (RNA Pol III) and prevents transcription of 5S RNA and tRNAs (Huber et al, 2009). In favorable conditions, meaning nutrients rich medium, TORC1 phosphorylates Sch9, and Sch9 on its turn phosphorylates Maf1 (Fig. 6). This phosphorylation renders Maf1 incapable of inhibiting RNA Pol III by two actions: Sch9 prevents binding of Maf1 to RNA Pol III and stimulates cytoplasmic translocation.

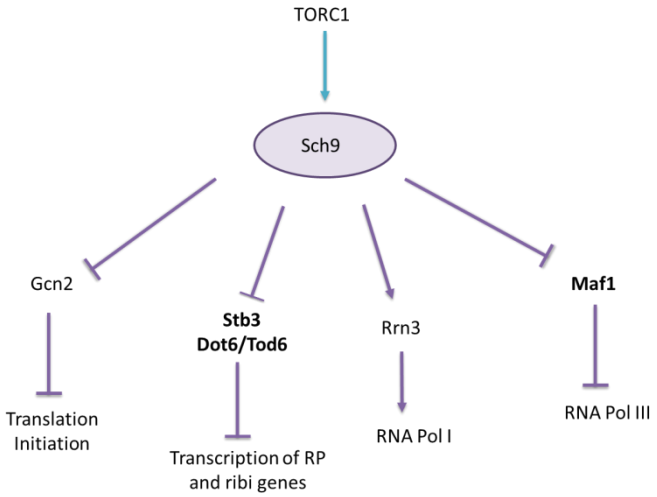

Figure 6: TORC1-dependent signaling of Sch9. Arrows indicate positive regulation and flat arrows represent negative regulation. The proteins in bold interact physically with Sch9.

The function of ribonucleic acid polymerase I (RNA Pol I) is to transcribe ribosomal deoxyribonucleic acids (rDNA). Rrn3 is a transcription initiator factor that binds to RNA Pol I and stimulates transcription by recruiting RNA Pol I onto rDNA promoters. Sch9 stimulates the recruitment of RNA Pol I onto rDNA and enhances the processing process of rRNA, but more research is needed to determine the mechanism by which this happens (Fig.6) (Huber et al, 2009; Peyroche et al, 2000).

Sch9 regulates protein synthesis also at translation level. Transcription initiator eIF2α is a subunit of eIF2 protein complex, which allows tRNA to bind on the translation machinery. In amino acid poor environment, protein kinase Gcn2 is activated by high levels of uncharged tRNA. Acitvated Gcn2 subsequently phosphorylates eIF2, rendering the protein complex inactive (Zaborske et al, 2010). Urban *et al.* showed that phosphorylation of transcription initiaton factor eIF2α is dependent of Sch9, but the mechanism by which this happens is unkown and possibly Sch9 mediates eIF2α phosphorylation through Gcn2 (Huber et al, 2009; Urban et al, 2007; Zaborske et al, 2010).

2.2.2. Control of cell size

In budding yeast, cells must grow till a critical size before cell division can occur. The critical size is dependent of the available nutrients. In nutrient rich medium, the threshold is higher than in nutrient poor medium. Throughout genetic analysis, Sch9 was one of the identified genes, that when mutated, lead to a small cell size (Jorgensen et al, 2002; Toda et al, 1988). This phenomenon, called Whi phenotype, is the consequence of accelerating cell division with respect to cell growth. *sch9*Δ mutants had 40% less cell volume than wild type cells and formed smaller colonies.

Ribogenesis as well is a major factor in cell size regulation (Rudra & Warner, 2004). Deletion of ribosomal genes induces small cell size phenotype (Jorgensen et al, 2002; Jorgensen et al, 2004). Given Sch9 is also involved in ribosome synthesis in a TORC1 dependent manner, Sch9 potentially couples ribogenesis to cell size and suggests Sch9 regulates cell size dependent of TORC1.

2.2.3. Stress response and life span

Yeast cells protect themselves against stress, e.g. nutrient starvation, heat and oxidative stress, by expressing stress response element (STRE) and post diauxic-shift (PDS) genes (Swinnen et al, 2006). The function of these genes is on the one hand regulated by the TORC1 and Sch9, and on the other hand by protein kinase A (PKA), the main protein of the PKA pathway. TORC1 and Sch9 primarily respond to nitrogen and carbon source availability, while PKA mainly reacts only to carbon availability. All the three proteins suppress the expression of STRE- and PDS genes through phosphorylation of the signaling integrator Rim15.

Under stress free conditions, Sch9, independent of TORC1, phosphorylates Rim15 at S1061 (Wanke et al, 2008) and TORC1 phosphorylates Rim15 at T1075 (Wanke et al, 2005). These phosphorylation actions stimulate the binding of Rim 15 binds to 14-3-3 protein Bmh2 and thereby cause cytoplasmic sequestration of Rim15 (Smets et al, 2010). Retaining Rim15 in the cytoplasm prevents activation of STRE-and PDS genes. PKA inactivates Rim15 through another mechanism. When G protein coupled receptor Gpr1 and Ras2 sense the presence of glucose in the environment, they stimulate the formation of cAMP by activating adenylate cyclase (AC). cAMP activates PKA and the latter phosphorylates Rim15 resulting in inactive Rim15 (Roosen et al, 2005) (Fig. 7).

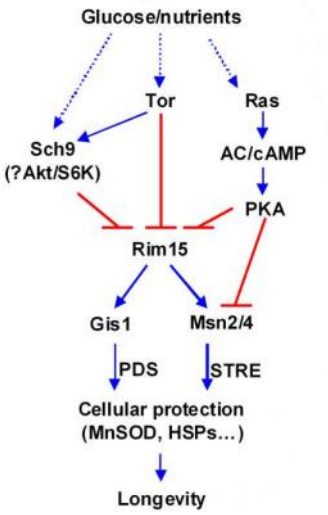

Figure 7: Scheme of different factors mediating life span extension through Rim15. Sch9, Tor and Ras prevent Rim15 from phosphorylationg Gis1 and Msn2/4 and consequently inhibit expression of PDS- and STRE-genes, modified figure from (Wei et al, 2008).

On the contrary, in stress conditions, Rim15 is not phosphorylated by Sch9, TOR or PKA. Unphosphorylated Rim15 doesn't bind to Bmh2 and migrates to the nucleus. In the nucleus Rim15 activates the transcription factors Gis1, Msn2 and Msn4 (Msn2/4) (Swinnen et al, 2006). Activated Gis1 will bind on the PDS-element, in the promoter of specific genes, and induce transcription of these genes. Parallel to Gis1, Msn2/4 activates expression of genes containing STRE elements in their promoter (Fabrizio et al, 2003; Wei et al, 2008). The genes stimulated by Gis1 and/or Msn2/4 help the cells to survive in stress conditions e.g. heat shock proteins for protein refolding, mitochondrial superoxide dismutase (MnSOD) for neutralization of oxygen radicals (Fabrizio et al, 2003) and PDS proteins for shifting from fermentation to respiration and promote entry into the stationary phase (Pedruzzi et al, 2003; Reinders et al, 1998).

These cellular protection pathways are involved in life span (Smets et al, 2008). Mutants with defective Sch9, Tor1 or PKA show extended RLS and CLS (Longo & Fabrizio, 2012). Wei *et al.*, compared the life span extension of *tor1*Δ, *sch9*Δ or *ras2*Δ strains to the life span extension of analogue mutant strains with additional *rim15*Δ, *msn2/4*Δ or *gis1*Δ mutation (Wei et al, 2008). CLS measurements indicated that the life span prolongation caused by *tor1*Δ, *sch9*Δ or *ras2*Δ were reversed when *RIM15*, *MSN2/4* or *GIS1* were also deleted. Next to Tor1, Sch9 and PKA, there are other factors that mediate life span, these regulation mechanisms can be Rim15-dependent and Rim15-independent (Wanke et al, 2005; Wei et al, 2008).

Sch9 also regulates stress response and independently of TORC1 and Rim15. For instance, when cells are grown under osmotic stress, Sch9 will phosphorylate and thereby activate transcription factor Sko1 (Pascual-Ahuir & Proft, 2007b). Subsequently, phosphorylated Sko1 will bind on cAMP response element (CRE), in the promoter of osmotic responsive genes, and activate transcription of these genes. Sch9 is essential in the protection of the cell against osmotic stress as *sch9*Δ mutant cells display a clear growth defect on medium with high osmotic stress.

Remarkably, next to being an upstream regulation factor of Sch9, recently the mitochondrion has been identified as a Sch9 downstream target. Sch9 regulates, in a TORC1 dependent manner, translation of oxidative phosphorylation subunits (OXPHOS), which are encoded by mitochondrial DNA (Pan & Shadel, 2009). Decreased Sch9 activity, due to reduced TORC1 signaling, enhances OXPHOS formation, and thereby stimulates respiration. Increased respiration leads to elevated reactive oxygen species (ROS) production during exponential and early PDS phase (Pan et al, 2011). These increased levels of ROS during growth stimulate down-regulation of mitochondrial activity and thus ROS production in the stationary phase. Although mechanism through which this happens remains elusive, this process has been proven to elongate CLS.

2.2.4. Autophagy

Autophagy is mechanism by which dysfunctional proteins and organelles are removed from the cytosol and transported into the vacuole for degradation (Glick et al, 2010). During starvation, autophagy is induced, and provides a mechanism to release molecules in the vacuoles back into the cytosol, where they are used for energy production, as building blocks for proteins and for fatty acids synthesis.

PKA and Sch9 work redundantly in autophagy regulation. TORC1 is also a known down-regulator of autophagy and given Sch9 is a downstream effector of TORC1, Yorimitsu *et al.* studied whether Sch9-dependent autophagy induction is TORC1 dependent. Autophagy induction was observed in cells with active TORC1 and inactive Sch9 and PKA, indicating Sch9 regulates autophagy in a TORC1-independent manner.

TORC1, Sch9 and PKA regulate stress response in through Rim15. Also for the induction of autophagy, PKA and Sch9 act, in part, via Rim15 (Yorimitsu et al, 2007). On the contrary, assays to investigate the dependence of TORC1 autophagy induction to Rim15 elucidated that TORC1 regulates autophagy independent of Rim15.

2.3. The human orthologue of Sch9

Sch9 was first characterized as a PKA homologue, as the two proteins were proven to be functional redundant for cell size regulation in yeast (Toda et al, 1988). Geykens *et al.,* aligned Sch9 and protein kinase B (PKB), showing that Sch9 has more similarity to mammalian PKB than to PKA (Geyskens et al., 2001). Further investigation, in which functional homology of mammalian PKB to Sch9 was studied by introducing vectors coding for mammalian PKB in *sch9*Δ strains, have proven that mammalian PKB is able to rescue cells from slow growth and small colony *sch9*Δ phenotype. Mammalian PKB expression also largely restored repression of stress response genes induced in *sch9*Δ mutant cells.

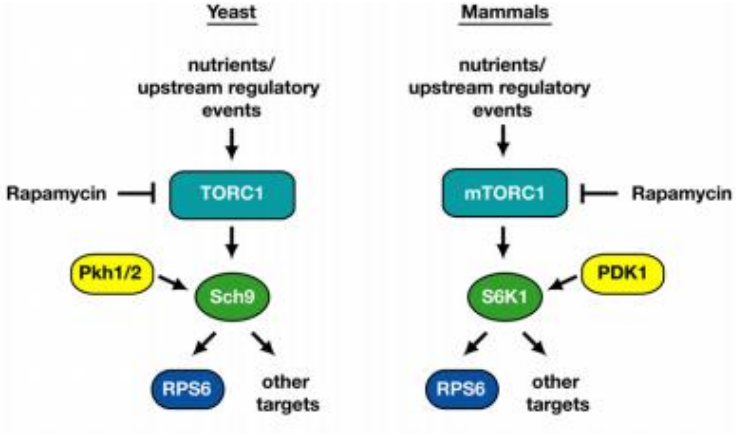

Figure 8: Model of TORC1-Sch9 signaling conservation in human and yeast, proposed by Urban et al., 2007 modified figure from (Powers, 2007).

Next to the theory for PKB as functional homologue for Sch9, there are research groups which suggest that Sch9 is more likely orthologous to S6 kinase 1 (S6K1) (Powers, 2007; Urban et al, 2007). The latter theory is supported by the fact that both S6K1 and Sch9 regulate protein synthesis, in part by phosphorylating Rps6 and are also both phosphorylated by (mammalian) TORC1 and phosphoinositide-dependent kinases (Fig. 8). PKB is a downstream target of mammalian TORC2 (mTORC2) and evidence of Sch9 being phosphorylated by TORC2 in yeast remains elusive.

The only complementation study that has been reported thus far is the mammalian PKB complementation study by Geyskens *et al* (Geyskens et al., 2001). During this study it was proven that PKB can complement certain phenotypes of *sch9*Δ. A similar study for complementation of *sch9*Δ by S6K1 has not been documented. More research is needed to elucidate whether S6K1 complements Sch9. Alongside of the phenotypes studied by Geyskens *et al.*, more *sch9*Δ phenotypes could be examined.

Further investigation is required to elucidate which protein, S6K1 or PKB, is the Sch9 orthologue or whether they are both orthologues of Sch9, depending on which function of Sch9 is investigated.

3. Vacuolar proton-translocating ATPase

Vacuolar proton-translocating ATPase (V-ATPase) is a proton pump present in all eukaryotic cells. Despite of V-ATPase being well conserved amongst eukaryotic cells, yeast is the main model organism being used to study the proton pump, because loss of V-ATPase activity in eukaryotes other than fungi is lethal (Kane, 2007).

3.1. V-ATPase assembly

The V-ATPase is composed of two subcomplexes, the pheripheral V_1 subcomplex and the integral V_0 subcomplex (Graham et al, 2000) (Fig. 9). The V_1 subcomplex is encoded by eight genes, *VMA1*, *VMA2*, *VMA4*, *VMA5*, *VMA7*, *VMA8*, *VMA10* and *VMA13*, each coding for a different subunit. After synthesis of all the subunits, they assemble and form a V_1 subcomplex in the cytosol. On the other hand, the V_0 subcomplex is encoded by six genes, *VMA3*, *VMA6*, *VMA11*, *VMA16, VPH1* and *STV1*, also each coding for a specific V_0 subcomplex subunit. Translation of these genes happens in the cytosol, subsequently Vma3, Vma11, Vma16 and Vph1 or Stv1 are translocated to the membrane of the endoplasmic reticulum (ER) where they assemble to form the V_0 subcomplex. To complete the V_0 assembly, Vma6 binds on the complex formed by the other subunits. The binding of Vma6 stimulates transport of the V_0 subcomplex to the vacuole. Once the V_0 subcomplex is inserted into the vacuolar membrane the V_1 subcomplex will bind on it and form a functional V-ATPase pump.

Loss of function of one of the subunits completely inhibits V-ATPase activity. When one of the V_1 subunits is deleted, the other V_1 subunits will still assemble, but the formed V_1 subcomplex will not bind to V_0 subcomplex (Graham et al, 2000; Kane, 2007). When one of the V_0 subunits is deleted, the assembly and localization of V_0 subcomplex will be disrupted and the V_1 subcomplex will remain in the cytosol.

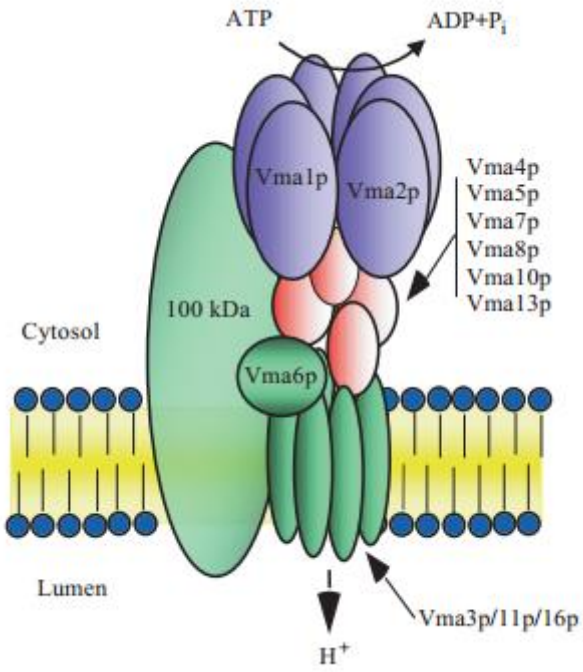

Figure 9: Schematic representation of V-ATPase. The subunits of the V_0 subcomplex are shown in green and the subunits of the V_1 subcomplex are represented in red and blue. The blue subunits, vma1 and vma2, are the hydrolysis catalytic subunits. The 100 kDa subunit can be Vph1 or Stv1, depending on the localization (Graham et al, 2000).

Next to the fourteen subunits mentioned above, an extra V_0 subcomplex subunit Vma9 has been identified (Compton et al, 2006). Furthermore, *VMA9* and other additional genes, *VMA12*, *VMA21* and *VMA22*, are essential for V-ATPase assembly. Cells lacking either of these genes failed to form a functional V-ATPase due to unsuccessful V-ATPase assembly.

3.2. Regulation of V-ATPase activity

The V-ATPase activity is regulated through acting on the assembly process of V_0 and V_1 subunits, and through changing of V-ATPase specific activity.

External pH mediates V-ATPase activity through the specific activity. To examine this, cells were grown on minimal media at buffered extracellular pH 5 and pH7, subsequently the specific activity of the V-ATPases of these cells was measured (Diakov & Kane, 2010). V-ATPases of cells grown on minimal media at buffered extracellular pH 7 exhibited higher activity than V-ATPases of cells grown on minimal media at buffered extracellular pH 5, showing V-ATPase activity is dependent of extracellular pH.

Glucose and cytosolic pH on the other hand control V-ATPase activity through the V-ATPase assembly process. This was elucidated via research in which the glucose dependence of V-ATPase assembly process and cytosolic pH was investigated (Dechant et al, 2010). In glucose poor medium V-ATPase disassembled, and addition of glucose enhanced V-ATPase

assembly. Analogous, the cytosolic pH declined when cells were glucose starved and adding glucose to the media, made the cytosolic pH rise back to physiological pH (~7.5). Investigation of the relation between V-ATPase assembly and cytosolic pH demonstrated V-ATPase disassembled upon intracellular acidification.

The results of both studies suggest that integrated pH and metabolic inputs determine the final assembly state and activity of the V-ATPase (Diakov & Kane, 2010).

3.3. Functions of V-ATPase

The main function of V-ATPase is acidifying cell organelles, but genetic screens lead to the hypothesis that V-ATPase may be involved in more cellular processes. Further investigations have proven V-ATPase to be associated with oxidative stress and upstream regulation of the PKA pathway.

3.3.1. The V-ATPase proton pump

In yeast, two types of V-ATPase are synthesized (Graham et al, 2000). One type of V-ATPase, which contains the Vph1 subunit, is vacuolar specific, while the second type includes the Stv1 subunit, and is present in the membrane of the other acidic cell organelles, such as endosomes and the Golgi apparatus. Both types acidify the lumen of the cell organelles on whose membrane they are present. The V_1 subcomplex catalyzes hydrolysis of ATP in the cytosol, the energy released from this reaction is used to pump protons from the cytosol into the lumen.

The main function of the Golgi apparatus is modifying, sorting and packaging macromolecules for secretion, exocytosis, or use within the cell (Bryant & Stevens, 1998). Endosomes, on the other hand, are essential in endocytosis. They transport molecules to the Golgi apparatus or the vacuole. Next to its role in protein degradation, the vacuole is also used as a storage organelle. Amino acids, ions and phosphates are stored in the vacuole and when these components are not present in the media, they will be released back into the cytosol. Furthermore, the vacuole is essential in osmoregulation and pH homeostasis (Rubenstein & Schmidt, 2010). Activity of V-ATPase is essential for proper functioning of these cell organelles.

Through genetic screens, several vacuolar membrane ATPase deletion (*vma*Δ) phenotypes have been characterized. Cells without V-ATPase activity can't grow on pH 7.5 buffered medium, lack the ability to grow on non-fermentable sugars and show an increased sensitivity to Ca^{2+} concentrations in the environment compared to wild type cells (Kane, 2006). The sensitivity to Ca^{2+} concentrations has been connected to the disability of the vacuole to regulate cytosolic Ca^{2+}concentrations, but most of the mechanisms behind these

*vma*Δ phenotypes, like how is V-ATPase involved in growth on non-fermentable sugars, are to be elucidated.

3.3.2. V-ATPase regulates the PKA pathway

The PKA pathway is a nutrient sensing pathway, which is activated when yeast cells are put in glucose rich environment. As mentioned above, glucose levels and cytosolic pH mediate V-ATPase activity through its assembly process. The latter combined with research that showed cAMP synthesis after glucose addition is significantly decreased in *vma*Δ strains (Dechant et al, 2010) lead to the following hypothesis: Cells in glucose rich medium metabolize glucose, leading to high cellular ATP and ethanol concentrations. This causes the cytosolic pH to increase through a mechanism that is not clarified yet. The increased pH stimulates V-ATPase assembly, which subsequently stimulates cAMP synthesis resulting in PKA activation (Fig. 10) (Rubenstein & Schmidt, 2010).

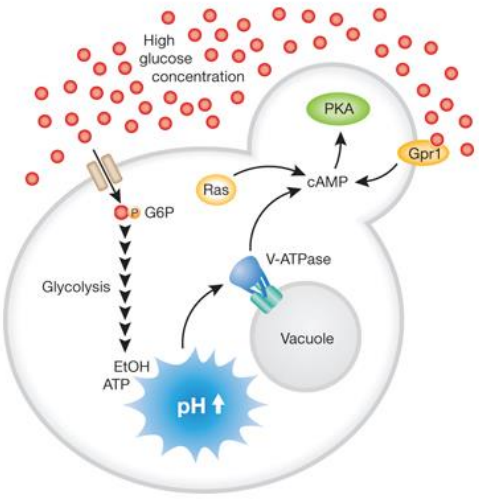

Figure 10: The V-ATPase activates the PKA pathway in glucose rich environment by stimulating synthesis of cAMP (Rubenstein and Schmidt, 2010).

3.3.3. V-ATPase activity protects from oxidative stress

Cells have several mechanisms to neutralize ROS, byproducts of aerobic respiration. These include both non-enzymatic anti-oxidants like glutathione, D-erythro-ascorbate and ubiquinol, as well as enzymes that neutralize ROS, such as catalases and superoxide dismutases. When these mechanisms fail to antagonize the reactive species, ROS concentrations increase and cause oxidative stress.

Genome wide screening for genes responsible for oxidative stress protection, revealed *vma*Δ strains were hypersensitive to oxidative stress (Thorpe et al, 2004). Further studies

confirmed strains without V-ATPase activity to be more sensitive to oxidative stress than wild type (Milgrom et al, 2007). Noteworthy, *vma*Δ strains showed increased ROS levels even when no oxidative stress was applied. These results suggest that the V-ATPase is involved in cellular protection against endogenous stress. During respiration, there is a high level of electron transport in the mitochondria. The possibility of this organelle being the source of endogenous stress was examined by comparing oxidative stress in *vma*Δ strains, in which respiration was disabled, to *vma*Δ strains with functional mitochondria (Milgrom et al, 2007). Respiration disabled *vma*Δ strains, didn't show an aberrant oxidative stress phenotype, proving the mitochondria cannot be the source of endogenous stress. The source of endogenous stress remains elusive.

Objectives

The protein kinase Sch9 is a signaling mediator that receives signals from upstream intracellular and extracellular cues and transmits these to downstream targets by phosphorylating them.

During preliminary studies, a synthetic genetic array (SGA) was performed to identify the genes that interact with *SCH9*. The *sch9*Δ strain was crossed with a collection of gene deletion strains present in the laboratory, and synthetic sick and synthetic lethal genetic interactions were determined. The results showed that the crossing of some *vma*Δ strains with the *sch9*Δ strain led to a synthetic sick phenotype. *VMA* genes code for subunits of the multiprotein complex V-ATPase, which is responsible for acidification of cell organelles, such as the vacuole. Due to these results, genetic interaction between the *VMA* genes and *SCH9* further analyzed, and the role of Sch9 in the vacuolar function was investigated.

Several approaches were followed in our study. To start, we confirmed the genetic sick phenotype of *sch9*Δ*vma*Δ double deletions by tetrad analysis, followed by an in-depth analysis of the growth properties of single and double deletion strains, as well as a characterization of the phenotypic overlap of *sch9*Δ and *vma*Δ strains. As both Sch9 and the V-ATPase function are regulated by nutrient availability, we chose to investigate possible effects of Sch9 on V-ATPase function and localization. Reciprocally, as Sch9 localization is enriched at the vacuolar membrane (Jorgensen et al, 2004), we tested for possible Sch9-Vma interactions, as well as phosphorylation of Vma subunits by Sch9. Finally, one of the well known phenotypes of the *sch9*Δ strain is its higher chronological life span (Fabrizio et al, 2001). Effects of V-ATPase functioning on CLS are largely unknown. Therefore, we set out to test how the observed genetic interaction between the V-ATPase and *SCH9* might influence survival in the stationary phase. (Baars et al, 2007)

Materials and Methods

4. Media

The composition of the different media for growing yeast and bacterial cells are described in the Addendum.

5. Yeast strains used in this study

Table 1: Genotype of strains used throughout this study.The genetic background of the wild type BY4741 strain is his3Δ1 leu2Δ0 met15Δ0 ura3Δ0. sch9Δ MATa was used during experiments unless stated otherwise.

Strain	Genetic background
WT	BY4741 MATa
*sch9*Δ	MATα; sch9::NATMX2
*sch9*Δ	MATa; sch9::NATMX2
*vma1*Δ	MATa; vma1::KANMX4
*vma2*Δ	MATa; vma2::KANMX4
*vma3*Δ	MATa; vma3::KANMX4
*vma4*Δ	MATa; vma4::KANMX4
*vma5*Δ	MATa; vma5::KANMX4
*vma6*Δ	MATa; vma6::KANMX4
*vma7*Δ	MATa; vma7::KANMX4
*vma8*Δ	MATa; vma8::KANMX4
*vma10*Δ	MATa; vma10::KANMX4
*vma11*Δ	MATa; vma11::KANMX4
*vma13*Δ	MATa; vma13::KANMX4
*vma16*Δ	MATa; vma16::KANMX4
*vph1*Δ	MATa; vph1::KANMX4
*stv1*Δ	MATa; stv1::KANMX4
*vma1*Δ *sch9*Δ	MATa; vma1::KANMX4 sch9::NATMX2
*vma2*Δ *sch9*Δ	MATa; vma2::KANMX4 sch9::NATMX2
*vma3*Δ *sch9*Δ	MATa; vma3::KANMX4 sch9::NATMX2
*vma4*Δ *sch9*Δ	MATa; vma4::KANMX4 sch9::NATMX2
*vma5*Δ *sch9*Δ	MATa; vma5::KANMX4 sch9::NATMX2
*vma6*Δ *sch9*Δ	MATa; vma6::KANMX4 sch9::NATMX2
*vma7*Δ *sch9*Δ	MATa; vma7::KANMX4 sch9::NATMX2
*vma8*Δ *sch9*Δ	MATa; vma8::KANMX4 sch9::NATMX2
*vma10*Δ *sch9*Δ	MATa; vma10::KANMX4 sch9::NATMX2
*vma11*Δ *sch9*Δ	MATa; vma11::KANMX4 sch9::NATMX2
*vma13*Δ *sch9*Δ	MATa; vma13::KANMX4 sch9::NATMX2
*vma16*Δ *sch9*Δ	MATa; vma16::KANMX4 sch9::NATMX2
*vph1*Δ *sch9*Δ	MATa; vph1::KANMX4 sch9::NATMX2
*stv1*Δ *sch9*Δ	MATa; stv1::KANMX4 sch9::NATMX2
WT vma1-Myctag	MATα; vma1-Myctag
WT vma2-Myctag	MATα; vma2-Myctag
WT vma4-Myctag	MATa; vma4-Myctag
WT vma5-Myctag	MATa; vma5-Myctag
WT vma6-Myctag	MATa; vma6-Myctag
WT vma7-Myctag	MATa; vma7-Myctag
WT vma10-Myctag	MATa; vma10-Myctag
WT vma13-Myctag	MATa; vma13-Myctag
*sch9*Δ *vma1-Myctag*	MATa; vma1-Myctag
*sch9*Δ *vma2-Myctag*	MATa; vma2-Myctag
*sch9*Δ *vma4-Myctag*	MATa; vma4-Myctag
*sch9*Δ *vma5-Myctag*	MATα; vma5-Myctag
*sch9*Δ *vma6-Myctag*	MATα; vma6-Myctag
*sch9*Δ *vma7-Myctag*	MATa; vma7-Myctag
*sch9*Δ *vma10-Myctag*	vma10-Myctag
*sch9*Δ *vma13-Myctag*	vma13-Myctag

6. Tetrad analysis

Tetrad analysis was performed in order to investigate genetic interactions between *SCH9* and the different *VMA* genes, and to isolate *vma*Δ*sch9*Δ double mutants. This experiment was carried out in *S. cerevisiae* yeast cells derived from the BY4741 background with the genotypes summarized in Table 1.

Haploid *sch9Δ* and *vmaΔ* cells of opposite mating type were crossed, and diploid cells were isolated on YPD medium containing both ClonNat (for selection of sch9::NATMX2) and geneticin (for selection of vmax::KANMX4). The diploids were cultured for 1 day on liquid medium, spun down and spotted on solid sporulation medium. After 3 – 6 days, cells were scraped from sporulation plates, treated with lyticase, after which spores were dissected with the micromanipulator (Singer Instruments MSM System) and positioned on a YPD plate. To determine the genotype of the isolated spores, cells were replica plated on YPD plates containing either ClonNat (for selection of sch9::NATMX2) or geneticin (for selection of vmax::KANMX4). A more detailed description of this protocol can be found in the Addendum.

7. Growth assays

7.1. Growth curve analysis

The growth profiles of wild type (WT), *sch9*Δ, *vma*Δ and the generated *vma*Δ*sch9*Δ strains were determined in order to examine the influence of the different deletions on the growth. Three single colonies of strains in Table 1 and the corresponding double mutants were inoculated in YPD medium. Because the double mutant strains grow very slow, the cells were incubated at 30 °C, shaking at 200 rpm, for at least 36 hours to reach the stationary phase.

The cultures were diluted to an optical density of 0.01 at 600 nm (OD_{600}) in a 96-well microtiter plate. All the strains were diluted in YPD medium and also in YPD medium, buffered at pH 5. The growth of the strains was followed at 30 °C in Multiskan GO spectrophotometer (Thermo Fisher Scientific Inc., Waltham, USA), which measured the OD_{600} every 2 hours for a total duration of 48 hours. The growth curves are shown as the mean values of the independent cultures, standard deviations (STDEV) are depicted as error bars.

7.2. Spot tests

In order to study phenotypic overlap between *sch9*Δ and *vma*Δ strains, spot tests were performed in different conditions.

7.2.1. Medium preparation

The specific solid medium conditions, listed in Table 2, were prepared as explained in section 1.1.

Table 2: Solid media conditions used for spot assays. Gly: glycerol, EtOH: ethanol.

pH dependence				
YPD pH 5	YPD pH 6	YPD pH 7	YPD pH 7,5	YPD pH 8
C-sources				
YP 3% Gal pH 5	YP 3% Gly pH 5	YP 3% Gly 2% EtOH pH 5	YP 3% lactate pH 5	YP 0,3% lactate pH 5
Ca^{2+} dependence				
YPD 60 mM $CaCl_2$	YPD 150 mM $CaCl_2$	YPD 60 mM $CaCl_2$ pH 5	YPD 150 mM $CaCl_2$ pH 5	YPD 60 mM $CaCl_2$ pH 7,5
Osmotic stress				
YPD 1 M KCl		YPD 1 M NaCl		
Metals				
YPD 2 mM $MnCl_2$		YPD 4 mM $ZnCl_2$		
Rapamycin				
50 nM rapamycin				

7.2.2. Performing the spot test

The single mutant and WT strains listed in Table 1 were inoculated in YPD and grown to the stationary phase at 30 °C, shaking at 200 rpm. Subsequently, the cultures were diluted to OD_{600} 1 in YP and 3 times a 10 fold serial dilution was made in a 96-well microtiter plates. 5µL of each dilution was spotted on plates listed above (Table 1). The plates were incubated for 3 days, at 30°C.

8. Yeast two-hybrid (Y2H) screening

After confirming the genetic interaction between *SCH9* and the *VMA* genes, Y2H was performed to screen the Vma proteins for physical interaction with the Sch9 protein. The used protocol is based on the protocol described by Woodsmith *et al.*(Woodsmith et al, 2012). The host strain for testing Y2H interaction is the PJ64-4a/α strain (genotype MAT**a**/α *trp1-901 leu2-3,112 ura3-52 his3-200 gal4Δ gal80Δ LYS2::GAL1-HIS3, GAL2-ADE2 met2::GAL7-lacZ*). This strain cannot grow on medium lacking either histidine or adenine, unless the target proteins interact with each other, which results in the formation of a functional Gal4 transcription factor, thereby inducing expression of the *HIS3* and *ADE2* genes. Expression of *HIS3* can be leaky, and as such, the addition of 3-aminotriazole (3-AT), which is a competitive inhibitor of the gene product of *HIS3*, is often employed to increase the dependency of *HIS3* expression on *bona fide* interaction between the target proteins.

Appropriate Y2H vectors were made with the Gap repair method, and the detailed protocol is described in the Addendum. As such, pGBAE-vectors were generated in which the GAL4 DNA binding domain is fused with the protein of interest. In addition, pACTBE-vectors are made in which the DNA activation domain is fused with the protein of interest. Both *SCH9* and the *VMA* genes were cloned into both the pGBAE- and pACTBE-vectors, and transformed into the PJ69-4a and PJ69-4α strains, resp.

Next, diploid cells were made by crossing pGBAE-*SCH9* clones in PJ69-4a cells with pACTBE-*VMA* clones in PJ69-4α and vice versa, by crossing pACTBE-*SCH9* bait clones in PJ69-4α cells with pGBAE-*VMA* prey clones in PJ69-4a. Diploid cells were isolated SD-Trp-Leu plates.

To test for interaction between the Sch9 and Vma proteins, the diploid strains were inoculated in SD-Leu-Trp and grown to stationary phase at 30 °C, shaking at 200 rpm. Subsequently, the strains were diluted to OD_{600} 1, after which a 10 fold serial dilution was performed 3 times in a 96-well microtiter plate. 5µL of each dilution was spotted on plates with the following selective media. As a control for growth, the strains were spotted on SD-Leu-Trp. To investigate physical interaction, the strains were spotted on SD-Leu-Trp-Ade and SD-Leu-Trp-His. Finally, to increase the dependency of growth on medium lacking histidine on true interaction of the target proteins, the cultures were also spotted on SD-Leu-Trp-His containing 2.5 mM and 5 mM 3-AT. The plates were incubated for 9 days at 30 °C.

9. *In silico* research: phosphorylation sites

To investigate the probability of Vma proteins being phosphorylated, the Vma amino acid sequences were analyzed. Identification of the conserved RxxS and RxxT phosphorylation motifs in the different Vma proteins was carried out using http://biodev.extra.cea.fr/strip/Default.aspx. Results are shown in Table S5.

10. Western blots

Western blots were performed to study the possibility of Sch9 affecting the expression and/or phosphorylation of V_1 subunits and Vma6. For this, the genes encoding the different V_1 subunits, as well as *VMA6*, were chromosomally tagged at their C-terminus with the 9Myc epitope in *SCH9*/*sch9*Δ heterozygous diploids. Subsequently, WT and *sch9*Δ haploid cells expressing the Myc-tagged *VMA* genes were generated by sporulating the diploid cells isolating the proper haploid strains.

After protein extraction with the TCA method, protein levels were determined via the Bradford method. Equal amounts of protein were run on a SDS-PAGE gel, followed by blotting onto a Immobilon-P membrane (Millipore). Detection of the Myc-tagged Vma proteins was performed with an anti-Myc antibody. In addition, the 'housekeeping protein' Adh2 was also detected to verify whether the same amount of protein was loaded in each lane. In addition to running the samples on a standard gel, phosphate-affinity gels ("Phos-tag" gels) were used to study possible effects of phosphorylation. On Phos-tag gels, a compound is added to the gel, so that phosphorylated protein isoforms are preferentially retained in the gel, leading to a larger separation of fosfo-isoforms, which can lead to detection of phosphorylation events which are not seen on regular gels. See Addendum for more details.

11. Co-immunoprecipitation (Co-IP)

To confirm the physical interaction between Vma6 and Sch9, observed in the Y2H assay, a Co-IP was performed. For this, strains expressing the Vma6-9Myc fusion proteins were transformed with a plasmid encoding a HA-tagged version of Sch9. After isolation of protein extracts, an antibody-mediated pull-down (immunoprecipitation) of either the Vma6-Myc or HA-Sch9 was performed, after which the presence of both tagged proteins was assayed by a standard SDS-PAGE and Western blotting. If both (tagged) proteins interact, one should be able to detect the HA-Sch9 in the extract immunoprecipitated with the anti-Myc antibody (pull-down of Vma6-Myc) and vice versa. A detailed description of the procedure for transformation, protein extraction and immunoprecipitation can be found in the Addendum.

12. Fluorescence study

To investigate the vacuolar morphology, two independent methods were employed. First of all, vacuolar morphology is often studied by staining yeast cells with the red fluorescent FM4-64 dye. This dye is incorporated into the plasma membrane of yeast cells, after which it is transported to the vacuolar membrane by the process of endocytosis. In short, FM4-64 staining is performed by adding 2µl of a FM4-64 stock solution to 50µl yeast cells, and incubating the cells for 30 min in the dark. Alternatively, vacuolar membranes can be visualized by expressing the Vph1-GFP protein. Vph1 is part of the V_0 subunit of the V-ATPase, which is localized in the vacuolar membrane in WT cells.

In a separate set of experiments, the intracellular localization of Sch9 was analyzed, making use of a plasmid encoding a GFP-tagged version of Sch9.

Cells containing GFP-tagged proteins and/or stained with FM4-64 are visualized with a Leica DM400 B fluorescence microscope, using a green or red filter, resp. More details on the handling of yeast cells for fluorescence microscopy can be found in the Addendum.

13. Longevity

In order to investigate whether the genetic interaction between *vma*Δ and *sch9*Δ strains has an impact on the life span of yeast cells, selected strains were analyzed for survival during stationary phase, as well as for accumulation of superoxide species. For this longevity study, yeast strains were grown in synthetic complete, glucose-containing, (SD) medium till stationary phase, which was determined as the first day following the day in which the cells were growing exponentially. For survival, a colony forming unit (CFU) method was applied, in which the amount of CFUs is determined for each strain at different time point in the stationary phase. The CFU count at the first day in stationary phase is set to 100% for each strain, after which subsequent CFU counts are expressed as percentages, relative to this initial 100%. Determination of superoxide levels was done be staining yeast cells with the superoxide-specific fluorescent dye DHE (dihydroethidium). Analysis of DHE fluorescence was done both by a microtiterplate reader (Beckmann DTX880) and by flow cytometry (Guava EasyCyte 8HT system). A detailed protocol is described in the Addendum.

Results

14. Interaction between *SCH9* and *VMA*s

14.1. Confirmation of the interaction between *SCH9* and *VMA*s

During a SGA screening, several *VMA* genes were found to genetically interact with *SCH9*, displaying a synthetic sick phenotype for several *vma*Δ*sch9*Δ double mutants. As SGA is a high-throughput technique, it is known to produce false-positive results. Therefore, to verify the results of the screening and investigate whether *SCH9* also genetically interact with other *VMA* genes, tetrad analysis was performed.

The V-ATPase complex is encoded by 15 genes, each coding for a specific Vma subunit. The *vma1*Δ*, vma2*Δ*, vma3*Δ*, vma4*Δ*, vma5*Δ*, vma6*Δ*, vma7*Δ*, vma8*Δ*, vma10*Δ*, vma11*Δ*, vma13*Δ*, vma16*Δ*, vph1*Δ and *stv1*Δ strains were crossed with a *sch9*Δ strain. Crossing of the *sch9*Δ strain with the 15th *VMA* gene deletion mutant strain, *vma9*Δ, failed to produce diploids in two separate attempts for reasons unknown. After sporulation of the diploids, the tetrads were separated and examined.

To determine the genotype of the tetrads, these were spread out on plates containing geneticin or ClonNAT. The *vma*Δ strains contain a gene in their genome which enables them to grow on geneticin plates and *sch9*Δ strains have a gene allowing them to grow on ClonNAT (table 3). Tetrads that were able to grow only on plates containing geneticin were genotyped as *vma*Δ strains, while those that exclusively grew on ClonNAT plates were genotyped as *sch9*Δ strains. Cells which grew on both type of plates were identified as *vma*Δ*sch9*Δ double mutants. Wild-type (WT) strains didn't grow on ClonNAT plates or on plates containing geneticin.

Comparison of the colony size and the genotype shows that overall, *vma*Δ*sch9*Δ strains are the smallest, followed by *sch9*Δ and *vma*Δ mutants (Fig. 11), with exception to the *vph1*Δ *and stv1*Δ strains. WT colonies are the largest, and *vph1*Δ and *stv1*Δ have an equivalent size.

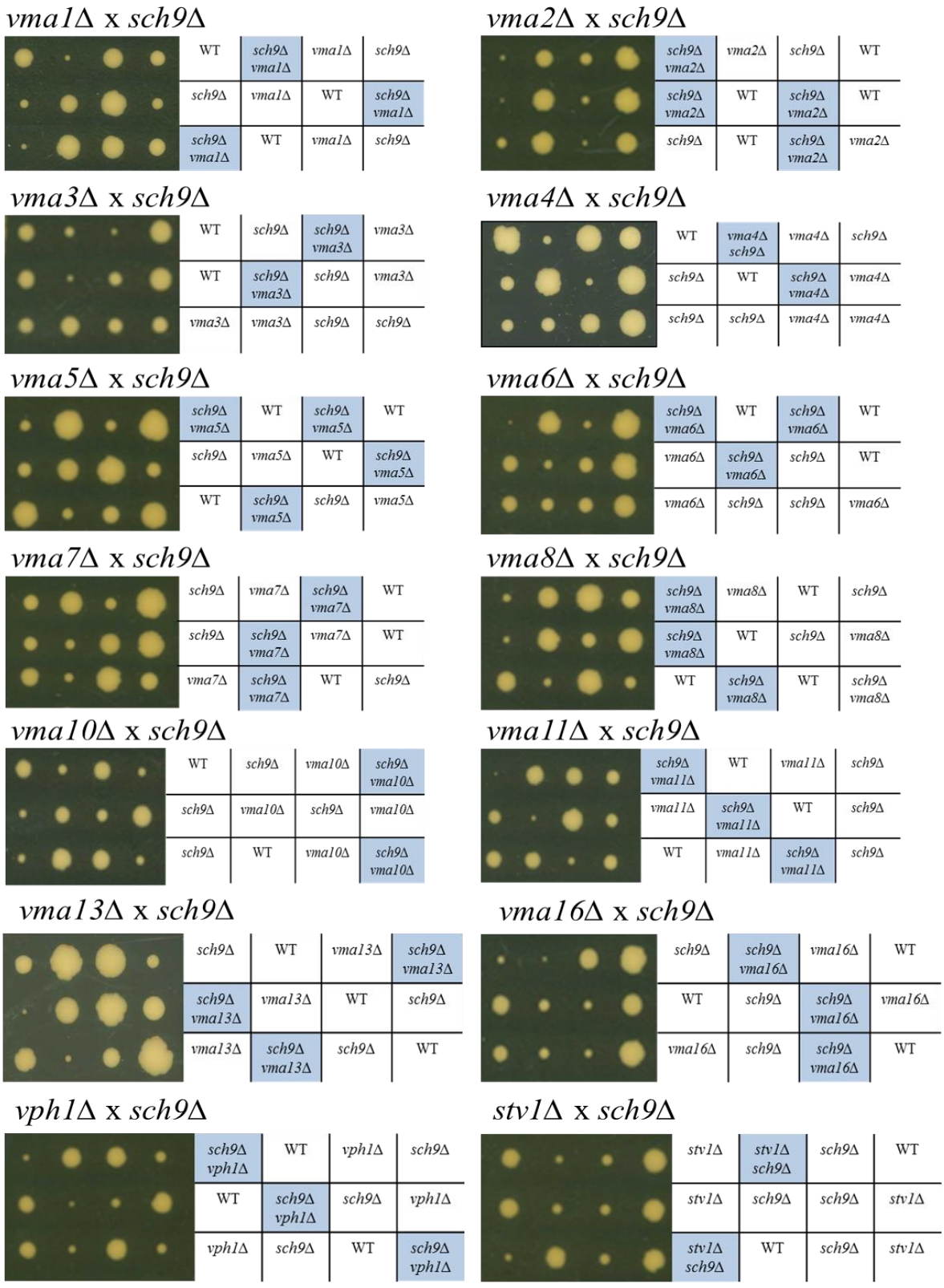

Figure 11: Tetrad analysis of diploids generated by crossing the sch9Δ strain with strains deleted for genes encoding subunits of the V-ATPase complex.

The observed difference in colony size between the double mutants, single mutants and WT, proves that next to *SCH9* (Jorgensen et al, 2002; Toda et al, 1988), *VMA*s also regulate colony size, and further that *SCH9* and *VMA* genetically interact to control colony size. *VPH1* and *STV1* are functionally redundant (Baars et al, 2007; Graham et al, 2000), and thereby *vph1*Δ *and stv1*Δ show no effect on colony size. Given that the difference in colony size is perceived for all the *vma*Δ*sch9*Δ double mutants, and that deletion of one of the *VMA* genes leads to a non-functional V-ATPase (Graham et al, 2000), the colony size phenotype is not regulated by a specific Vma subunit, rather by a non-functional V-ATPase.

These results clearly show that *VMA* genes mediate colony size, and *SCH9* and *VMA* genetically interact to regulate the colony size. As a next step, investigation of additional phenotypes being affected was carried out by assaying growth rate in liquid cultures, as well as spot assays on solid media, using different conditions.

14.2. Growth assay of *vma*Δ and *vma*Δ*sch9*Δ in liquid media

Sch9 is known to control the growth process of yeast cells (Jorgensen et al, 2004). By determining the growth curves of strains deleted for *SCH9* and/or *VMA* genes, a quantitative approach was used to study the genetic interaction between *SCH9* and *VMA* in liquid YPD medium. As *vma*Δ strains are known to grow better in medium buffered at pH 5 (Diakov & Kane, 2010), and to study whether the double deletions also grow better at pH 5, the same experiment was carried out in YPD, buffered at pH 5.

As expected, the *sch9*Δ strain display a longer lag phase, a slower growth during their exponential phase, and grow to a higher final OD in stationary phase than WT cells (Fig. 12). Compared to the *sch9*Δ strain, the *vma*Δ strains, except *vph1*Δ and *stv1*Δ strains*,* generally have an even longer lag phase, the same growth rate during exponential phase, and enter the stationary phase at a lower OD, even lower than the WT strain. The *vph1*Δ and *stv1*Δ single mutants display growth properties comparable to the WT strain. For the double deletion strains, growth of most of the *vma*Δ*sch9*Δ strains is impaired compared to both single deletion strains.

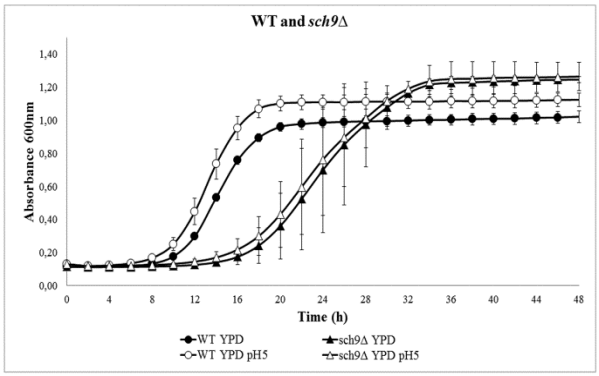
WT and sch9Δ
Absorbance 600nm
Time (h)
WT YPD
sch9Δ YPD
WT YPD pH5
sch9Δ YPD pH5

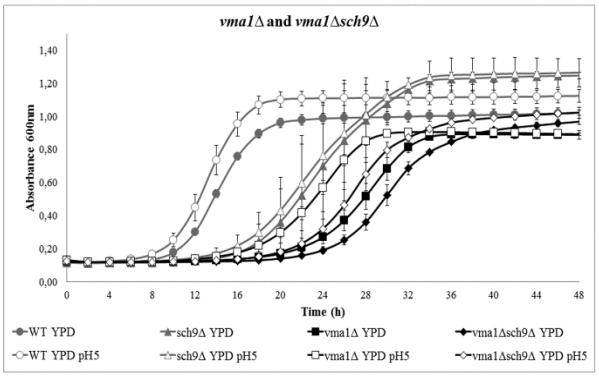
vma1Δ and vma1Δsch9Δ
Absorbance 600nm
Time (h)
WT YPD
sch9Δ YPD
vma1Δ YPD
vma1Δsch9Δ YPD
WT YPD pH5
sch9Δ YPD pH5
vma1Δ YPD pH5
vma1Δsch9Δ YPD pH5

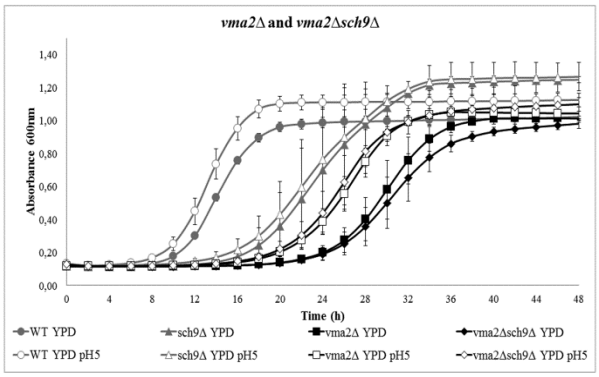
vma2Δ and vma2Δsch9Δ
Absorbance 600nm
Time (h)
WT YPD
sch9Δ YPD
vma2Δ YPD
vma2Δsch9Δ YPD
WT YPD pH5
sch9Δ YPD pH5
vma2Δ YPD pH5
vma2Δsch9Δ YPD pH5

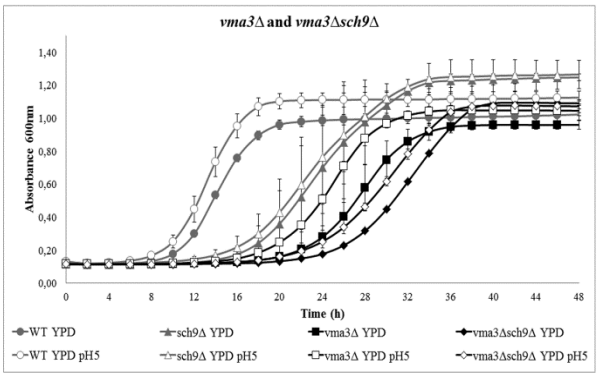
vma3Δ and vma3Δsch9Δ
Absorbance 600nm
Time (h)
WT YPD
sch9Δ YPD
vma3Δ YPD
vma3Δsch9Δ YPD
WT YPD pH5
sch9Δ YPD pH5
vma3Δ YPD pH5
vma3Δsch9Δ YPD pH5

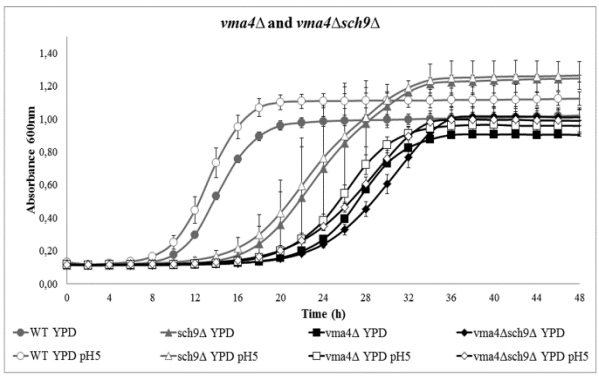
vma4Δ and vma4Δsch9Δ
Absorbance 600nm
Time (h)
WT YPD
sch9Δ YPD
vma4Δ YPD
vma4Δsch9Δ YPD
WT YPD pH5
sch9Δ YPD pH5
vma4Δ YPD pH5
vma4Δsch9Δ YPD pH5

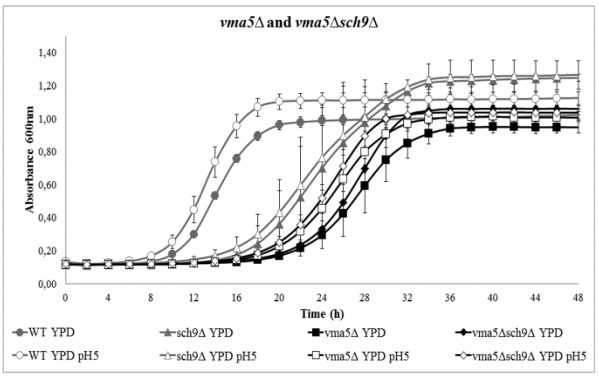
vma5Δ and vma5Δsch9Δ
Absorbance 600nm
Time (h)
WT YPD
sch9Δ YPD
vma5Δ YPD
vma5Δsch9Δ YPD
WT YPD pH5
sch9Δ YPD pH5
vma5Δ YPD pH5
vma5Δsch9Δ YPD pH5

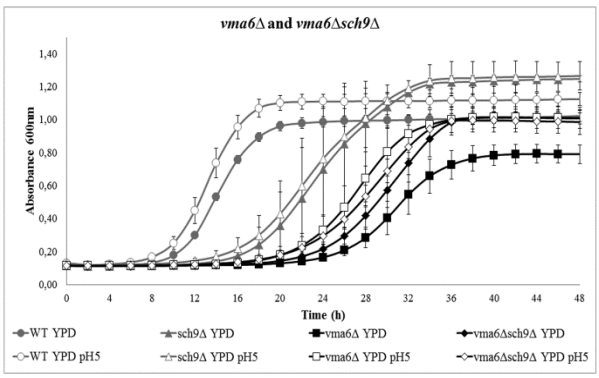
vma6Δ and vma6Δsch9Δ
Absorbance 600nm
Time (h)
WT YPD
sch9Δ YPD
vma6Δ YPD
vma6Δsch9Δ YPD
WT YPD pH5
sch9Δ YPD pH5
vma6Δ YPD pH5
vma6Δsch9Δ YPD pH5

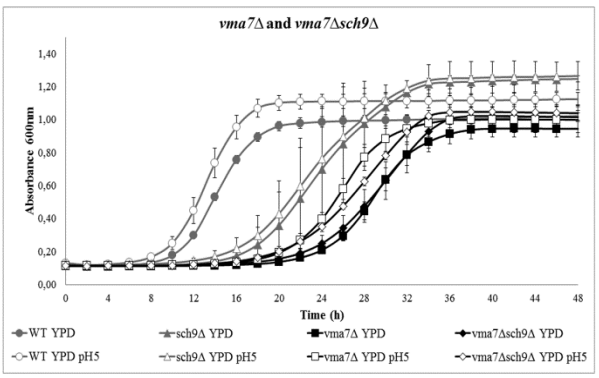
vma7Δ and vma7Δsch9Δ
Absorbance 600nm
Time (h)
WT YPD
sch9Δ YPD
vma7Δ YPD
vma7Δsch9Δ YPD
WT YPD pH5
sch9Δ YPD pH5
vma7Δ YPD pH5
vma7Δsch9Δ YPD pH5

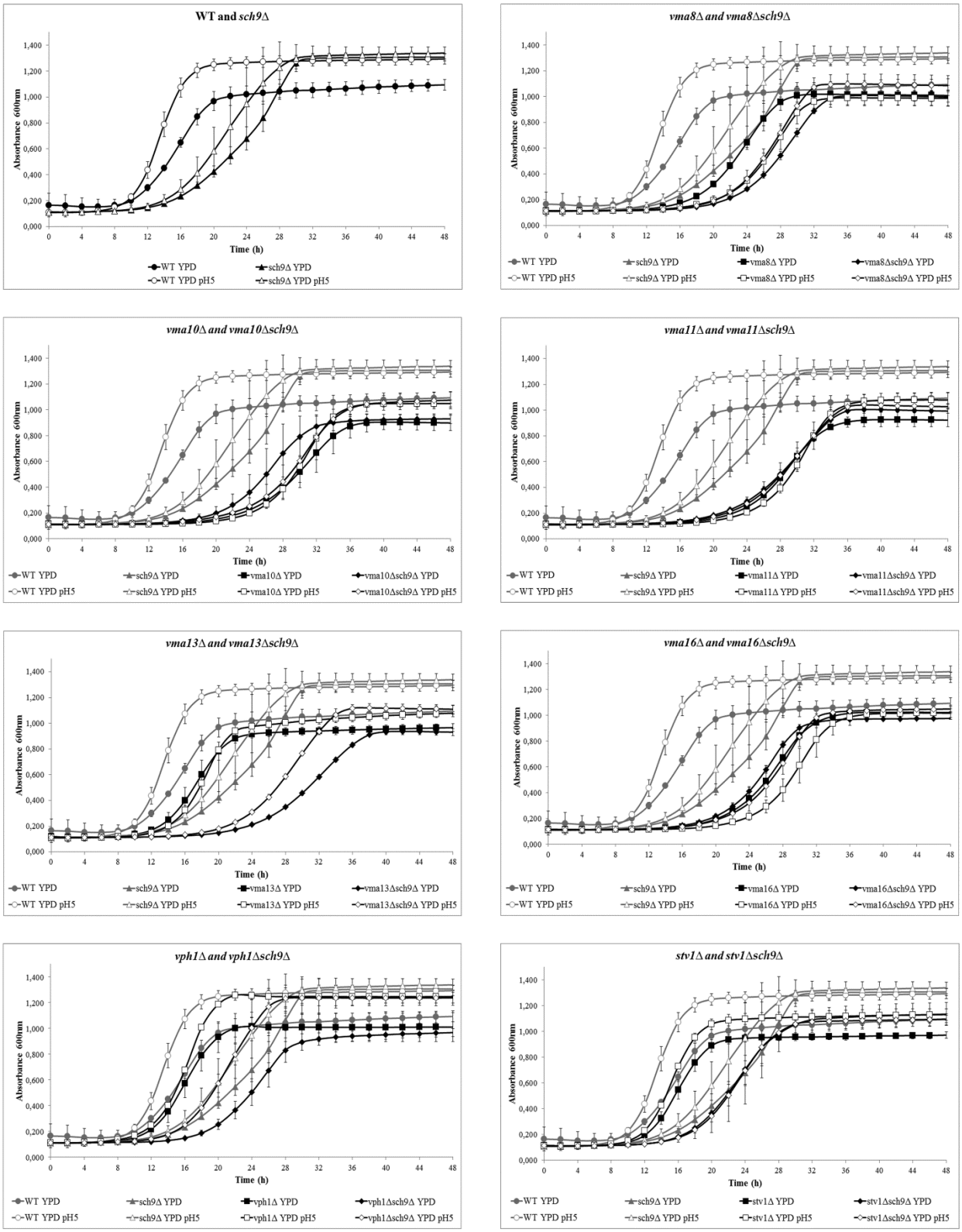

Figure 12: Growth curves of WT, sch9Δ, vmaΔ, and the vmaΔsch9Δ double deletion strains on standard YPD and YPD buffered to pH5. Results shown are the average of three independent cultures for each strain. Error bars indicate standard deviations.

These results indicate that, in addition to colony size, *SCH9* also genetically interacts with the V-ATPase coding genes to regulate growth properties in liquid cultures. Indeed, albeit some variation, double deletion strains widely grow slower than *vma*Δ and *sch9*Δ strains, which confirms the interaction between *SCH9* and *VMA* genes. As stated above, *VPH1* and *STV1* are functionally redundant, and have growth properties similar to the WT strain.

The growth curves additionally demonstrate that, next to the *vma*Δ strains, also the WT, *sch9*Δ and *vma*Δ*sch9*Δ strains grow better in YPD buffered at pH 5. At this lower pH (unbuffered YPD has an initial pH around 6.5), all the strains have a shorter lag phase, a faster growth during exponential phase and enter the stationary phase at a higher OD. The observed upregulation of growth in the WT, and generally in the *vma*Δ and *vma*Δ*sch9*Δ strains is higher than the growth upregulation observed in the *sch9*Δ strain.

As such, by growing the cells at pH 5, the growth defect of *vma*Δ and *vma*Δ*sch9*Δ strains is partially relieved but the *vma*Δ*sch9*Δ strains still have a larger growth defect than *vma*Δ strains, indicating that lowering the extracellular pH does not abolish the observed genetic interaction.

Similar to the tetrad analysis results, the growth curves suggest a general genetic interaction between *SCH9* and the V-ATPase complex genes that does not appear to be attributed to specific Vma subunits.

14.3. Phenotypic overlap of the *sch9Δ* and *vmaΔ* strains

Cells without a functional V-ATPase typically cannot grow on medium buffered to alkaline pH, cannot utilize non-fermentable C-sources, and have an increased sensitivity to Ca^{2+} and heavy metals compared to WT (Graham et al, 2000; Kane, 2006).

On the other hand, *sch9*Δ strains have been reported to display growth defects on non-fermentable carbon sources (Crauwels et al, 1997), and to be sensitive to hyperosmotic stress (Pascual-Ahuir & Proft, 2007b), as well as the addition of the anti-fungal rapamycin (Lamming & Sabatini, 2011; Wanke et al, 2008).

As such, both *sch9*Δ and *vmaΔ* cells share the growth defect on medium supplemented with non-fermentable carbon sources. To test additional phenotypic overlap, we assayed growth of the *sch9*Δ strain on media known to impair growth of *vmaΔ* cells, and vice versa, using spot assays with conditions summarized in table 2.

14.3.1. Growth of the sch9Δ strain is partially impaired at high pH

Nelson *et al*. elucidated that cells lacking V-ATPase activity show a pH-dependent conditional lethality (Kane, 2006; Nelson & Nelson, 1990), as *vma* mutant strains were able to grow at acidic pH (~5) but failed to grow at neutral pH (7) or higher.

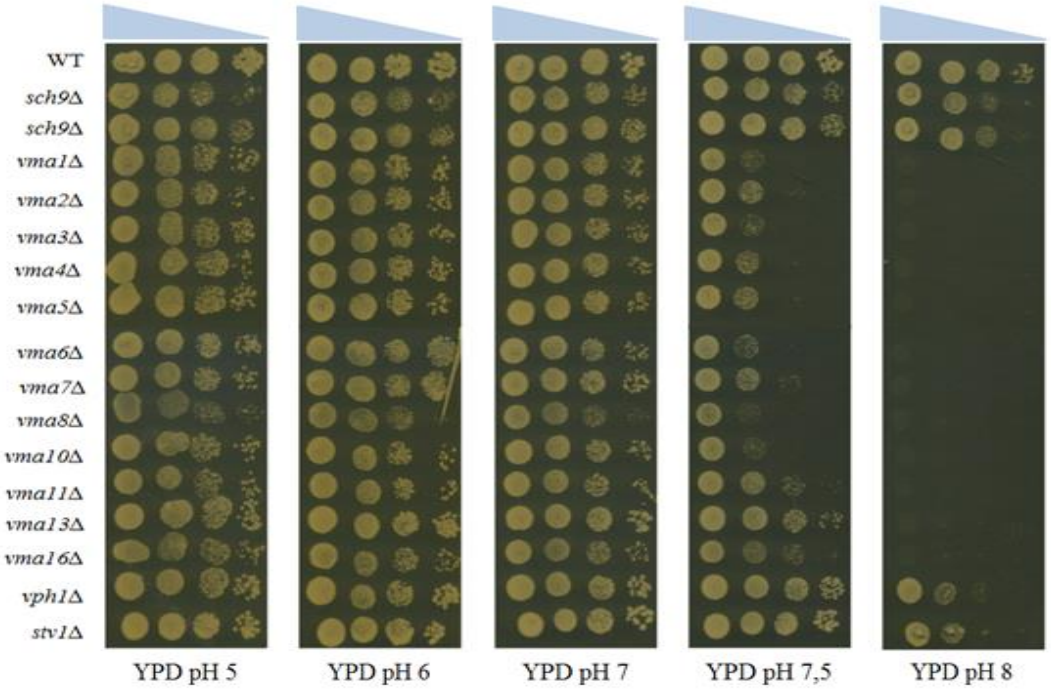

Figure 13: pH dependence for growth. The indicated strains were spotted on YPD medium buffered to different pH values.

The performed spot assay shows to some extent equivalent results. All strains grow well on YPD buffered at acidic pH (5 and 6), and in contrary with previous research, the *vma*Δ strains also grow on YPD buffered at neutral pH 7 (Fig. 13). When spotted on YPD buffered at pH 7,5, the *vma*Δ strains have a growth defect in comparison with the WT and *sch9*Δ strains, and at pH 8 they did not grow anymore. The *sch9*Δ strain, as well as the *vph1*Δ and *stv1*Δ strains, was able to grow up till pH 8 similar as the WT.

The *sch9*Δ strain thus exhibits very little growth sensitivity to buffered pH when compared to the *vma*Δ strains (Table 3).

14.3.2. Growth of the sch9Δ and vmaΔ strains is inhibited by specific non-fermentable carbon sources

In the literature, *sch9*Δ and *vmaΔ* cells, have been described to be unable to grow on medium supplemented with non-fermentable carbon sources (Crauwels et al, 1997; Foury, 1990). In this experiment, growth of these strains was examined on YP buffered with a variety of non-fermentable carbon sources. We chose to perform these assays in medium

which was buffered to pH5, optimal for growth of *vma⊿* strains, to exclude possible interferences of pH with observed growth defects.

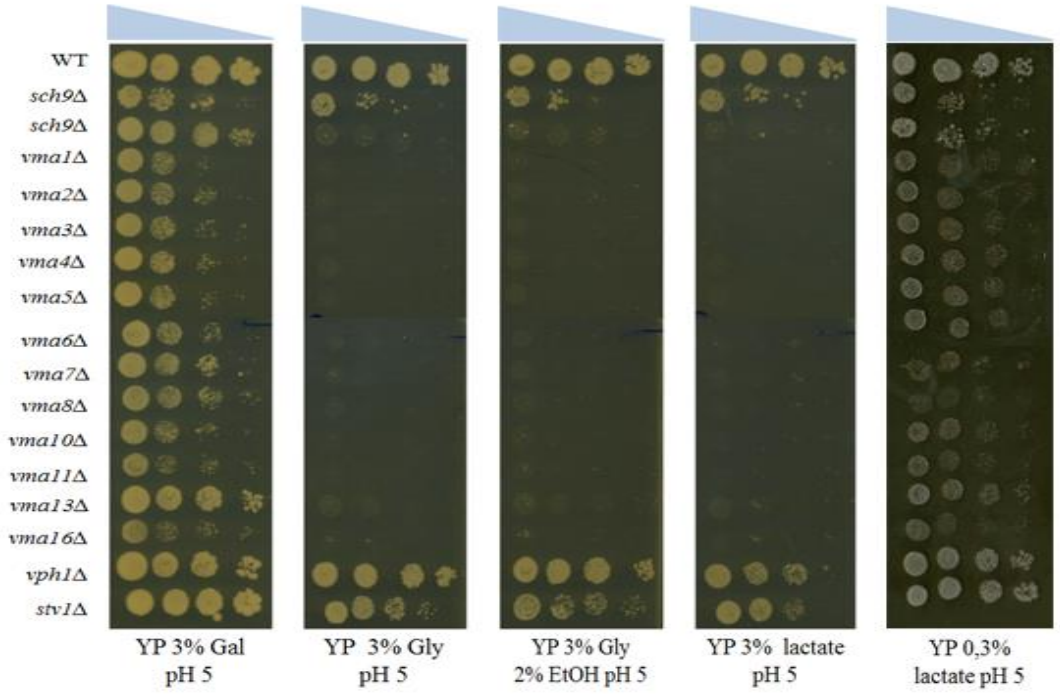

Figure 14: Carbon source dependence for growth. The indicated strains were spotted on YP medium buffered to pH 5 with different carbon sources, as described in the figure.

In general, the growth of the *vma⊿* strains is impaired on medium supplemented with 3% galactose, and completely absent on medium containing 3% glycerol, 3% glycerol/2% ethanol and 3% lactate (Fig. 14). A similar picture was seen for the *sch9⊿* strain, although we note that the first ***sch9***Δ culture on the spot assays grows on all tested conditions. As previous research demonstrated that the ***sch9***Δ strain is unable to grow on non-fermentable carbon sources, this strain most probably contains suppressor mutations. Interestingly, lowering the lactate concentration to 0.3% resulted in a partial relief of the growth defect of the *vma⊿* and *sch9⊿* strains. This effect has been annotated before to lower the amount of reactive oxygen species (ROS) formed during respiration of the non-fermentable carbon source (Milgrom et al, 2007). As a final note, the WT and functionally redundant *vph1*Δ *and* ***stv1***Δ strains grow on all tested non-fermentable carbon source conditions.

In conclusion, we can state that both the *SCH9* and the *VMA* genes are involved in pathways responsible for growth on non-fermentable carbon source, and that at least part of the growth defects observed may be due to oxidative stress generated by these strains when respiring these carbon sources (Table 3).

14.3.3. The sch9Δ strain shows a Ca^{2+}-dependent growth

Cells lacking V-ATPase activity aren't able to grow on media containing high Ca^{2+}-concentration (Kane, 2006). To investigate whether *SCH9* is also implicated in Ca^{2+}-homeostasis, spot assays were performed on YPD medium containing 60 and 150 mM $CaCl_2$. The *vma*Δ strains grow better at pH 5, therefore the influence of pH on growth at elevated Ca^{2+}-concentrations was studied by performing the spot assays also on YPD buffered at pH 5 and 7,5 supplemented with 60 and 150 mM $CaCl_2$.

In line with previous research, *vma*Δ strains, except *vph1*Δ and *stv1*Δ, didn't grow on YPD medium supplemented with 60 and 150 mM $CaCl_2$, regardless of medium pH. In contrast to the *vma*Δ strains, the *sch9*Δ, *vph1*Δ and *stv1*Δ strains grow on YPD containing 60 $CaCl_2$ (Fig. 15). However, further increasing the $CaCl_2$ concentration to 150mM has a clear inhibitory effect on the growth of the *sch9Δ*, compared to the WT strain, indicating that *sch9Δ* cells are sensitive to calcium, though to a lesser extent than *vmaΔ* cells. Interestingly, also the *vph1Δ* strain displayed a similar sensitivity to 150mM $CaCl_2$, while the *stv1Δ* strain did not. As such, the Vph1 and Stv1 proteins are not fully redundant in function. Finally, when spotted on YPD buffered at pH 7,5, supplemented with 60 mM $CaCl_2$, the *sch9Δ* as well as both the *vph1Δ* and *stv1Δ* strains display a comparable impairment of growth.

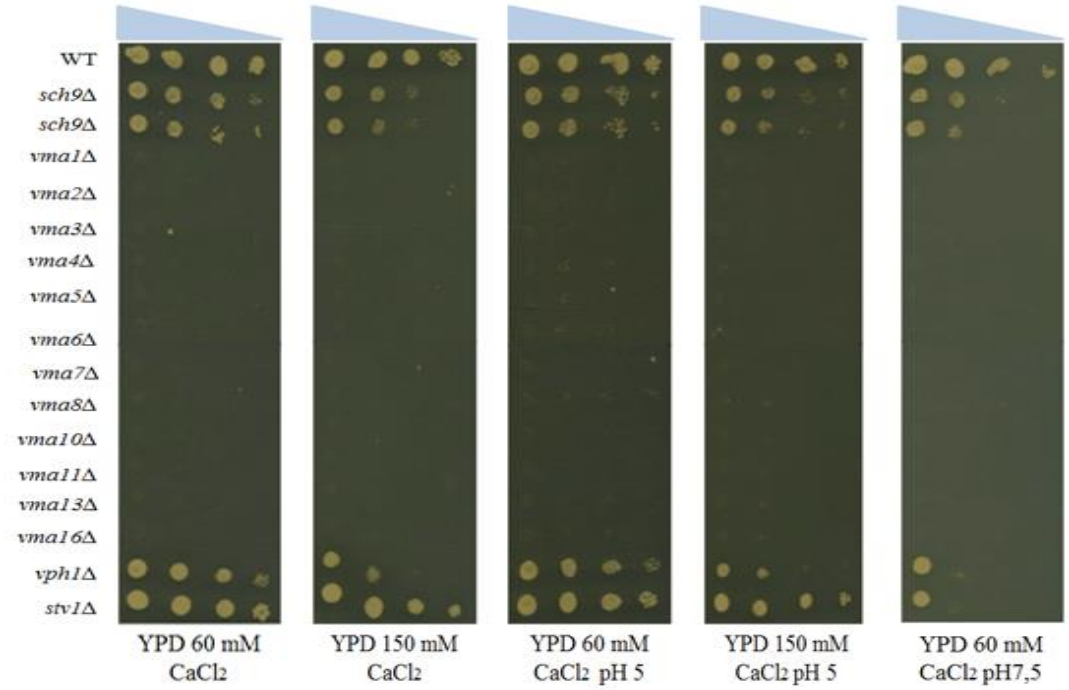

Figure 15: $CaCl_2$ dependence for growth. The indicated strains were spotted on YPD medium containing different CaCl2 concentrations and were buffered to different pH values.

We can conclude that loss of Sch9 leads to sensitivity to calcium, though less severe than when V-ATPase function is lost (Table 3). Furthermore, the Vph1 and Stv1 did not show complete redundancy in these tests, with Vph1 being more important in the resistance to high calcium levels, compared to Stv1.

14.3.4. Osmotic stress weakens growth of the sch9Δ strain and inhibits growth of the vmaΔ strains

Sch9 has been implicated in the transcriptional activation of osmostress inducible genes, and as such the *sch9*Δ strain was demonstrated to be sensitive to osmotic stress (Pascual-Ahuir & Proft, 2007a). With spot assays on YPD supplemented with 1 M NaCl or 1 M KCl, the sensitivity of the *vma*Δ strains to osmotic stress was investigated and compared to *sch9*Δ strains.

The spot assays show that the *sch9*Δ strain has a growth defect when grown on YPD medium containing either 1 M KCl or 1 M NaCl (Fig. 16). In both conditions, *vma*Δ strains, except *vph1*Δ and *stv1*Δ, display a similar growth defect. The WT and functionally redundant *vph1*Δ and *stv1*Δ strains grow equally well under these investigated conditions.

This assay thus proves that *SCH9* and the *VMA* genes are both involved in osmotic stress regulation (Table 3).

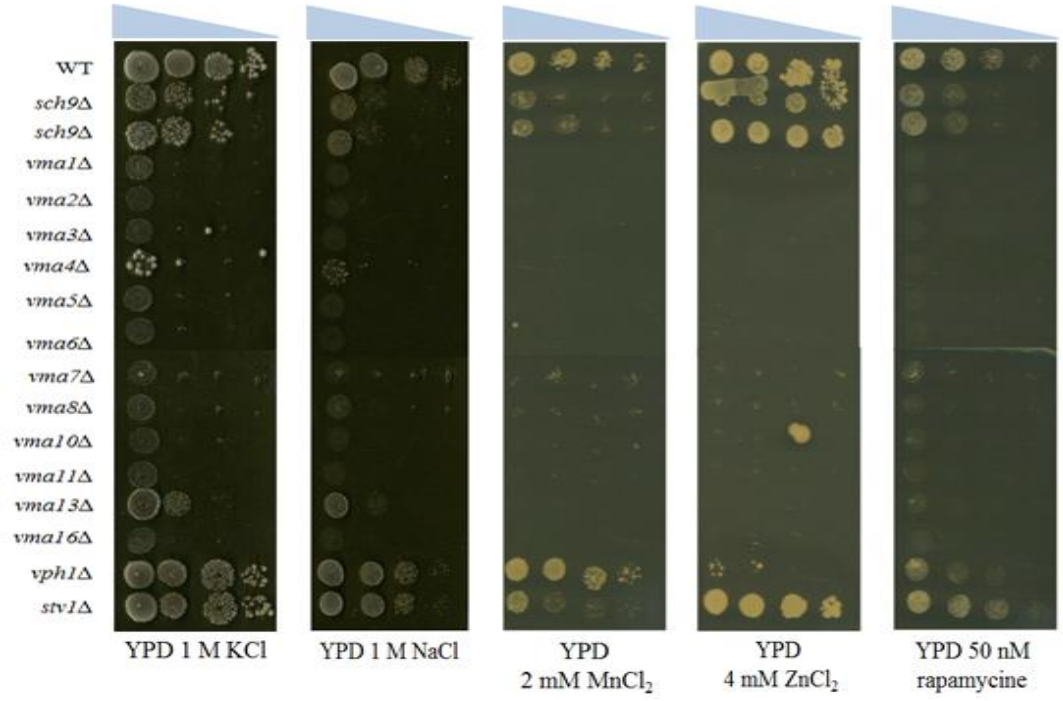

Figure 16: Osmotic stress, metal and anti-fungal dependence for growth. The indicated strains were spotted on YPD medium containing the indicated compounds.

14.3.5. Growth of the sch9Δ strain is metal-dependent

The involvement of the V-ATPase complex in metal ion homeostasis has been established (Eide et al, 2005). Loss of V-ATPase activity impairs the growth of yeast cells in environments with increased metal ions. To study whether *SCH9* is also involved in regulation of metal ion homeostasis, spot assays were performed on YPD supplemented with 2 mM $MnCl_2$ or 4 mM $ZnCl_2$.

As expected, no growth of the *vma*Δ strains, except *vph1*Δ and *stv1*Δ, under these conditions is observed (Fig. 16). The *sch9*Δ strain, however, has a severe growth defect on YPD medium supplemented with 2 mM $MnCl_2$, while growth on YPD plates supplemented with 4 mM $ZnCl_2$ was hardly affected. A similar pattern was seen for the *stv1Δ* strain, while the *vph1Δ* strain showed the opposite, i.e. normal growth in the presence of $MnCl_2$ and sensitivity to $ZnCl_2$. The latter again indicates that Vph1 and Stv1 cannot completely take over each other's function under all conditions. Tolerance to zinc is assumed to be mediated mainly by the vacuole (Li & Kane, 2009), while manganese tolerance may require additional, non-vacuolar, mechanisms, such as the Golgi-resident Ca^{2+}/Mn^{2+} ATPase Pmr1 (Devasahayam et al, 2007; Devasahayam et al, 2006). The latter is supported by the specific sensitivity of *stv1Δ* cells to $MnCl_2$, as Stv1 is reported to be mainly located in non-vacuolar compartments, such as the Golgi (Kane, 2006).

*14.3.6. The vma*Δ *strains are hypersensitive to rapamycin*

The Sch9 protein is phosphorylated by the TORC1 complex. When cells are treated with rapamycin, the function of TORC1 complex is inhibited and thereby cannot phosphorylate the Sch9 protein. The degree of Sch9 phosphorylation in the cells decreases, which inhibits growth of cells (Urban et al, 2007). The growth of *vma*Δ strains on YPD medium supplemented with 50 nM rapamycin was investigated to verify whether the V-ATPase is also a potential downstream effector of rapamycin.

The spot assay demonstrates that the *vma*Δ strains are hypersensitive to rapamycin addition. Indeed, cells lacking *SCH9* also display a clear growth defect, though less severe than *vma*Δ cells (Fig. 16). Rapamycin-induced growth impairment of the *vph1*Δ *and stv1*Δ strains is less obvious, indicating partial redundancy under this condition.

These results indicate that the V-ATPase somehow interacts with TORC1 signaling. This finding is further supported by the report that manganese may act via inhibiting TORC1 signaling (Devasahayam et al, 2007), and our finding that the V-ATPase is required for tolerance to both rapamycin and manganese.

14.3.7. Conclusion of the spot assay results

Table 3: Overview scheme of the spot assay results. (+) indicates the tested strains grow as good as the WT strain, (-) indicates the tested strain is more sensitive to the medium than the WT strain and (- -) indicates the strains were very sensitive in comparison to the WT strain/ no growth was observed. The asterisk (*) indicates that although cells still display a growth defect compared to WT cells, reducing the amount of lactate partially negates the growth defect of mutant cells on this carbon source.

Phenotype	*sch9*Δ	*vma*Δ strains (except *vph1*Δ *and stv1*Δ)
YPD pH 5	+	+
YPD pH 6	+	+
YPD pH 7	+	+
YPD pH 7,5	+	-
YPD pH 8	+	- -
YP 3% Gal pH 5	-	-
YP 3% Gly pH 5	- -	- -
YP 3% Gly 2% EtOH pH 5	- -	- -
YP 3% lactate pH 5	- -	- -
YP 0,3% lactate pH 5	- *	- *
YPD 60 mM $CaCl_2$	-	- -
YPD 150 mM $CaCl_2$	-	- -
YPD 60 mM $CaCl_2$ pH 5	-	- -
YPD 150 mM $CaCl_2$ pH 5	-	- -
YPD 60 mM $CaCl_2$ pH 7,5	-	- -
YPD 1 M KCl	-	- -
YPD 1 M NaCl	-	- -
YPD 2 mM $MnCl_2$	-	- -
YPD 4 mM $ZnCl_2$	+	- -
50 nM rapamycin	-	- -

The results of these spot assays indicated new phenotypic overlaps between *sch9*Δ and *vma⊿* cells. Next to the known phenotypic overlap of these strains, i.e. the inability to grow on non-fermentable carbon sources, *sch9*Δ and *vma⊿* strains both display sensitivity to Ca^{2+}, osmotic stress, Mn^{2+} and rapamycin. Based on the observed phenotypic overlaps and the knowledge that *SCH9* and *VMA*s interact, it is reasonable to suggest that the Sch9 – V-ATPase interaction could be implicated in the regulation of one or some of these phenotypes. Analysis of the pathways via which the Sch9 and Vma proteins influence these phenotypes and subsequent investigation of pathway overlap can help clarify at which step in the pathway these proteins exert their effect. In general, it seems that phenotypes which are thought to be mediated largely by the V-ATPase mediated acidification of the vacuole, such as growth at high pH and zinc tolerance, are not shared with the *sch9*Δ strain. For certain other phenotypes of *vma*Δ strains, no obvious link is established with vacuolar acidification (these are sometimes annotated as “moonlighting” functions of the V-ATPase). These

include its inability of growth on non-fermentable carbon sources and higher internal oxidative stress (Kane, 2007). Thus, Sch9 may be involved in the regulation of such moonlighting functions of the V-ATPase, which may be separate from the enzyme's proton pump function.

15. Screening for physical interaction between Sch9 and Vma proteins: Sch9 interacts with Vma6.

After screening for genetic interaction between the *VMA* genes and *SCH9*, we investigated whether Sch9 physically interacts with the Vma proteins using the GAL4 yeast two-hybrid (Y2H) assay. The DNA sequences coding for the Sch9 and Vma proteins were inserted into the pGBAE- and the pATCBE- expression vectors and transformed respectively into PJ69-4a cells and PJ69-4α cells. Next, two sets of screening were performed: The first screening assay was performed with the PJ69-4a cells containing the pGBAE-*SCH9* vector (Sch9a) crossed with PJ69-4α cells transformed with pATCBE-*VMA* (Vma#α). In the second screening, the Y2H vectors were switched for Sch9 and Vma constructs, so that the PJ69-4a strain containing the pGBAE-*VMA* vector (Vma#a) crossed with PJ69-4α cells transformed with pATCBE-*SCH9* (Sch9α). We generated two positive and two negative control strains for this assay.

As a first negative control, haploid cells containing expression vectors with a *GFP* coding sequence as insert were crossed. The latter vectors are used as 'empty vector controls', as the Gfp protein is generally assumed not to lead to specific interactions with yeast proteins or with itself. As this combination should never grow on medium without histidine or adenine, it serves as a general negative control of the experiment. The second negative control was designed to exclude auto-activation by Sch9 constructs. To this end, diploid cells were generated by crossing haploid cells containing the Sch9 constructs with haploid cells from opposite mating type, transformed with complementing Y2H vectors containing the GFP insert. We did not combine the empty vector with all Y2H-Vma constructs in our first screening round, as this would greatly increase the amount of combinations to test in our screen. Instead, Y2H-Vma that are retrieved in our first screening round to interact with Sch9, will be retested in a second phase with appropriate empty vector controls to asses auto-activation of these Y2H-Vma constructs.

As a first positive control for the assay, the genes coding for two proteins that interact, *STE4* and *GPA1*, were inserted into the expression vectors and the obtained haploid cells were crossed. Since Sch9 and Pkh1 are known to interact, as a second positive control, the *PKH1* coding sequence was inserted into the pATCBE- and pGBAE- vectors and the transformed

cells were crossed respectively with the pGBAE-*SCH9* and pATCBE-*SCH9* vector containing cells.

Given that the host strains contain *ADE2* and *HIS3* as reporter genes, the interaction between these proteins was assayed by spotting the strains on SD-L-W-A and SD-L-W-H. To reduce auto-activation, the cells were also spotted on SD-L-W-H medium supplemented with 3-aminotriazole, which is a competitive inhibitor of the gene product of *HIS3* (imidazoleglycerol-phosphate dehydratase).

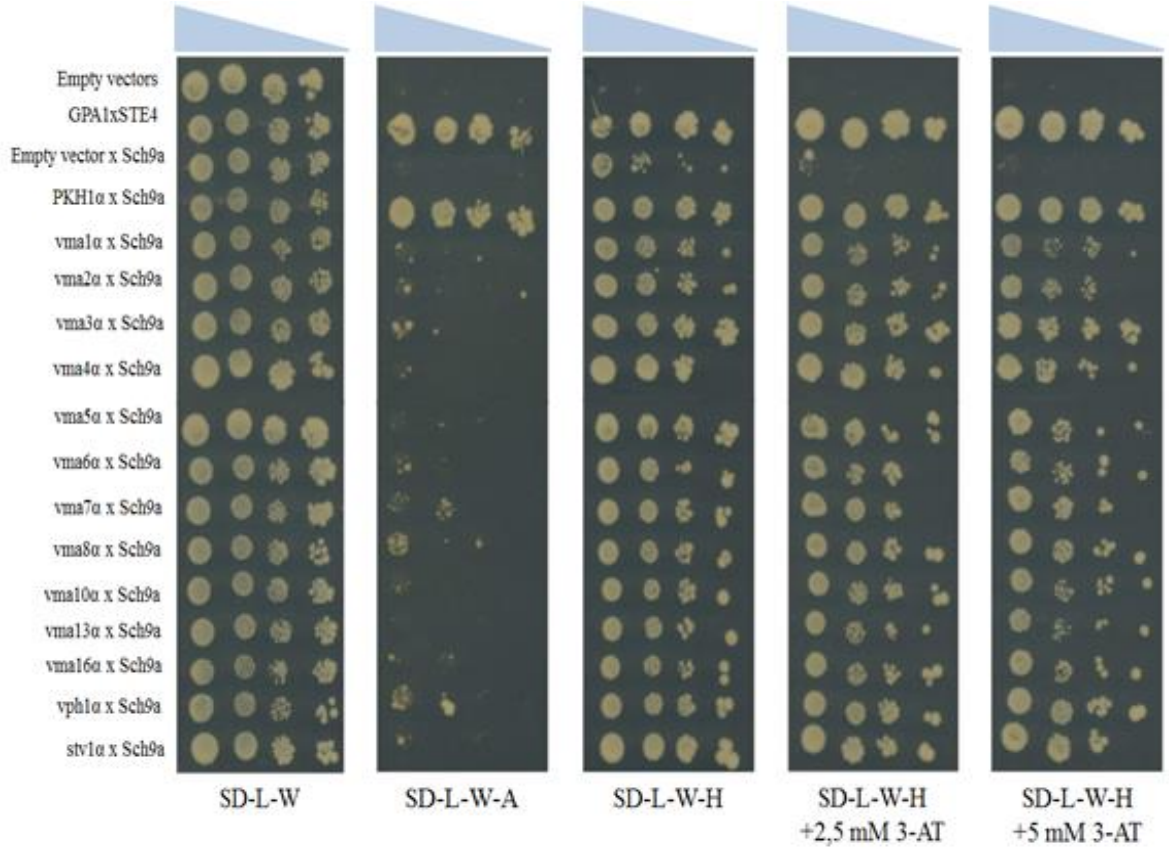

Figure 17: Y2H assay of the diploids generated by crossing the PJ69-4a cells containing the pGBAE-SCH9 vector (Sch9a) with PJ69-4α cells transformed with pATCBE-VMA (Vma#α). Scans were taken after growing the cells for 9 days at 30 °C.

The spot assay on SD-L-W medium shows that the crossing of PJ69-4a cells containing the pGBAE-*SCH9* vector (Sch9a) with PJ69-4α cells transformed with pATCBE-*VMA* (Vma#α) successfully generated diploids containing the pGBAE-*SCH9* and pATCBE-*VMA* (Fig. 17). We observe that pGBAE-*SCH9* leads to auto-activation on SD-L-W-H. Transcription of this vector causes the formation of a DNA binding domain-Sch9 complex, suggesting that Sch9 acts as the transcription activator. This is in line with literature, where the role of Sch9 in promoting transcription of osmostress-responsive genes by acting as a chromatin-associated transcriptional activator (Pascual-Ahuir & Proft, 2007b) has been shown. Addition of 3-AT in

the medium is able to reduce the background growth caused by auto-activation of the pGBAE-*SCH9* construct. As expected, the positive controls grow well on SD-L-W-A, SD-L-W-H and SD-L-W-H supplemented with 3-AT. This shows that the strong interaction between Ste4 and Gpa1 and between Sch9 and Pkh1 is able to stimulate transcription of *ADE2* and *HIS3*. When spotted on SD-L-W-A medium, none of the Sch9a x Vma#α strains is able to grow, but when spotted on SD-L-W-H medium all the Sch9a x Vma#α strains grow very well, even on SD-L-W-H medium supplemented with 3-AT. These results were compared to the Vma#a x Sch9α strains Y2H screening.

The growth observed on SD-L-W indicates that the generation of diploids containing the pGBAE-*VMA* vector (Vma#a) and pATCBE-*SCH9* (Sch9α) was successful (Fig. 18). In contrast to the pGBAE-*SCH9* construct, the pATCBE-*SCH9* vector does not auto-activate, given that we don't perceive growth of this strain on any of the interaction selection plates. The positive controls, as expected, grow well on the different selection medium. In this screening assay only the Sch9α x Vma6a strain is able to grow on SD-L-W-H, though this growth is impaired by the addition of 3-AT. Since the Vma6 protein also doesn't grow on SD-L-W-A, this indicates that the interaction between Sch9 and Vma6 may be weak, compared to observed interaction between Sch9 and Pkh1.

Vma6 is the only protein that interacts with Sch9 in both screening. Before retesting this observed interaction, we generated controls for testing possible auto-activation of the Vma constructs. This was performed by crossing haploid cells containing the Vma6 constructs with haploid cells from opposite mating type, transformed with complementing Y2H vectors containing the GFP insert. Figure 19 shows that none of the Vma6 constructs auto-activates and confirms the interaction between Sch9 and Vma6.

As next, we set out to verify the interaction between Vma6 and Sch9 with Co-immunoprecipitation assay.

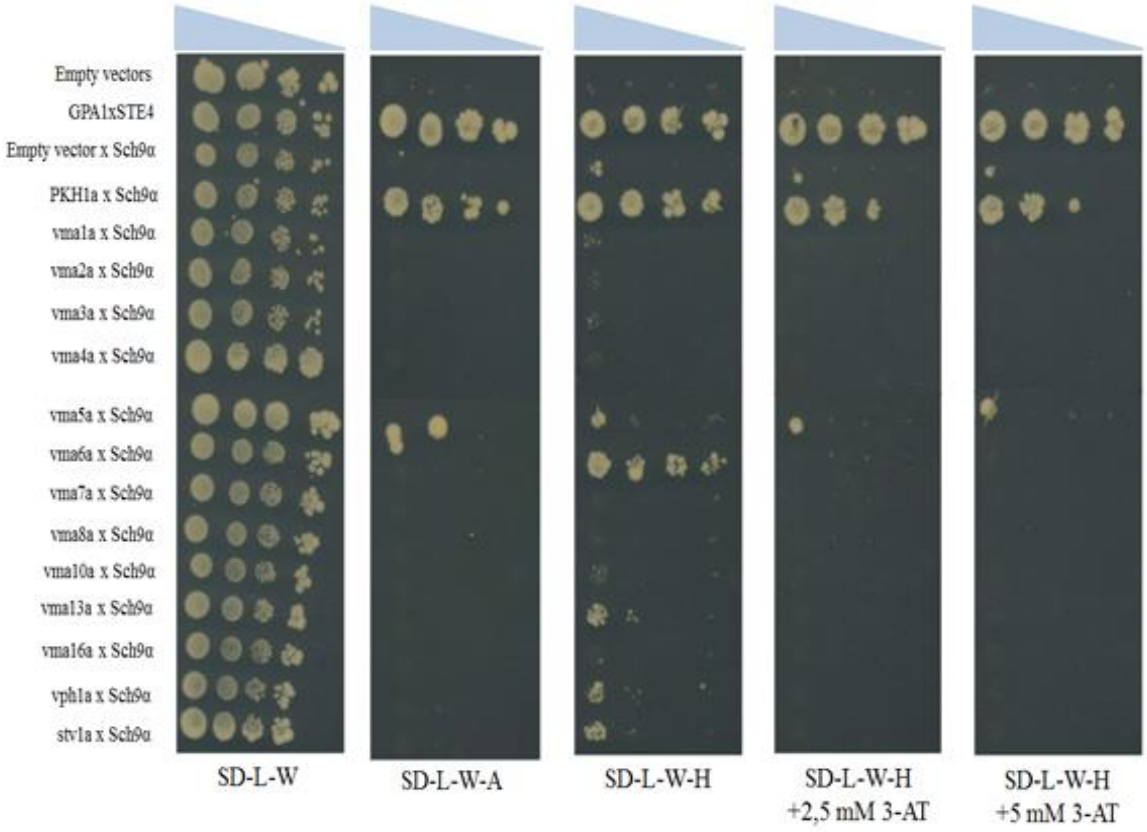

Figure 18: Y2H assay of the diploids generated by crossing the PJ69-4a strain containing the pGBAE-VMA vector (Vma#a) crossed with PJ69-4α cells transformed with pATCBE-SCH9 (Sch9α). Scans were taken after growing the cells for 9 days at 30 °C.

.

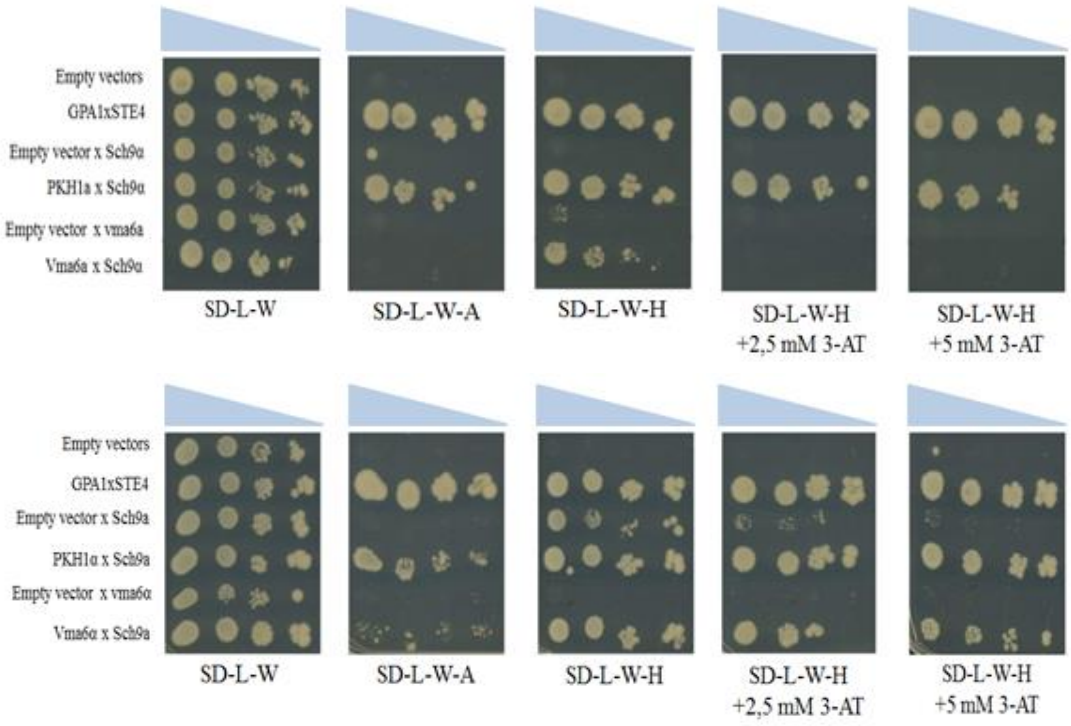

Figure 19:Y2H assay for the confirmation of interaction between Sch9 and Vma6. The diploid strains were generated the same way as explained above.

16. Confirmation of the interaction between Vma6 and Sch9

The Y2H screening indicated that Vma6 and Sch9 interact. To verify these results, we performed co-immunoprecipitation (Co-IP). The *sch9*Δ strain with chromosomal Myc-tagged *VMA6* was transformed with a plasmid encoding N-terminal 6HA-tagged Sch9 (HA-Sch9). To generate controls, the HA-Sch9 plasmid was transformed into the *sch9*Δ strain (with native, non-tagged *VMA6*), and the empty vector into the *sch9*Δ Vma6-Myc cells. Due to contamination of the precultures of the controls, we were only able to carry out the Co-IP with the protein extracts of the *sch9*Δ Vma6-Myc strain transformed with HA-Sch9 plasmid.

As depicted in Figure 20, if Sch9 and Vma6 interact within the yeast cell, we expect that both proteins will be extracted by immunopurification of either one of the interacting partners. As such, we should be able to detect HA-Sch9 after purifying Vma6-Myc from the cellular protein extract. In addition, the Vma6-Myc should be detected after immunoprecipitation of HA-Sch9. We see in Figure 21 that this was indeed the case. Therefore, as we proved that Sch9 interacts with Vma6 in both the co-immunoprecipitation as well as the Y2H experiment (see previous section), we can conclude that Sch9 and Vma6 will indeed physically interact *in vivo* in yeast.

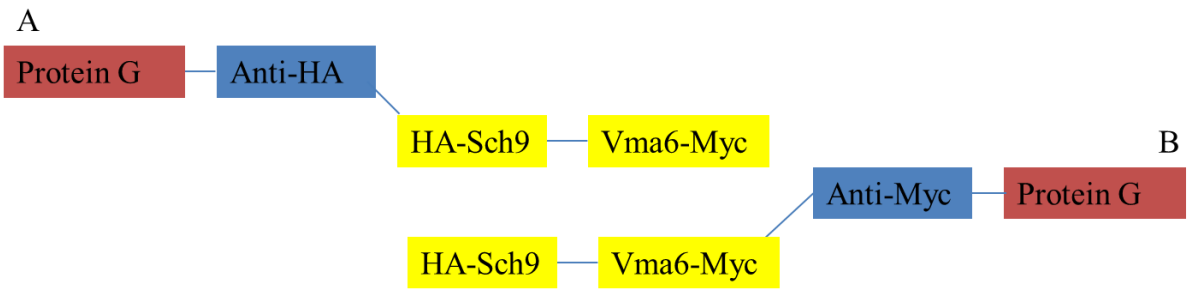

Figure 20: Schematic representation of the performed pull down experiments. If Sch9 and Vma6 interact in the yeast cell, we expect that we can isolate this protein complex by precipitation with either anti-HA or anti-Myc antibodies. A=pull down performed with Anti-HA and B=performed with Anti-Myc. Protein G beads are the magnetic beads used for isolation of protein complexes. The beads are coated with specific antibodies used in the pull-down experiments.

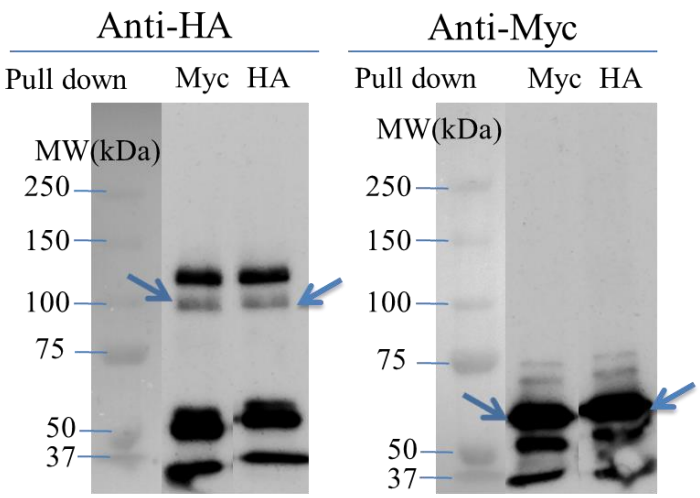

Figure 21: Co-IP with protein extracts of the sch9Δ Vma6-Myc strain transformed with HA-Sch9 protein. Immunoprecipitation ("pull down") was carried out with protein G beads, coated with either the anti-Myc antibody ("Myc", to pull down Vma6-9Myc protein) or the anti-HA antibody ("HA", to pull down the 6HA-Sch9 protein). After immunoprecipitation, protein extracts were boiled, separated from the protein G beads, and were run on a SDS-PAGE. Detection was carried out with anti-HA antibody (left) to detect the presence of 6HA-Sch9 protein (+/- 100 kDa) or with the anti-Myc antibody (right) to detect the presence of the Vma6-9Myc protein (+/- 50 kDa), indicated with arrows. As 6HA-Sch9 is detected after immunoprecipitation of Vma6-9Myc, and the Vma6-9Myc protein is detected after immunoprecipitation of 6HA-Sch9, this indicates that Sch9 and Vma6 interact in vivo.

To study the functional consequence of this interaction, we examined the influence of Sch9 on V-ATPase activity, and investigated whether the Sch9 protein kinase might be required for phosphorylation of certain Vma subunits, such as Vma6.

17. The vacuolar morphology is independent of the activity of the Sch9 protein

To study the effect of Sch9 on vacuolar morphology and function, two different approaches were used to visualize vacuoles in yeast cells. The first approach makes use of the lipophilic, red fluorescent dye FM4-64. This dye inserts into the plasma membrane, after which it is taken up by the cell via the process of endocytosis, and via endosomes the dye is finally transported to the vacuolar membrane. As such, this dye is often used to stain cellular vacuoles. However, this staining method depends on endocytosis, a process which itself relies on proper V-ATPase activity for proper acidification of endosomic organelles. In a second approach, we made use of a GFP-tagged Vph1 protein. The Vph1 protein is a subunit of the V_0 subcomplex of the V-ATPase. As mentioned in the literature review, Vph1 is synthesized in the cytosol and then translocated to the membrane of the endoplasmic reticulum (ER) where it assembles with the other V_0 subunits (Graham et al, 2000). Thereafter, the Vma6 protein binds to the assembled V_0 subunits and stimulates the transport of the V_0 subcomplex into the vacuolar membrane. Thus, both approaches depend on different cellular processes to stain the vacuolar membrane. For our analysis, the WT, *sch9*Δ, *vma2*Δ*, vma3*Δ*, vma5*Δ and *vma6*Δ strains containing the Vph1-GFP encoding plasmid were harvested during the exponential phase and stained with FM4-64.

Figure 22 shows that the vacuolar staining of the WT and the *sch9*Δ strains is different from that of the *vma*Δ strains. Whereas we observe a clear staining of the vacuolar membrane by FM4-64 in the WT and the *sch9*Δ cells, this staining shows that in the *vma*Δ strains small inclusions around the vacuoles are formed. Next to the inclusions, a smear of low FM4-64 signal is perceived throughout the cytosol in the *vma*Δ strains. Given that the vacuolar staining of the *sch9*Δ cells is the same as that of the WT cells, and that the FM4-64 staining depends on V-ATPase activity, we can assume the Sch9 protein is not required for proper functioning of the V-ATPase under our condition. FM4-64 labeling of the *vma*Δ strains confirms that deletion of one of the *VMA* genes disrupts proper staining of the vacuolar membrane by this dye (Graham et al, 2000).

For our second approach, we observe a GFP signal at the vacuolar membrane in the WT, *sch9*Δ, *vma2*Δ and *vma5*Δ strains, but in the *vma6*Δ and *vma3*Δ strains no clear GFP fluorescence is visible at this location. The Vma2 and Vma5 proteins are subunits of the V_1 subcomplex, and the Vma3 and Vma6 proteins are V_0 subunits. Previous research showed that when one of the V_0 subunits is deleted, the assembly and vacuolar localization of V_0 subcomplex will be disrupted (Tomashek et al, 1997). Our results are in line

with this theory. In the *vma2*Δ and *vma5*Δ cells, all the V_0 subunits are available in the cell and they assemble and translocate into the vacuolar membrane. The *vma6*Δ and *vma3*Δ strains cannot synthesize a functional V_0 subcomplex due to the lack of one of the V_0 subunits. In the *vma6*Δ strain, a smear of Vph1-GFP signal is perceived throughout the cell whereas in the *vma3*Δ strain no GFP signal is observed. We assume that in the *vma6*Δ strain the present V_0 subunits still assemble, but because of the absence of the Vma6 protein, the formed complex is not translocated into the vacuolar membrane. In the *vma3*Δ cells the present V_0 subunits do not assemble.

Overlay of the GFP and FM4-64 fluorescence signal show that the two signals overlap in the WT and the *sch9*Δ strains, but do not completely overlap in the *vma*Δ strains. This is because the WT and *sch9*Δ cells have a functional V-ATPase, in contrast to the *vma*Δ strains. In conclusion, we demonstrated that lack of the Sch9 protein does not impact on vacuolar morphology and V-ATPase function under our experimental conditions. Next, we set out to investigate whether the V-ATPase activity regulates the localization of Sch9.

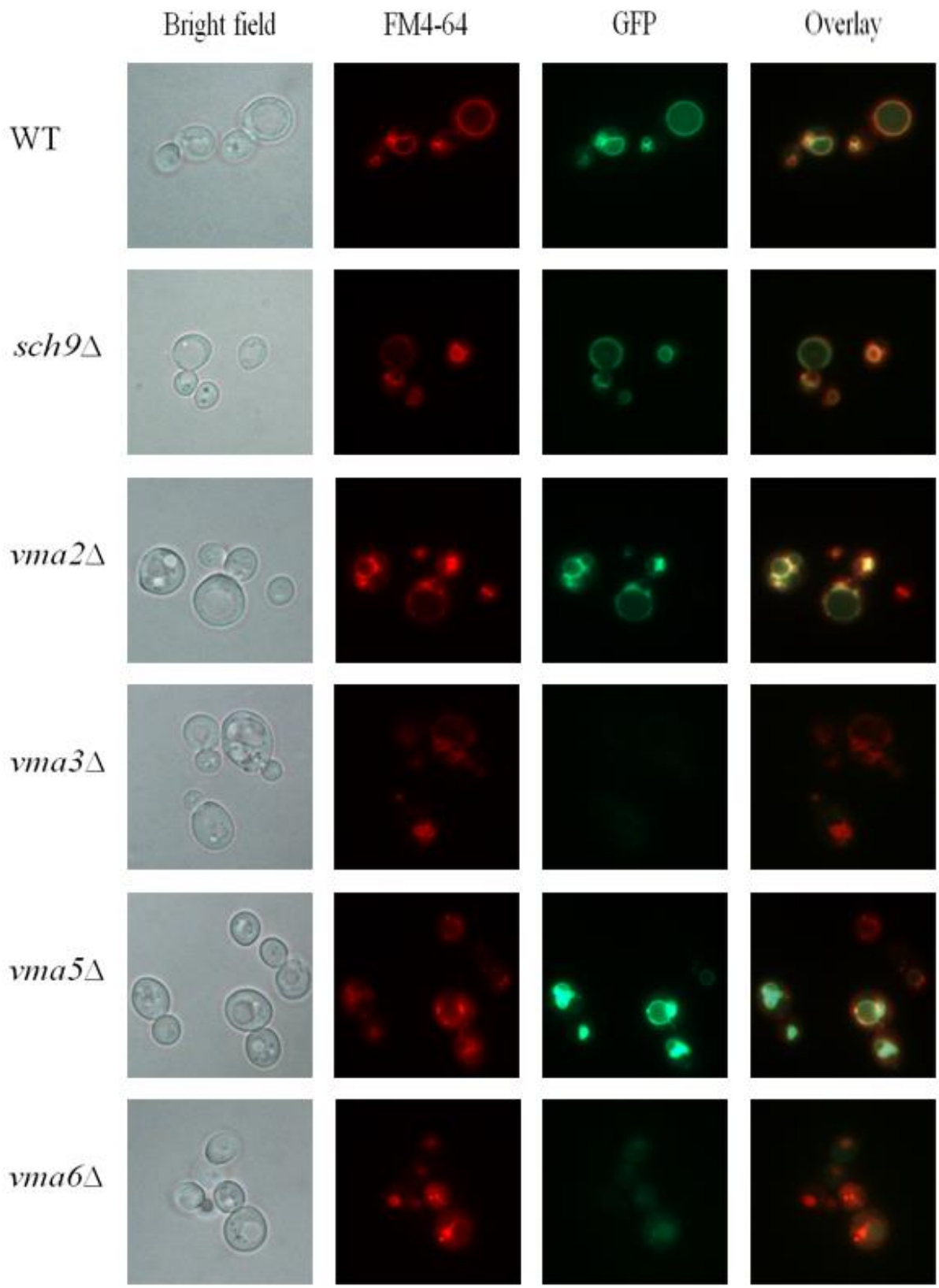

Figure 22: FM4-64 labeling of the strains transformed with the Vph1-GFP plasmid. Proper stainging of the vacuolar membrane depends on V-ATPase activity, while proper translocation of Vph1-GFP to the vacuolar membrane depends on the presence of all V_0 subunits, though not on the presence of V_1 subunits.

18. V-ATPase activity do not mediate Sch9 localization

The Sch9 protein is present throughout the cytosol and is enriched at the vacuole (Jorgensen et al, 2004). To investigate whether V-ATPase activity is involved in the regulation of the localization of Sch9, cultures of the WT, *sch9*Δ, *vma2*Δ, *vma3*Δ, *vma5*Δ and *vma6*Δ strains transformed with the GFP-Sch9 plasmid were grown to the exponential phase and stained with FM4-64. The localization of Sch9 was examined with the fluorescence microscope.

As explained above, the pictures of the FM4-64 staining indicate that the V-ATPase function/vacuolar morphology of *sch9*Δ cells is the same as that of WT cells, while being different from that of the *vma*Δ strains.

The perceived GFP-Sch9 signal is similar in all the tested strains (Fig. 23). We observe a GFP signal throughout the cytosol and a stronger signal at the vacuolar membrane. Superposition of the GFP and FM4-64 fluorescence signal in the WT and *sch9Δ* strains show that overlap of the two signals at the vacuole. These results validate Sch9 is spread throughout the cell, but enriched at the vacuolar membrane. In the different *vma* strains, the loss of V-ATPase activity negates proper staining of the vacuolar membrane by FM4-64. However, the vacuolar structures are clearly seen in the bright field pictures, and indicate that loss of V-ATPase activity has no influence on Sch9 localization.

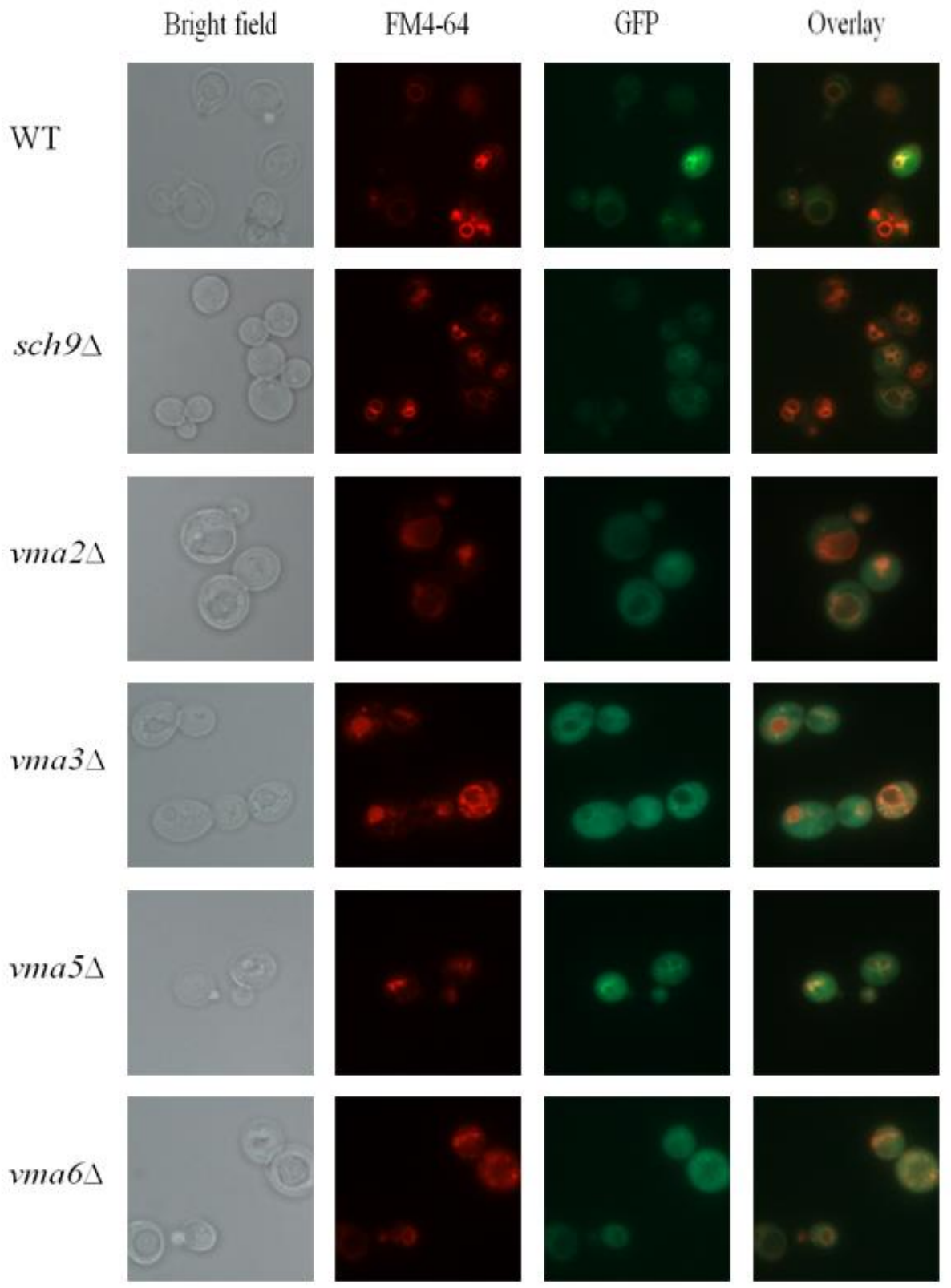

Figure 23:FM4-64 labeling of the strains transformed with the GFP-Sch9 plasmid. GFP-Sch9 is enriched at the vacuolar membrane, independent of V-ATPase activity. Colocalization with the vacuolar membrane is seen by comparing the GFP signals with the brightfield photos, which show clear vacuolar structures. In addition, FM4-64 staining of the vacuolar membrane is seen in WT and sch9Δ cells, but not in vmaΔ strains, as this staining method depends on V-ATPase activity.

19. Phosphorylation of the Vma proteins

To further elaborate on the functional connection between Sch9 and the Vma proteins, we chose to investigate whether the Sch9 protein affects the expression and/or phosphorylation of V-ATPase subunits. To this end, we genomically tagged different *VMA* genes at their C-terminus, so that Vma-9Myc fusions proteins are produced. Genomic tagging was performed in a WT/ *sch9*Δ heterozygous diploid. Subsequent sporulation and tetrad analysis produced haploid VMA-9MYC fusions constructs in both a WT background as in the *sch9*Δ strain. We started out with the analysis of the different Vma components of the V_1 subunit of the V-ATPase, in part because an *in silico* revealed that all the V_1 subunits, except Vma10, contained the R-x-x-S/T consensus sequence for phosphorylation by AGC kinases (such as Sch9) (supplement 5). In addition, we included the Vma6 protein in our analysis, since we already demonstrated that Vma6 interacts with Sch9 *in vivo*. As the activity of Sch9 and V-ATPase is regulated by nutrient availability (Dechant et al, 2010; Jorgensen et al, 2004), we also investigated the effect of glucose deprivation on phosphorylation and expression of the Vmas. Therefore, samples for protein extraction were taken of cells growing exponentially on glucose, as well as after 30 min of glucose deprivation. Western blots of the samples run on regular gels were performed and detected with anti-Myc and anti-Adh2 antibodies. Detection of Adh2, a housekeeping protein, serves as a control for the presence of the same amount of proteins in all the samples, whereas the anti-Myc antibody detects the Myc-tagged proteins. This analysis can give insight into potential effects of Sch9 on the expression of Vma subunits. In addition, as Sch9 is a kinase, we wanted to analyze possible phosphorylation of Vma proteins by Sch9. Phosphorylation of proteins leads to the formation of isoforms with a higher molecular weight (Mw) due to the incorporation of phosphate groups. Since these phospho-isoforms only slightly differ in Mw from the corresponding non-phosphorylated species, phosphorylation events are not always detectable with standard SDS-PAGE techniques. In contrast, on Phos-tag gels, phosphorylated protein isoforms are preferentially retained in the gel, leading to a larger separation of phospho-isoforms, which can lead to detection of phosphorylation events which are not seen on regular gels (Bontron et al, 2012). Therefore, we included an analysis of the Vma-Myc proteins on Phos-tag gels. As such, we expect that phosphorylation events are detected by two possible scenarios. First, phosphorylation can be apparent on a regular gel by additional bands at slightly higher Mw than the unphosphorylated form. These bands are then expected to be resolved (i.e. separated from the non-phosphorylated form) even more in the Phostag gel. Secondly, it can be that no phospho-isoforms can be detected by a regular gel, though they become visible as additional bands above the non-phosphorylated form on a Phos-tag gel.

Before we start our discussion on the results, we note that several attempts to separate and grow the tetrads of the Vma8-Myc WT/ *sch9*Δ diploid cells failed for unknown reason. Therefore the analysis of Vma8-Myc couldn't be performed. In addition, protein extraction of the WT Vma5-Myc strain deprived of glucose was unsuccessful.

Looking at the results displayed in Fig. 24, it is already clear that both deletion of *SCH9* or removal of glucose for 30 minutes does not have an impact on the expression levels of all the Vma proteins tested. This can be best seen by looking at the regular gels detected with the anti-Myc antibody.

In what follows, the additional effects are described, especially potential phosphorylation of the different Vma proteins. Regarding the Vma1 protein, regular gel detection indicates an additional band just above the expected size. However, this band is not apparent in the Phos-tag gel, so we are not convinced that this represents a phosphorylation event. In addition, this pattern is unaffected by glucose presence or deletion of *SCH9*.

When examining Vma2, a similar additional band, slightly higher than the expected (non-phosphorylated) size was detected on a normal gel, as well as on the Phos-tag gel. Interestingly, we perceive a change of this pattern in the *sch9Δ* strain. In this deletion strain, the additional band seems to shift upwards upon glucose removal, which in the Phos-tag gel is reflected by the appearance of two additional higher Mw band compared to *sch9Δ* strain with glucose. As such, Vma2 may be phosphorylated and Sch9 may be involved in this phosphorylation in a glucose-dependent manner.

Both Vma4 and Vma13 appear to be present as single, monomeric, non-phosphorylated species.

In case of Vma5, we also observed an additional, higher-Mw band. This pattern does not appear to change in the Phos-tag gel, thus also here we do not assume that this represents a phosphorylation event. Since the protein extraction in the WT strain upon glucose removal was unsuccessful, we cannot accurately speculate on how glucose and/or Sch9 might affect this higher-Mw Vma5 signal.

We previously demonstrated *in vivo* that Sch9 and Vma6 interact physically. As such, phosphorylation of Vma6 by Sch9 would be a likely scenario. Although a higher-Mw Vma6-Myc species on both regular and Phos-tag gels is detected, this pattern seems largely unresponsive to the presence of glucose and/or Sch9. Arbitrarily, a small decrease might be observed for the higher-Mw Vma6-Myc in the *sch9Δ* strain. Since this will have to be confirmed, we cannot assume specific phosphorylation of Vma6 by Sch9.

Finally, regarding both the Vma7 and Vma10 proteins, higher-Mw species are observed for which the pattern is highly dependent on both glucose and Sch9 presence. In case of Vma7, WT cells show an additional signal which could point to dimerization of Vma7. However, in the *sch9Δ* strain, the additional signal appears at a lower Mw than in the WT, which indicates that other factors besides the Vma7 protein itself may be present in these higher-Mw species. These higher-Mw species disappear after glucose removal in both WT and *sch9Δ* cells, indicating that Vma7 could be involved in the glucose-dependent regulation of V-ATPase activity. When examining Vma10, two different higher Mw-species are observed only in the *sch9Δ* strain, and of these only the upper one disappears upon glucose removal.

In conclusion, only for the Vma2 protein, possible phosphorylation is observed. We could also perceive higher-Mw species for other Vma proteins. Even though the specific components of these higher-Mw species remain unidentified, they might be involved in the glucose- and/or Sch9-dependent regulation of V-ATPase function, as demonstrated in our analysis of the Vma7 and Vma10 proteins.

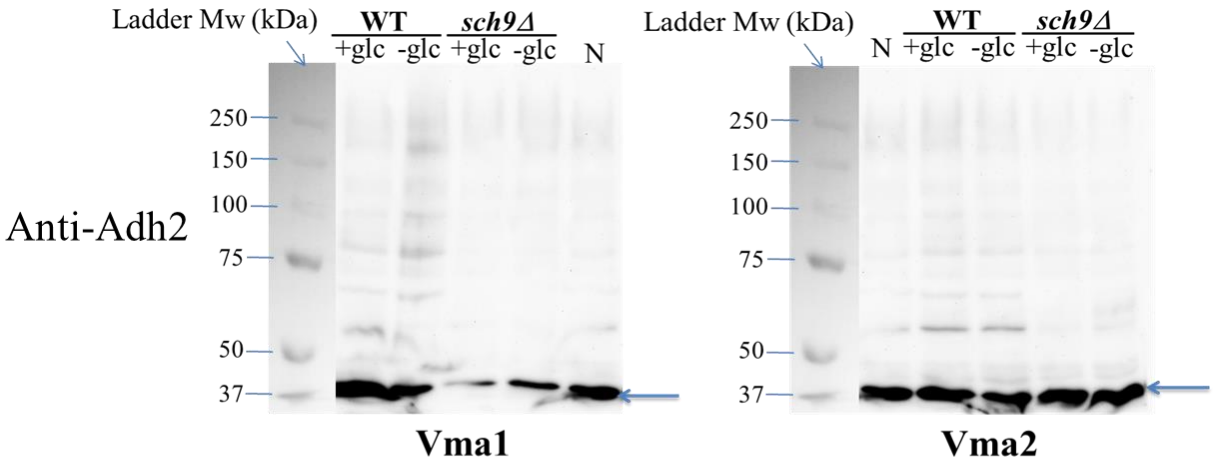
Ladder Mw (kDa)
WT
sch9Δ
+glc -glc +glc -glc N
250
150
100
75
50
37
Anti-Adh2
Vma1
Vma2

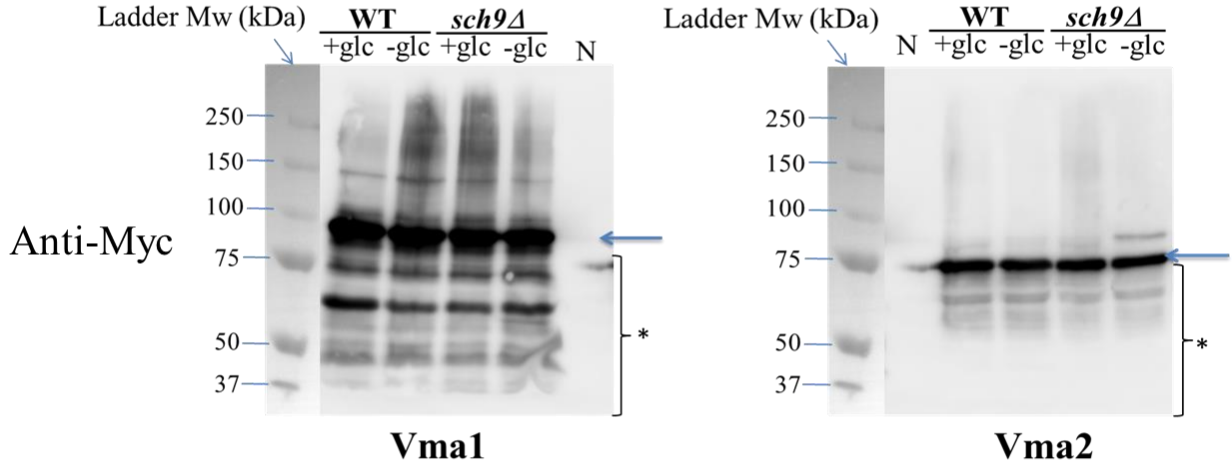
Ladder Mw (kDa)
WT
sch9Δ
+glc -glc +glc -glc N
250
150
100
75
50
37
Anti-Myc
*
Vma1
Vma2

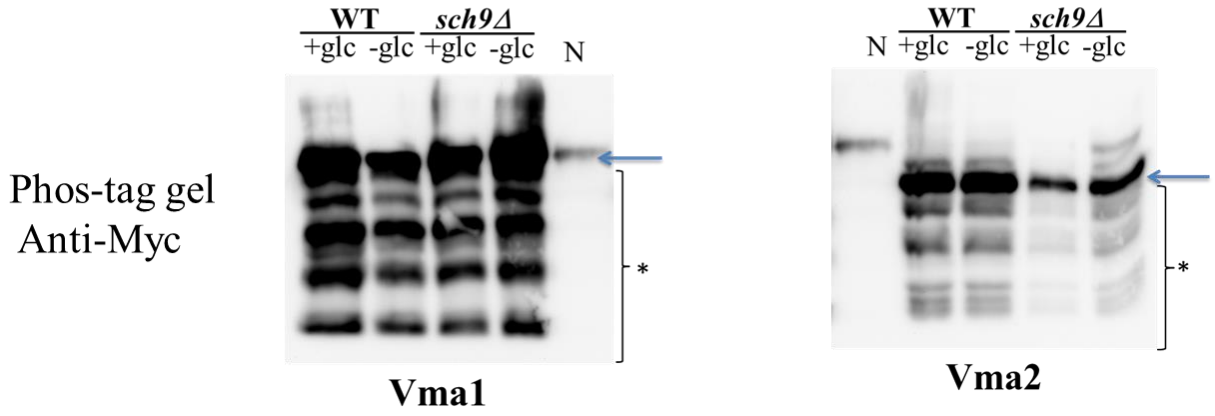
WT
sch9Δ
+glc -glc +glc -glc N
Phos-tag gel
Anti-Myc
*
Vma1
Vma2

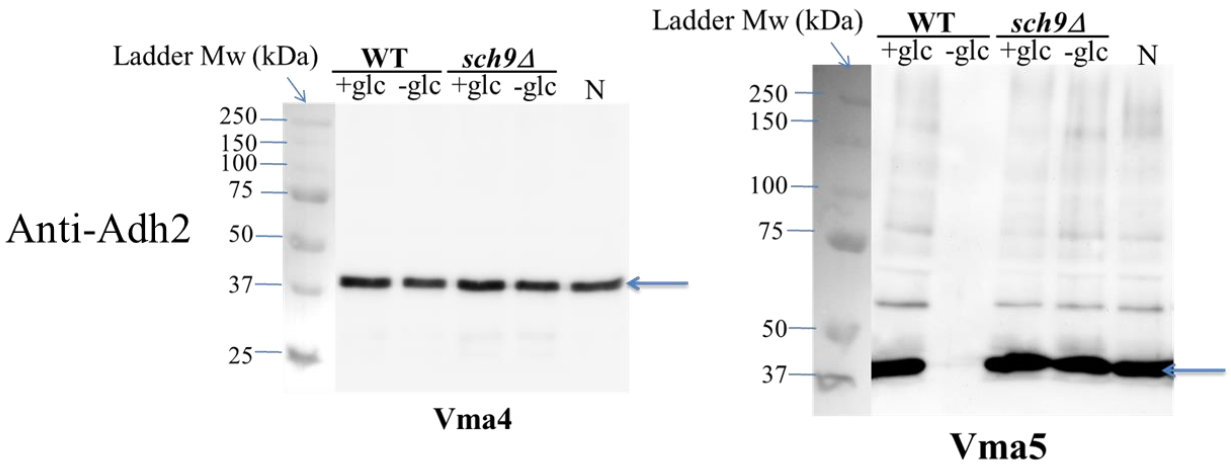
Anti-Adh2
Ladder Mw (kDa)
WT
sch9Δ
+glc -glc +glc -glc N
250
150
100
75
50
37
25
Vma4
Ladder Mw (kDa)
WT
sch9Δ
+glc -glc +glc -glc N
250
150
100
75
50
37
Vma5

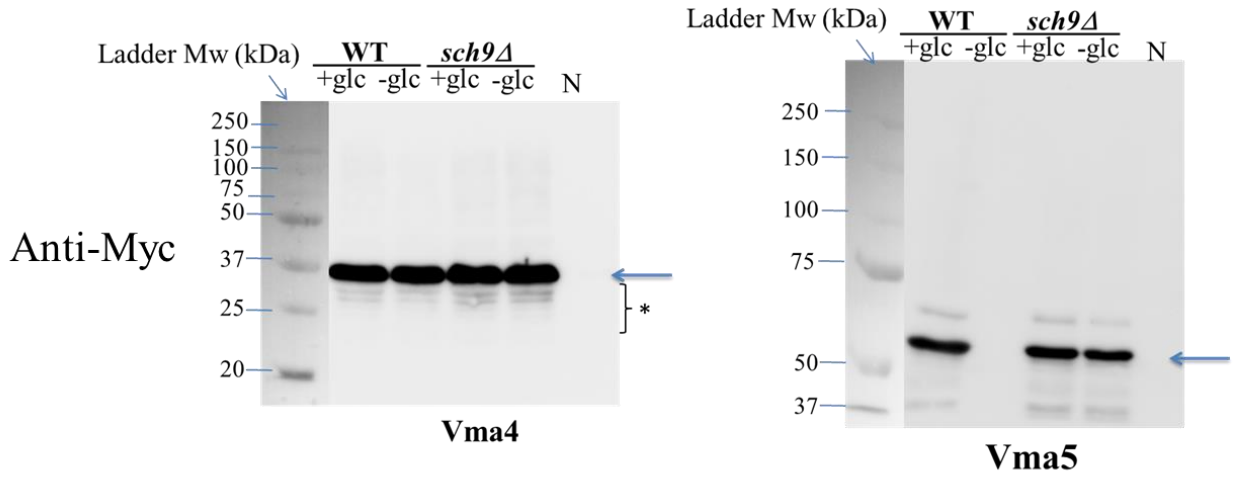
Anti-Myc
Ladder Mw (kDa)
WT
sch9Δ
+glc -glc +glc -glc N
250
150
100
75
50
37
25
20
*
Vma4
Ladder Mw (kDa)
WT
sch9Δ
+glc -glc +glc -glc N
250
150
100
75
50
37
Vma5

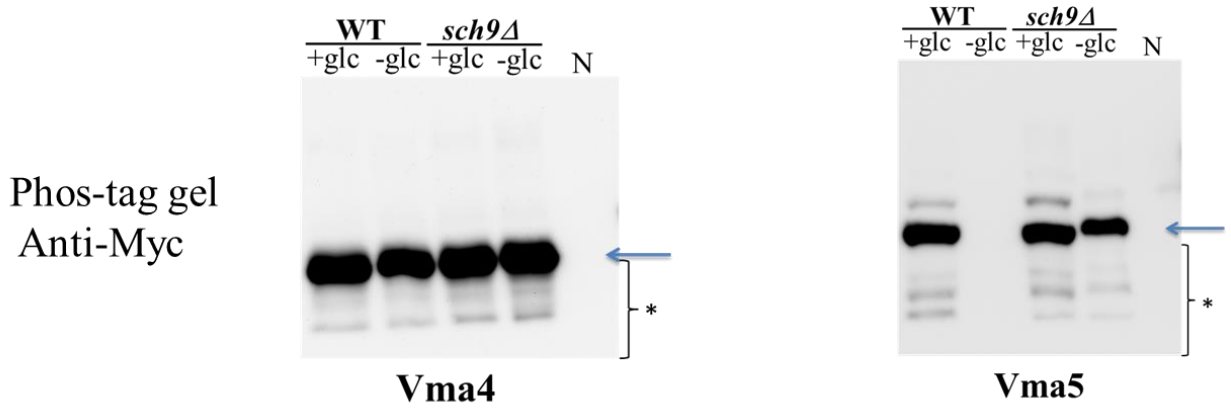
Phos-tag gel
Anti-Myc
WT
sch9Δ
+glc -glc +glc -glc N
*
Vma4
WT
sch9Δ
+glc -glc +glc -glc N
*
Vma5

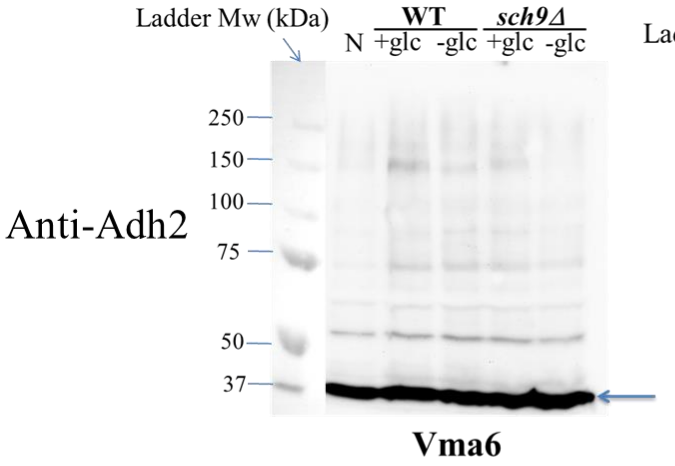
Anti-Adh2
Ladder Mw (kDa)
WT
sch9Δ
N +glc -glc +glc -glc
250
150
100
75
50
37
Vma6

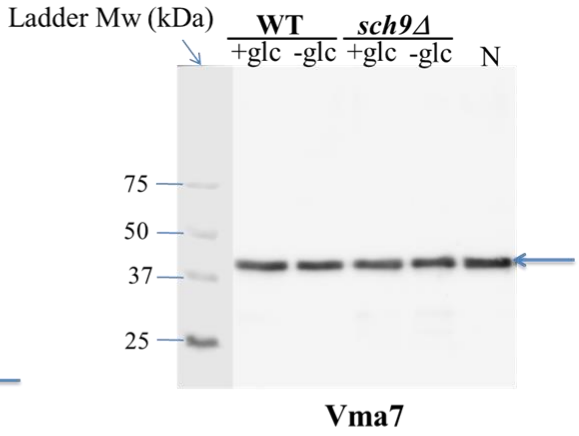
Ladder Mw (kDa)
WT
sch9Δ
+glc -glc +glc -glc N
75
50
37
25
Vma7

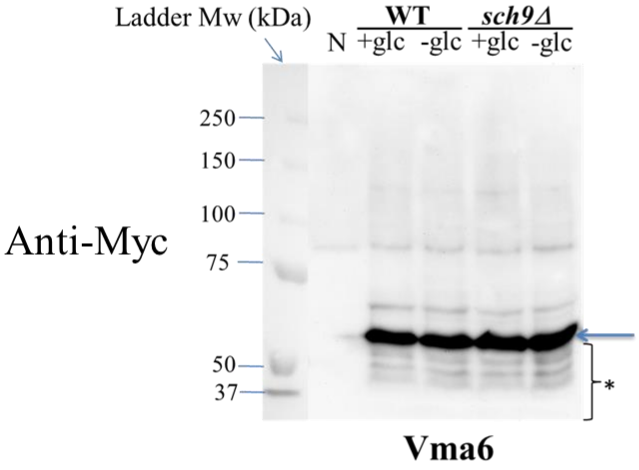
Anti-Myc
Ladder Mw (kDa)
WT
sch9Δ
N +glc -glc +glc -glc
250
150
100
75
50
37
*
Vma6

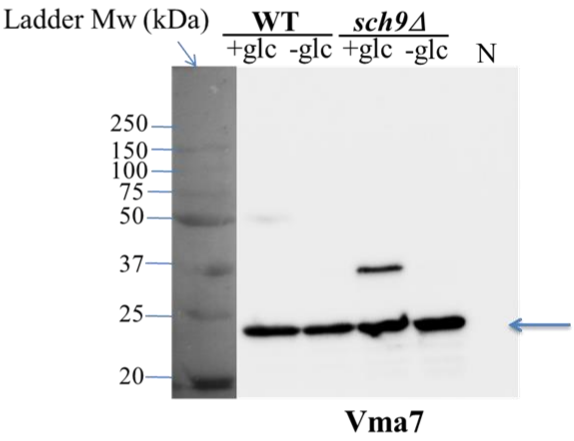
Ladder Mw (kDa)
WT
sch9Δ
+glc -glc +glc -glc N
250
150
100
75
50
37
25
20
Vma7

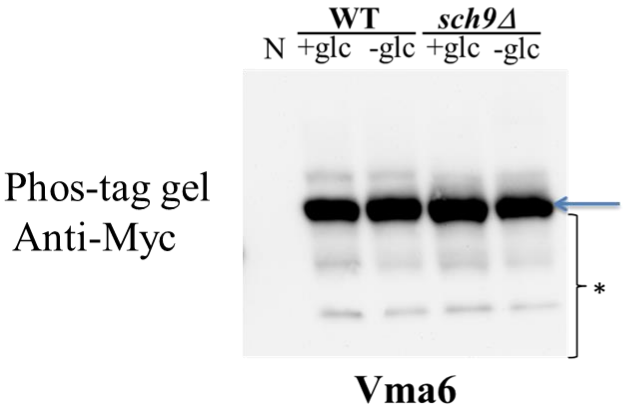
Phos-tag gel
Anti-Myc
WT
sch9Δ
N +glc -glc +glc -glc
*
Vma6

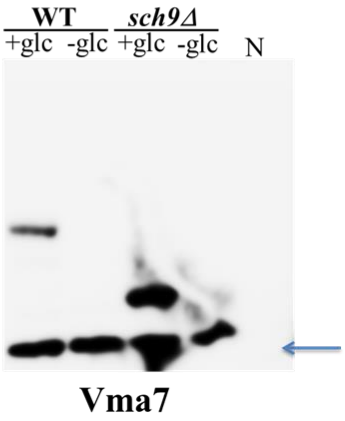
WT
sch9Δ
+glc -glc +glc -glc N
Vma7

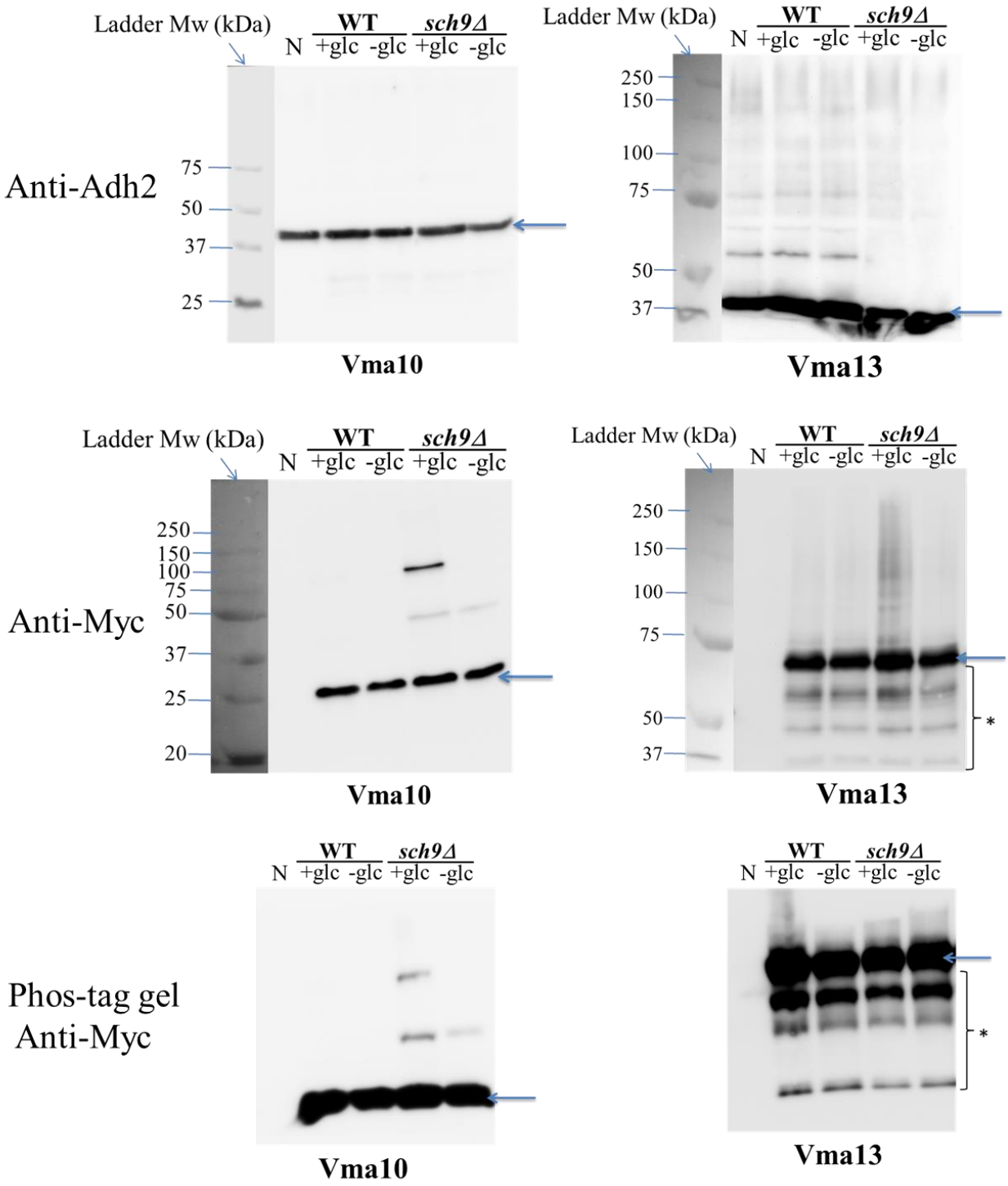

Figure 24: Western blots for strains expressing Vma-9Myc fusion proteins. Extracts were loaded on standard SDS-PAGE for detection of the housekeeping protein Adh2 ("anti-Adh2") or the Vma-Myc proteins ("anti-Myc"). In addition, samples were loaded on a phosphate-affinity gel (Phos-tag gel) to detect potential phosphorylation events not detectable on the standard SDS-PAGE. Arrows indicate the expected sizes of the Adh2 or Vma-9Myc proteins. Asterikses (*) indicate Vma-Myc proteolytic products. N annotates the negative control, which is the WT strain without Myc tagged constructs.

20. The involvement of the V-ATPase activity in life span

Sch9 is a negative regulator of the chronological life span (CLS)(Wei et al, 2009). To investigate whether the genetic interaction between *vma*Δ and *sch9*Δ strains regulates life span, we measured the reactive oxygen species (ROS) levels of the WT and *sch9*Δ *vma2*Δ, *vma2*Δ*sch9*Δ, *vma6*Δ and *vma6*Δ*sch9*Δ strains and simultaneously determined the CLS of those strains. During periods of environmental stress e.g. poor-quality carbon, yeast cells switch from fermentation to aerobic respiration and, in comparison to cells grown in glucose rich medium, produce higher ROS due to increased mitochondrial respiration. Cells have protection mechanisms that convert ROS into non-damaging compounds, but when these mechanisms fail to remove all the ROS, they accumulate in the cell. ROS cause cellular damage, which ultimately leads to cell death.

To study longevity, we analyzed the viability of the different strains using the CFU method (Fig. 25). In parallel, the superoxide levels were determined by staining cells with the fluorescent probe DHE, since this ROS species has been implicated as a major player in determining cell viability (Longo*, et al.*, 1996, Fabrizio*, et al.*, 2003). The latter method was performed on the one hand by a micro plate reader assay (Fig. 26) and on the other hand by flow cytometric analysis (Fig. 27 and Fig. 28) of DHE stained cells. With the micro plate reader assay the total amount of superoxide in a culture is determined, while the flow cytometric analysis characterizes the cells without ("DHE negative") and those with significant amount of superoxide ("DHE positive"). Next to measurements during the stationary phase, superoxide levels were also determined during exponential growth, as ROS levels during growth have been shown to have an impact on survival during the subsequent stationary phase (Pan*, et al.*, 2011).

20.1. Longevity

As shown in Figure 25, deletion of *SCH9* results in life span extension, which is equivalent to previous observations (Fabrizio*, et al.*, 2001, Wei*, et al.*, 2008). When examining the *vma2*Δ and *vma6*Δ strains, an initial increase in viability followed by a reduction in survival is perceived. At present, we cannot exclude that this initial increase in viability is due to dilution errors made for day 0, or whether this reflects a genuine property of these *vma* strains. However, the observed decrease in viability compared to the WT strain, is slow, thus we assume that impaired V-ATPase function results in an increased life span, similar to the *sch9*Δ strain.

The double mutants display a striking difference depending on which *VMA* gene is deleted in the *sch9*Δ background strain. In case of the *vma6*Δ*sch9*Δ strain, the perceived CLS follows a

pattern similar to *sch9*Δ cells, while the *vma2*Δ*sch9*Δ strain exhibits a rapid loss in viability, even faster than the WT strain.

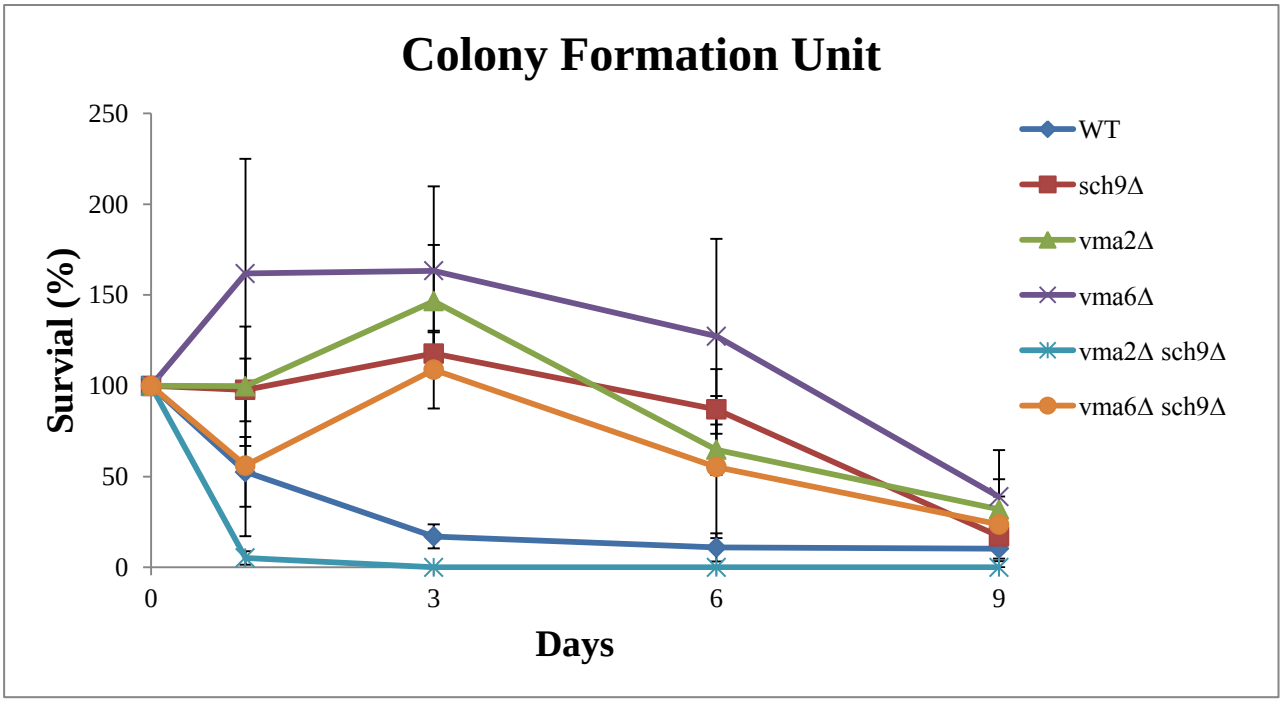

Figure 25: Colony formation unit assay of the indicated strains. Results shown are the average of four independent cultures for each strain. Error bars indicate standard deviations.

20.2. Superoxide levels

The superoxide levels determined by the micro plate reader assay show that compared to the WT strain, *vma2*Δ*sch9*Δ cells accumulate less ROS species during growth (Fig. 26). Although previous research revealed that loss of *SCH9* results in an increased respiration and thereby an augmentation of superoxide production during growth (Lavoie & Whiteway, 2008, Pan*, et al.*, 2011), it also leads to an induction of stress-responsive genes, e.g. superoxide dismutase encoding genes, by activating the Rim15 protein kinase (Wei*, et al.*, 2008). As such, the net outcome of superoxide levels is dependent of the balance between increased production and scavenging, which can variate among different background strains and culture conditions. Therefore, the decreased level of superoxide in the *sch9*Δ strain can be explained by these variables. Corresponding to the decreased DHE fluorescence detected with the micro plate reader assay, a significantly lower amount of *sch9*Δ cells were identified as DHE positive in the flow cytometric analysis (Fig. 27 and Fig. 28).

Regarding the *vma*Δ mutants, we observed higher total DHE fluorescence than for the WT strain during exponential growth (Fig. 26). However, analysis by flow cytometry indicated no significant difference in DHE positive cells between the WT, *vma2*Δ and *vma6*Δ strains (Fig.

27). The flow cytometry profiles of DHE staining (Fig. 28) indicates that the average fluorescence intensity of DHE positive cells is higher in *vma2*Δ and *vma6*Δ cells, when compared to the WT strain. As such, a same amount of DHE positive cells results in a higher total DHE fluorescence. Analysis of the double mutants revealed equivalent observations.

During the stationary phase, we observed a strong correlation between the increase in superoxide levels and the reduction in viability (Fig. 26, Fig. 27 and Fig. 28). This correlation is perceived in all the investigated strains, and is most accurate when using the flow cytometric data of DHE positive cells as a measure for superoxide levels. Indeed, the rapid decline of viability of the *vma2*Δ*sch9*Δ strain, compared to the WT strain, is correlated with a faster increase of DHE positive cells, with an almost 100% of DHE positive cells, already at day 1. Strains displaying an increased life span compared to WT cells, i.e. *sch9*Δ, *vma2*Δ and *vma6*Δ and v*ma6*Δ*sch9*Δ cultures, all contain less DHE positive cells during the time course of the longevity experiment.

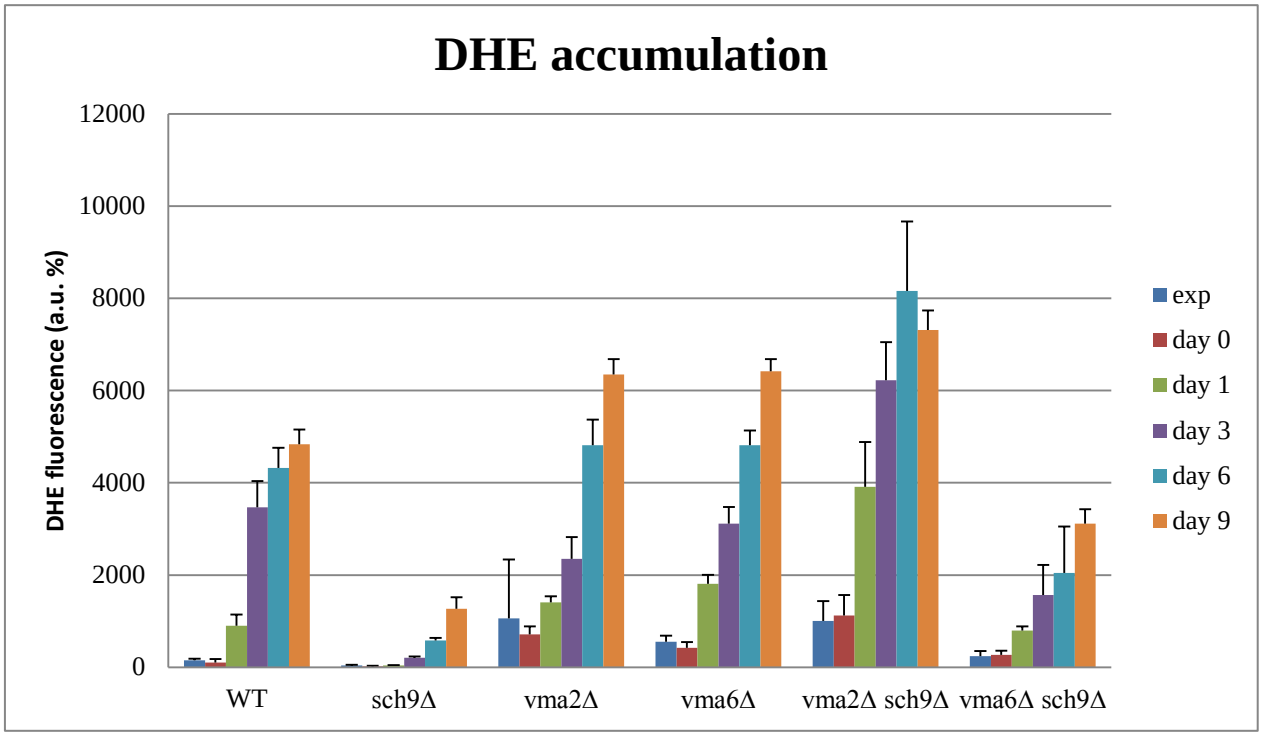

Figure 26: Total relative DHE fluorescence. DHE fluorescence of the indicated strains was measured using a micro titer plate reader (Beckman DTX880) and normalized for OD595. Results shown are the average of four independent cultures for each strain. Error bars indicate standard deviations.

In conclusion, we demonstrate, for the first time, that loss of V-ATPase function, by deletion of *VMA2* or *VMA6*, results in life span extension compared to the WT strain. The reason for the observed life span extension in *vma2*Δ and *vma6*Δ is unknown at present. Intriguingly, combining these *vma*Δ deletions with an additional deletion of *SCH9* resulted in striking different effects on longevity in the *vma2*Δ*sch9*Δ and *vma6*Δ*sch9*Δ strain. While vma6 sch9 strains display a longer life span than the WT strain, similar to sch9 strain. The vma2 sch9 strain, on the other hand, is characterized by a rapid loss in viability, resulting in a life span significantly shorter than the WT strain. The underlying mechanism remains unclear. In both double deletion strains, the V-ATPase is not functional, indicating that the high mortality in the vma2 sch9 strain is not due to loss of proton pumping activity of the V-ATPase. Still, a functional V_0 sector is present in this strain. This V_0 subunit is known to regulate certain processes independent of the V_1 sector, such as vacuolar fusion (Bayer*, et al.*, 2003, Baars*, et al.*, 2007). As such, absence of *SCH9* might specifically induce cell death in cells containing only a functional V0 sector of the V-ATPase, though further research is needed to confirm this.

The observed life span extension or reduction is, in all cases associated with a decrease or increase in superoxide production, resp., which is in line with previous studies showing that superoxide is a critical regulator for longevity.

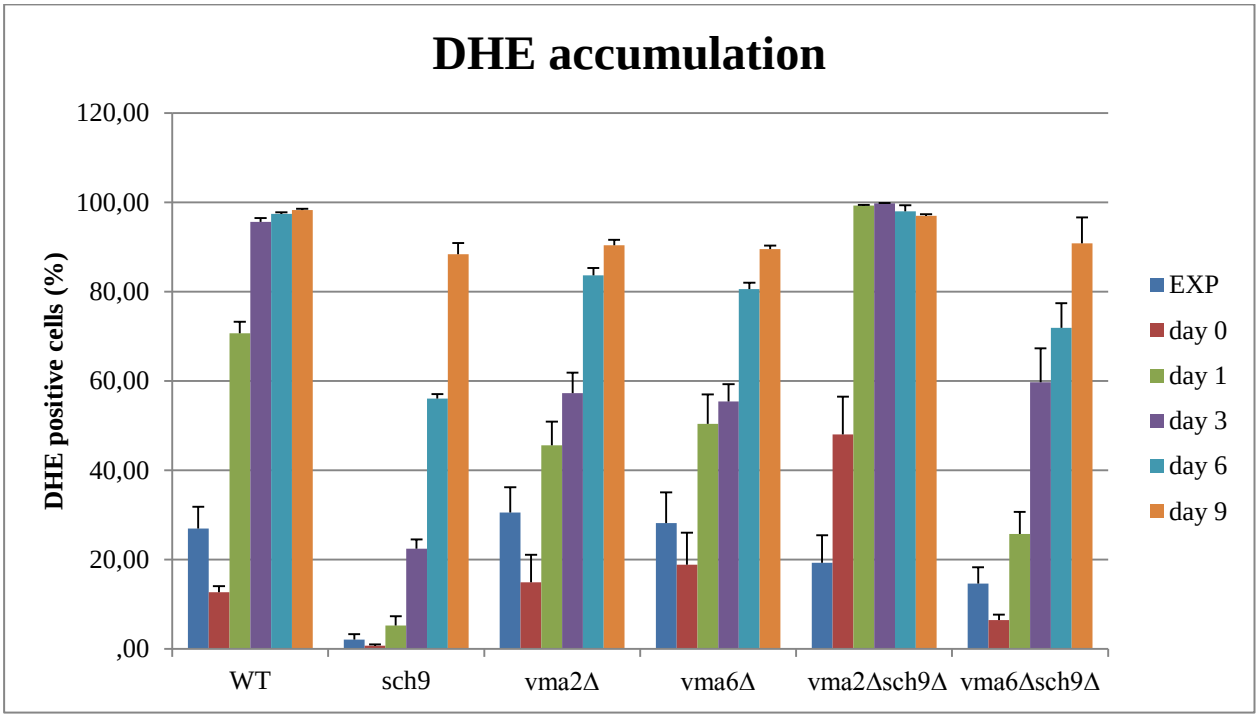

Figure 27: Average results of the amount of DHE positive cells for the indicated strains and time point shown in Figure 28. Results shown are the average of four independent cultures for each strain. Error bars indicate standard deviations.

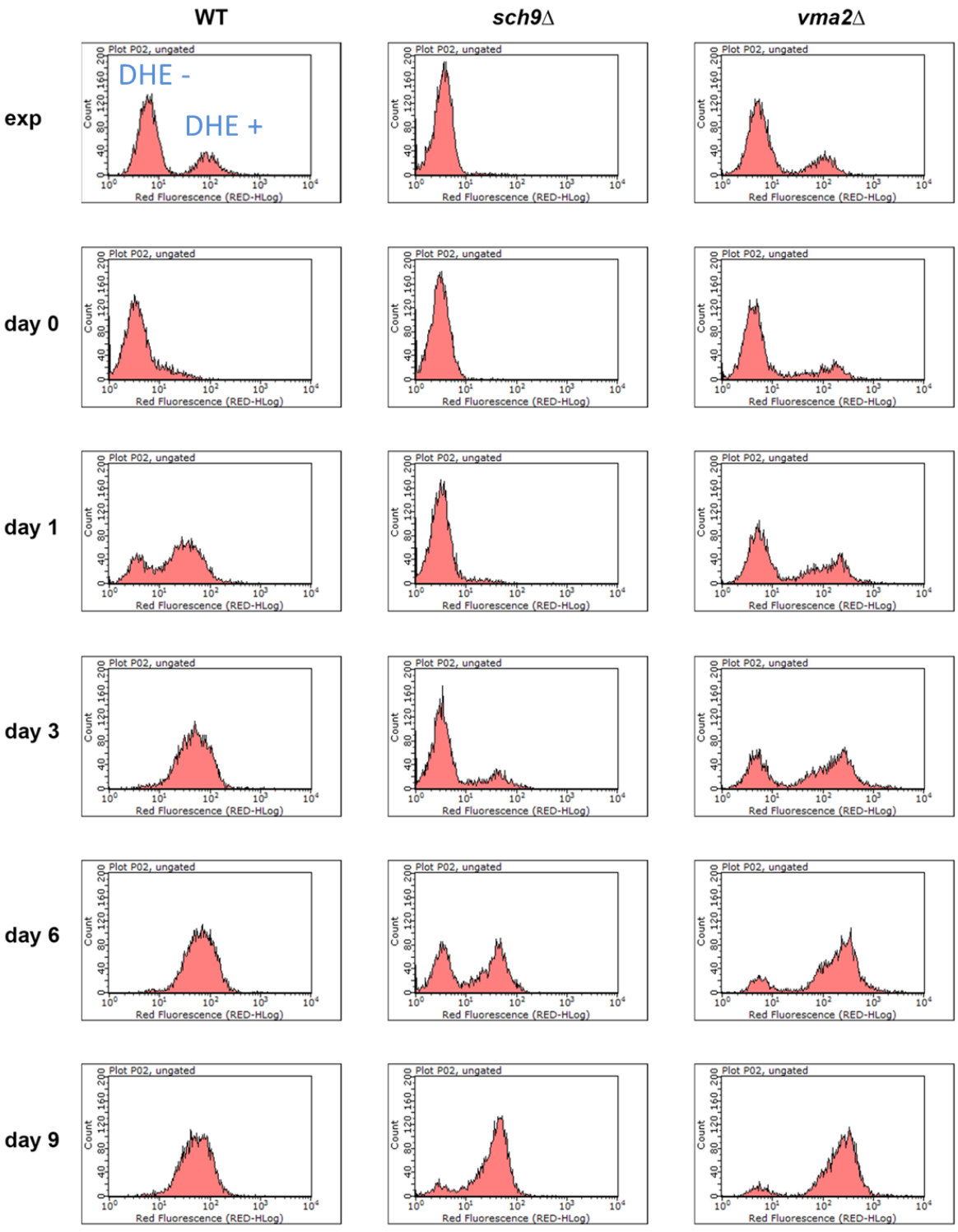
WT
sch9Δ
vma2Δ
exp
day 0
day 1
day 3
day 6
day 9
DHE -
DHE +
Plot P02, ungated
Count
Red Fluorescence (RED-HLog)

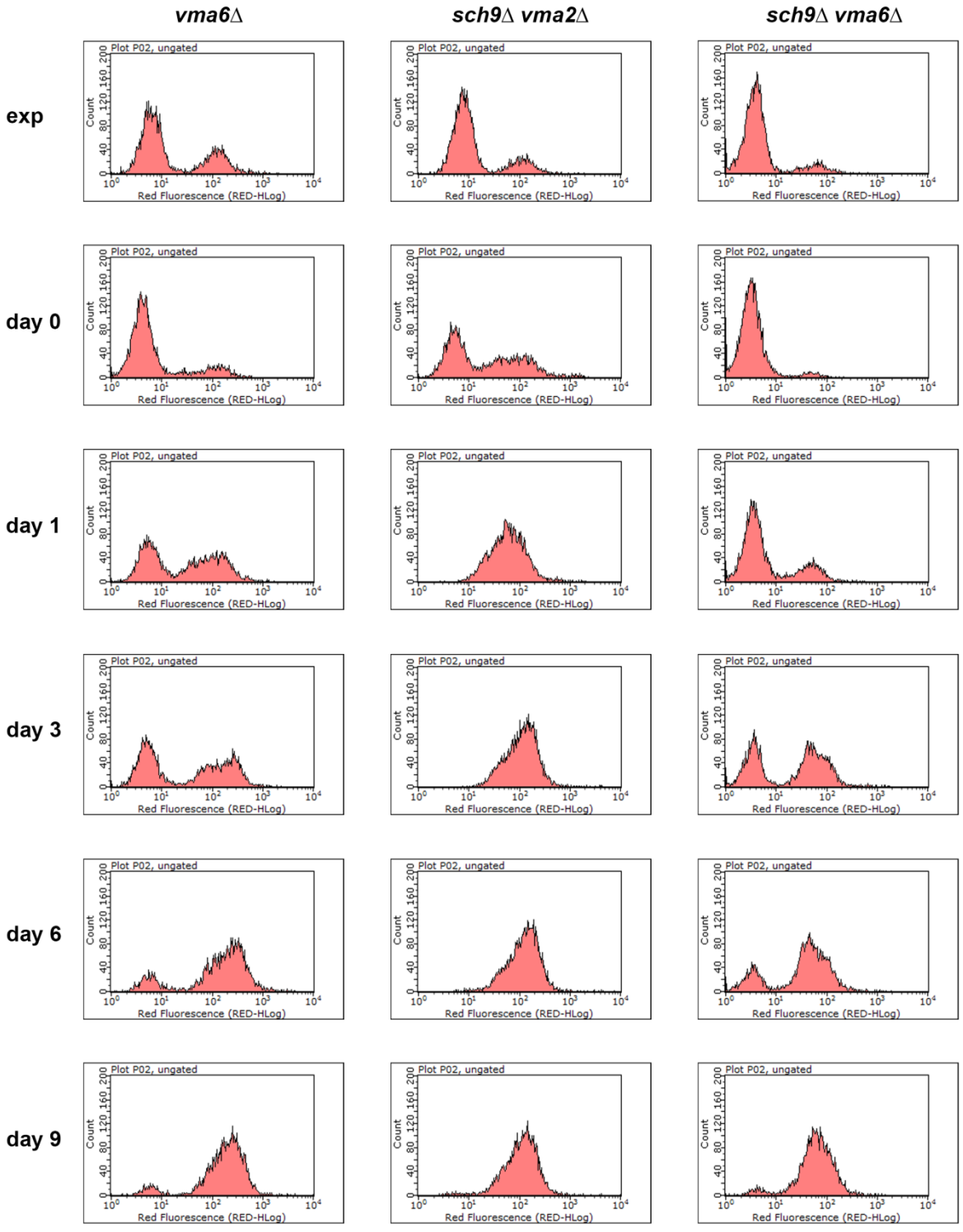

Figure 28: Flow cytometry analysis of DHE stained cells. Cells were stained with DHE and analyzed with the Guava EasyCyte 8HT system. Red fluorescence (DHE signal) is shown in. the X-axis (note the logarithmic scale), cell counts in the Y-axis. For the different time points, a representative results of four independent cultures for each strain is shown. As depicted for the WT strain during exponential growth, for each analysis the amount (% of cells) of DHE positive (DHE +) and DHE negative (DHE -) cells were determined. Average results of the amount of DHE positive cells for all strains and time points are shown in Figure 27.

Discussion

Preliminary data indicated that several *VMA* genes genetically interact with *SCH9,* since the *vma*Δ*sch9*Δ double mutants displayed a synthetic sick phenotype in a synthetic genetic array (SGA) analysis. The *VMA* genes are needed for the V-ATPase activity, a proton pump with a vital role in upholding pH gradients between the cytosol and different intracellular compartments, such as the vacuole (Graham et al, 2000), while the *SCH9* gene encodes the Sch9 protein kinase, which is a core mediator of nutrient sensing pathways (Smets et al, 2010). Therefore, during this dissertation, the genetic interaction between the *VMA* genes and *SCH9* was explored.

21. Genetic interaction

To start with, the outcome of the SGA screening was verified using tetrad analysis. The results demonstrated a genetic interaction between each *VMA* gene and *SCH9*, indicating that the genetic interaction cannot be ascribed to a particular *VMA* species. Rather, this interaction is the consequence of the combination of a non-functional V-ATPase and a deletion of *SCH9*. While performing tetrad analysis, the genetic interaction between genes is revealed by a difference in colony size. We furthermore illustrated that this genetic interaction is also observed when performing growth assays in liquid cultures.

Genetic interaction generally points out that both partners cooperate in the regulation of specific cellular mechanisms. As multiple processes that require Sch9 (Lamming & Sabatini, 2011; Pascual-Ahuir & Proft, 2007) and/or the V-ATPase (Kane, 2006) are known, we carried out spot assays in which *sch9*Δ and *vma*Δ mutant strains were grown under certain conditions that demand either Sch9 and/or the V-ATPase function. As such, we performed a phenotypic mapping to find processes that are regulated by both Sch9 and V-ATPase. The major outcomes were:

1) At elevated pH, the growth of the *sch9*Δ strain is not impaired. Since this is one of the conditions which requires the proton pump function of the V-ATPase for acidifying the vacuole. This finding was the first indication that Sch9 is not required for the enzymatic function of the V-ATPase complex.

2) Growth on non-fermentable carbon sources is highly reduced in both *sch9*Δ and *vma*Δ cells. By lowering the concentration of the non-fermentable carbon sources, a partial relief of the growth defect was perceived. We assume that the latter is a consequence of a decreased ROS production in the cell under these conditions, in line with previous

statements (Milgrom et al, 2007). As such, these observations indicate that both Sch9 and the V-ATPase are involved in the response to endogenous oxidative stress.

3) We established a functional relation between the V-ATPase and TORC1 signaling, since the *vma*Δ strains are sensitive to rapamycin and manganese, which are both known to affect the TORC1 signaling (Devasahayam et al, 2007; Devasahayam et al, 2006; Urban et al, 2007). Intriguingly, in mammalian cells, the V-ATPase pump is a mediator of the amino acid-dependent activation of the mTORC1 (Efeyan et al, 2012). More research is needed to elucidate whether a similar mechanism is operating in yeast cells.

Note that the latter two outcomes involve cellular functions of the V-ATPase for which there is no direct link to its enzymatic (proton-pumping) function. These functions are sometimes annotated as “moonlighting” functions of the V-ATPase. As such, our results indicate that the phenotypic overlap of functions between Sch9 and the V-ATPase seems to be directed specifically to these moonlighting functions.

22. Physical interaction

Subsequent to confirming genetic interaction between Sch9 and V-ATPase, we investigated possible physical interaction between these proteins. A yeast two-hybrid screening was performed, in which we discovered that Sch9 interacts with the Vma6 subunit. The latter interaction was confirmed by co-immunoprecipitation.

23. Functional interaction

To further elaborate on the functional implications of the observed genetic and physical interactions between Sch9 and the V-ATPase, we started out to investigate the vacuolar morphology in the *sch9*Δ strain, and showed that the vacuolar morphology is not modified upon deletion of *SCH9*. The WT, *sch9*Δ and *vma*Δ strains were stained with FM4-64, a fluorescent dye used to stain the vacuolar membrane. The FM4-64 dye is taken up by endocytosis, which depends on the acidification of endosomes and the vacuole by the V-ATPase. Therefore, this staining method is also an indication for the proper functioning of the vacuolar proton pump. Considering that the vacuolar staining of *sch9*Δ cells is equivalent to the WT cells and different from the *vma*Δ strain, these results are a second indication Sch9 is not essential for the proton pumping activity of the V-ATPase.

The Sch9 protein is known to be enriched at the vacuolar membrane (Jorgensen et al, 2004). Therefore, another potential role for the observed physical interaction between Sch9 and the V-ATPase could be that this interaction is required for targeting Sch9 to the vacuolar membrane. However, our results showed that this was not the case.

Finally, we did not observe a clear Sch9-dependent effects on either the expression or phosphorylation of specific Vma proteins. We did, however, observe some higher-Mw species of Vma7 and Vma10, dependent on the presence of glucose and/or Sch9. Still, the nature and function of these species are elusive at present.

In conclusion, we demonstrate that the observed physical interaction between Sch9 and Vma6 is not required for the regulation of proper vacuolar morphology, proton pumping activity of the V-ATPase, the recruitment of Sch9 to the vacuolar membrane, or phosphorylation of the tested Vma proteins by Sch9. We note that we did not include all the Vma proteins in our phosphorylation study, so testing the other Vma proteins is necessary to have a complete conclusion on Sch9-dependent phosphorylation of V-ATPase subunits. Another hypothesis is that the V-ATPase activity acts upstream of the TORC1/Sch9 signaling, similarly to what happens in mammalian cells (Efeyan et al, 2012), and that the observed physical interaction between Sch9 and V-ATPase subunit is required for activation of Sch9 by TORC1.

24. Chronological Life Span

It has been discovered a long time ago that Sch9 is a negative mediator of chronological life span (CLS) (Fabrizio et al, 2001), but the influence of the V-ATPase pump on CLS has not been studied to our knowledge. We show that deletion of *VMA* genes triggers a life span extension in comparison to the wild type, which was correlated to reduced levels of superoxide in the cell. Intriguingly, deleting the same *VMA* genes in a *sch9Δ* strain displays an apparent difference depending on the *VMA* gene deleted. The *vma6*Δ*sch9*Δ strain shows a survival pattern similar to *sch9*Δ cells, while *vma2*Δ*sch9*Δ cells unexpectedly demonstrate a rapid decrease in viability. Also here, the rapid decrease in viability is associated with a hyperaccumulation of superoxide levels. The underlying mechanisms are not known. Given that in both double deletion strains, no functional V-ATPase is present, the high mortality of *vma2*Δ*sch9*Δ cells cannot be appointed to loss-of-function of the vacuolar proton pump. However, the V_0 subunit, which is known to mediate certain processes independent of the V_1 subunit, e.g. vacuolar fusion (Baars et al, 2007; Bayer et al, 2003), is still present in the *vma2*Δ*sch9*Δ strain. As such, deletion of *SCH9* might specifically cause rapid cell death in cells containing only a functional V_0 sector of the V-ATPase, though further research is needed to validate this.

Summary

The protein kinase Sch9 plays a major role in nutrient signaling and the determination of life span in yeast. As Sch9 is the functional orthologue of the mammalian PKB/Akt and S6K1 kinases, yeast serves as a suitable model system for the elucidation of cellular processes involving these mammalian kinases. In the work presented here, we indicate a functional connection between Sch9 and the vacuolar H^+-ATPase (V-ATPase), a proton pump which serves to acidify intracellular organelles, such as the vacuole. Interestingly, although the V-ATPase complex is conserved from yeast to human, loss of V-ATPase activity in eukaryotes other than fungi is often lethal. Therefore, yeast is a prime model used to study the functions of this proton pump. Besides its direct role in organelle acidification, the V-ATPase also performs certain “moonlighting” functions in yeast, for which no direct link to its enzymatic (proton-pumping) function is apparent. Intriguingly, our evidence indicates that Sch9 is not required *per se* for the proton pumping activity of the V-ATPase. Instead, this kinase appears to be specifically involved in cellular processes involving the “moonlighting” functions of the V-ATPase, such as the response to endogenous oxidative stress and the regulation of signaling through the highly conserved TORC1 kinase. Our hypothesis that Sch9 and the V-ATPase collaborate to regulate certain cellular processes is strengthened by the fact that we revealed a direct, physical interaction between Sch9 and Vma6, a subunit of the V-ATPase. This interaction is not required for the regulation of a proper vacuolar morphology, proton pumping activity of the V-ATPase, the recruitment of Sch9 to the vacuolar membrane, or phosphorylation of several Vma proteins by Sch9. Therefore, the functional implication of the observed physical interaction is still unclear at this moment. Finally, we demonstrate that the V-ATPase plays a role in the regulation of yeast life span, possibly by modulating cellular levels of the toxic superoxide compound. Intriguingly, combining the deletion of *SCH9* with functional impairment of the V-ATPase leads to different results on life span, depending on which subunit of the V-ATPase is affected.

In conclusion, our data strongly indicate that Sch9 and the V-ATPase collaborate to regulate specific cellular processes, highlighted by the fact that we could demonstrate an *in vivo* physical interaction between these partners. As both Sch9 and the V-ATPase are highly conserved in mammalian cells, further elucidation of the molecular mechanisms by which these entities are connected in yeast will be of great value for unraveling new functions of their mammalian counterparts.

Samenvatting

Het proteïne kinase Sch9 speelt een belangrijke rol in nutriënt signalering en de bepaling van de levensduur in gist. Aangezien Sch9 het functionele ortholoog is van de PKB/Akt en S6K1 kinasen in zoogdiercellen, is gist een geschikt modelorganisme voor het vinden van nieuwe functies van deze orthologe kinasen. In dit eindwerk wordt een functionele link aangetoond tussen Sch9 en het vacuolaire H^+-ATPase (V-ATPase), een proton pomp die intracellulaire organellen zoals de vacuole verzuurt. Hoewel het V-ATPase complex geconserveerd is van gist tot de mens, is het verlies van V-ATPase activiteit in andere eukaryoten vaak lethaal, zodat gist een belangrijk modelorganisme is om de functies van deze proton pomp te bestuderen. Naast haar primaire rol in de verzuring van organellen, heeft het V-ATPase ook bepaalde "moonlighting" functies in gist, waarvoor geen directe link naar de enzymatische (proton-pomp) functie aanwezig lijkt. Onze waarnemingen tonen aan dat Sch9 niet strikt noodzakelijk is voor de enzymatische activiteit van het V-ATPase. Dit kinase blijkt echter wel betrokken te zijn bij cellulaire processen die door de “moonlighting” functies van het V-ATPase worden geregeld, zoals de respons op endogene oxidatieve stress en signalering via het geconserveerde TORC1 kinase. Onze hypothese dat Sch9 en het V-ATPase samen bepaalde cellulaire processen reguleren wordt versterkt door het feit dat we een directe fysieke interactie hebben aangetoond tussen Sch9 en Vma6, een subeenheid van het V-ATPase. Deze interactie blijkt echter niet nodig voor de regulatie van een correcte vacuolaire morfologie, voor de enzymatische activiteit van het V-ATPase, voor de rekrutering van Sch9 naar het vacuolaire membraan of voor de fosforylatie van verscheidene Vma proteïnen door Sch9. Bijgevolg zijn de functionele implicaties van de waargenomen fysieke interactie op dit moment nog niet gekend. Tenslotte hebben we aangetoond dat het V-ATPase betrokken is in de regulatie van de levensduur van gist, mogelijks door het moduleren van de cellulaire niveau’s van het toxische superoxide. Opmerkelijk, wanneer de deletie van *SCH9* gecombineerd wordt met een niet-functioneel V-ATPase, leidt dit tot verschillende effecten op de levensduur, afhankelijk van welke subeenheid van het V-ATPase wordt geïnactiveerd.
Samenvattend tonen onze data aan dat Sch9 en het V-ATPase samen specifieke cellulaire processen reguleren, wat benadrukt wordt door het feit dat we een *in vivo* fysische interactie tussen deze partners konden aantonen. Aangezien zowel Sch9 en het V-ATPase sterk geconserveerd zijn in zoogdiercellen, zal verder onderzoek naar de moleculaire mechanismen waarmee deze entiteiten zijn verbonden in gist van groot belang zijn voor het ontrafelen van nieuwe functies van hun equivalenten in zoogdiercellen.

References

Baars TL, Petri S, Peters C, Mayer A (2007) Role of the V-ATPase in regulation of the vacuolar fission-fusion equilibrium. *Mol Biol Cell* **18:** 3873-3882

Bayer MJ, Reese C, Buhler S, Peters C, Mayer A (2003) Vacuole membrane fusion: V0 functions after trans-SNARE pairing and is coupled to the Ca2+-releasing channel. *J Cell Biol* **162:** 211-222

Bontron S, Jaquenoud M, Vaga S, Talarek N, Bodenmiller B, Aebersold R, De Virgilio C (2012) Yeast Endosulfines Control Entry into Quiescence and Chronological Life Span by Inhibiting Protein Phosphatase 2A. *Cell Rep*

Breitenbach M, Laun P, Jazwinski SM (2012) Introduction. *Subcell Biochem* **57:** 1-12

Bryant NJ, Stevens TH (1998) Vacuole biogenesis in Saccharomyces cerevisiae: protein transport pathways to the yeast vacuole. *Microbiol Mol Biol Rev* **62:** 230-247

Compton MA, Graham LA, Stevens TH (2006) Vma9p (subunit e) is an integral membrane V0 subunit of the yeast V-ATPase. *J Biol Chem* **281:** 15312-15319

Crauwels M, Donaton MC, Pernambuco MB, Winderickx J, de Winde JH, Thevelein JM (1997) The Sch9 protein kinase in the yeast Saccharomyces cerevisiae controls cAPK activity and is required for nitrogen activation of the fermentable-growth-medium-induced (FGM) pathway. *Microbiology* **143 (Pt 8):** 2627-2637

Dechant R, Binda M, Lee SS, Pelet S, Winderickx J, Peter M (2010) Cytosolic pH is a second messenger for glucose and regulates the PKA pathway through V-ATPase. *Embo J* **29:** 2515-2526

Devasahayam G, Burke DJ, Sturgill TW (2007) Golgi manganese transport is required for rapamycin signaling in Saccharomyces cerevisiae. *Genetics* **177:** 231-238

Devasahayam G, Ritz D, Helliwell SB, Burke DJ, Sturgill TW (2006) Pmr1, a Golgi Ca2+/Mn2+-ATPase, is a regulator of the target of rapamycin (TOR) signaling pathway in yeast. *Proc Natl Acad Sci U S A* **103:** 17840-17845

Diakov TT, Kane PM (2010) Regulation of vacuolar proton-translocating ATPase activity and assembly by extracellular pH. *J Biol Chem* **285:** 23771-23778

Eide DJ, Clark S, Nair TM, Gehl M, Gribskov M, Guerinot ML, Harper JF (2005) Characterization of the yeast ionome: a genome-wide analysis of nutrient mineral and trace element homeostasis in Saccharomyces cerevisiae. *Genome Biol* **6:** R77

Fabrizio P, Hoon S, Shamalnasab M, Galbani A, Wei M, Giaever G, Nislow C, Longo VD (2010) Genome-wide screen in Saccharomyces cerevisiae identifies vacuolar protein sorting, autophagy, biosynthetic, and tRNA methylation genes involved in life span regulation. *PLoS Genet* **6:** e1001024

Fabrizio P, Liou LL, Moy VN, Diaspro A, Valentine JS, Gralla EB, Longo VD (2003) SOD2 functions downstream of Sch9 to extend longevity in yeast. *Genetics* **163:** 35-46

Fabrizio P, Pozza F, Pletcher SD, Gendron CM, Longo VD (2001) Regulation of longevity and stress resistance by Sch9 in yeast. *Science* **292:** 288-290

Fontana L, Partridge L, Longo VD (2010) Extending healthy life span--from yeast to humans. *Science* **328:** 321-326

Foury F (1990) The 31-kDa polypeptide is an essential subunit of the vacuolar ATPase in Saccharomyces cerevisiae. *J Biol Chem* **265:** 18554-18560

Glick D, Barth S, Macleod KF (2010) Autophagy: cellular and molecular mechanisms. *J Pathol* **221:** 3-12

Graham LA, Powell B, Stevens TH (2000) Composition and assembly of the yeast vacuolar H(+)-ATPase complex. *J Exp Biol* **203:** 61-70

Huang X, Liu J, Dickson RC (2012) Down-regulating sphingolipid synthesis increases yeast lifespan. *PLoS Genet* **8:** e1002493

Huber A, Bodenmiller B, Uotila A, Stahl M, Wanka S, Gerrits B, Aebersold R, Loewith R (2009) Characterization of the rapamycin-sensitive phosphoproteome reveals that Sch9 is a central coordinator of protein synthesis. *Genes Dev* **23:** 1929-1943

Huber A, French SL, Tekotte H, Yerlikaya S, Stahl M, Perepelkina MP, Tyers M, Rougemont J, Beyer AL, Loewith R (2011) Sch9 regulates ribosome biogenesis via Stb3, Dot6 and Tod6 and the histone deacetylase complex RPD3L. *EMBO J* **30:** 3052-3064

Jacinto E, Lorberg A (2008) TOR regulation of AGC kinases in yeast and mammals. *Biochem J* **410:** 19-37

Jorgensen P, Nishikawa JL, Breitkreutz BJ, Tyers M (2002) Systematic identification of pathways that couple cell growth and division in yeast. *Science* **297:** 395-400

Jorgensen P, Rupes I, Sharom JR, Schneper L, Broach JR, Tyers M (2004) A dynamic transcriptional network communicates growth potential to ribosome synthesis and critical cell size. *Genes Dev* **18:** 2491-2505

Kaeberlein M, Burtner CR, Kennedy BK (2007) Recent developments in yeast aging. *PLoS Genet* **3:** e84

Kaeberlein M, Kennedy BK (2005) Large-scale identification in yeast of conserved ageing genes. *Mech Ageing Dev* **126:** 17-21

Kane PM (2006) The where, when, and how of organelle acidification by the yeast vacuolar H+-ATPase. *Microbiol Mol Biol Rev* **70:** 177-191

Kane PM (2007) The long physiological reach of the yeast vacuolar H+-ATPase. *J Bioenerg Biomembr* **39:** 415-421

Kawai S, Urban J, Piccolis M, Panchaud N, De Virgilio C, Loewith R (2011) Mitochondrial genomic dysfunction causes dephosphorylation of Sch9 in the yeast Saccharomyces cerevisiae. *Eukaryot Cell* **10:** 1367-1369

Kim MD, Hong SP, Carlson M (2005) Role of Tos3, a Snf1 protein kinase kinase, during growth of Saccharomyces cerevisiae on nonfermentable carbon sources. *Eukaryot Cell* **4:** 861-866

Lamming DW, Sabatini DM (2011) A radical role for TOR in longevity. *Cell Metab* **13:** 617-618

Lavoie H, Whiteway M (2008) Increased respiration in the sch9Delta mutant is required for increasing chronological life span but not replicative life span. *Eukaryot Cell* **7:** 1127-1135

Li SC, Kane PM (2009) The yeast lysosome-like vacuole: endpoint and crossroads. *Biochim Biophys Acta* **1793:** 650-663

Liu K, Zhang X, Lester RL, Dickson RC (2005a) The sphingoid long chain base phytosphingosine activates AGC-type protein kinases in Saccharomyces cerevisiae including Ypk1, Ypk2, and Sch9. *J Biol Chem* **280:** 22679-22687

Liu K, Zhang X, Sumanasekera C, Lester RL, Dickson RC (2005b) Signalling functions for sphingolipid long-chain bases in Saccharomyces cerevisiae. *Biochem Soc Trans* **33:** 1170-1173

Longo VD, Fabrizio P (2012) Chronological Aging in Saccharomyces cerevisiae. *Subcell Biochem* **57:** 101-121

Longo VD, Gralla EB, Valentine JS (1996) Superoxide dismutase activity is essential for stationary phase survival in Saccharomyces cerevisiae. Mitochondrial production of toxic oxygen species in vivo. *J Biol Chem* **271:** 12275-12280

Lu JY, Lin YY, Sheu JC, Wu JT, Lee FJ, Chen Y, Lin MI, Chiang FT, Tai TY, Berger SL, Zhao Y, Tsai KS, Zhu H, Chuang LM, Boeke JD (2011) Acetylation of yeast AMPK controls intrinsic aging independently of caloric restriction. *Cell* **146:** 969-979

Martin DE, Hall MN (2005) The expanding TOR signaling network. *Curr Opin Cell Biol* **17:** 158-166

Milgrom E, Diab H, Middleton F, Kane PM (2007) Loss of vacuolar proton-translocating ATPase activity in yeast results in chronic oxidative stress. *J Biol Chem* **282:** 7125-7136

Nelson H, Nelson N (1990) Disruption of genes encoding subunits of yeast vacuolar H(+)-ATPase causes conditional lethality. *Proc Natl Acad Sci U S A* **87:** 3503-3507

Pan Y, Schroeder EA, Ocampo A, Barrientos A, Shadel GS (2011) Regulation of yeast chronological life span by TORC1 via adaptive mitochondrial ROS signaling. *Cell Metab* **13:** 668-678

Pan Y, Shadel GS (2009) Extension of chronological life span by reduced TOR signaling requires down-regulation of Sch9p and involves increased mitochondrial OXPHOS complex density. *Aging (Albany NY)* **1:** 131-145

Pascual-Ahuir A, Proft M (2007a) Control of stress-regulated gene expression and longevity by the Sch9 protein kinase. *Cell Cycle* **6:** 2445-2447

Pascual-Ahuir A, Proft M (2007b) The Sch9 kinase is a chromatin-associated transcriptional activator of osmostress-responsive genes. *EMBO J* **26:** 3098-3108

Pedruzzi I, Dubouloz F, Cameroni E, Wanke V, Roosen J, Winderickx J, De Virgilio C (2003) TOR and PKA signaling pathways converge on the protein kinase Rim15 to control entry into G0. *Mol Cell* **12:** 1607-1613

Peyroche G, Milkereit P, Bischler N, Tschochner H, Schultz P, Sentenac A, Carles C, Riva M (2000) The recruitment of RNA polymerase I on rDNA is mediated by the interaction of the A43 subunit with Rrn3. *EMBO J* **19:** 5473-5482

Powers T (2007) TOR signaling and S6 kinase 1: Yeast catches up. *Cell Metab* **6:** 1-2

Ptacek J, Devgan G, Michaud G, Zhu H, Zhu X, Fasolo J, Guo H, Jona G, Breitkreutz A, Sopko R, McCartney RR, Schmidt MC, Rachidi N, Lee SJ, Mah AS, Meng L, Stark MJ, Stern

DF, De Virgilio C, Tyers M, Andrews B, Gerstein M, Schweitzer B, Predki PF, Snyder M (2005) Global analysis of protein phosphorylation in yeast. *Nature* **438:** 679-684

Reinders A, Bürckert N, Boller T, Wiemken A, De Virgilio C (1998) Saccharomyces cerevisiae cAMP-dependent protein kinase controls entry into stationary phase through the Rim15p protein kinase. *Genes Dev* **12:** 2943-2955

Roelants FM, Torrance PD, Thorner J (2004) Differential roles of PDK1- and PDK2-phosphorylation sites in the yeast AGC kinases Ypk1, Pkc1 and Sch9. *Microbiology* **150:** 3289-3304

Roosen J, Engelen K, Marchal K, Mathys J, Griffioen G, Cameroni E, Thevelein JM, De Virgilio C, De Moor B, Winderickx J (2005) PKA and Sch9 control a molecular switch important for the proper adaptation to nutrient availability. *Mol Microbiol* **55:** 862-880

Rubenstein EM, Schmidt MC (2010) The glucose signal and metabolic p[H+]lux. *EMBO J* **29:** 2473-2474

Rudra D, Warner JR (2004) What better measure than ribosome synthesis? *Genes Dev* **18:** 2431-2436

Smets B, De Snijder P, Engelen K, Joossens E, Ghillebert R, Thevissen K, Marchal K, Winderickx J (2008) Genome-wide expression analysis reveals TORC1-dependent and -independent functions of Sch9. *FEMS Yeast Res* **8:** 1276-1288

Smets B, Ghillebert R, De Snijder P, Binda M, Swinnen E, De Virgilio C, Winderickx J (2010) Life in the midst of scarcity: adaptations to nutrient availability in Saccharomyces cerevisiae. *Curr Genet* **56:** 1-32

Stichternoth C, Fraund A, Setiadi E, Giasson L, Vecchiarelli A, Ernst JF (2011) Sch9 kinase integrates hypoxia and CO2 sensing to suppress hyphal morphogenesis in Candida albicans. *Eukaryot Cell* **10:** 502-511

Swinnen E, Wanke V, Roosen J, Smets B, Dubouloz F, Pedruzzi I, Cameroni E, De Virgilio C, Winderickx J (2006) Rim15 and the crossroads of nutrient signalling pathways in Saccharomyces cerevisiae. *Cell Div* **1:** 3

Thorpe GW, Fong CS, Alic N, Higgins VJ, Dawes IW (2004) Cells have distinct mechanisms to maintain protection against different reactive oxygen species: oxidative-stress-response genes. *Proc Natl Acad Sci U S A* **101:** 6564-6569

Toda T, Cameron S, Sass P, Wigler M (1988) SCH9, a gene of Saccharomyces cerevisiae that encodes a protein distinct from, but functionally and structurally related to, cAMP-dependent protein kinase catalytic subunits. Genes Dev 2: 517-527

Tomashek JJ, Graham LA, Hutchins MU, Stevens TH, Klionsky DJ (1997) V1-situated stalk subunits of the yeast vacuolar proton-translocating ATPase. J Biol Chem 272: 26787-26793

Urban J, Soulard A, Huber A, Lippman S, Mukhopadhyay D, Deloche O, Wanke V, Anrather D, Ammerer G, Riezman H, Broach JR, De Virgilio C, Hall MN, Loewith R (2007) Sch9 is a major target of TORC1 in Saccharomyces cerevisiae. Mol Cell 26: 663-674

Wanke V, Cameroni E, Uotila A, Piccolis M, Urban J, Loewith R, De Virgilio C (2008) Caffeine extends yeast lifespan by targeting TORC1. Mol Microbiol 69: 277-285

Wanke V, Pedruzzi I, Cameroni E, Dubouloz F, De Virgilio C (2005) Regulation of G0 entry by the Pho80-Pho85 cyclin-CDK complex. EMBO J 24: 4271-4278

Wei M, Fabrizio P, Hu J, Ge H, Cheng C, Li L, Longo VD (2008) Life span extension by calorie restriction depends on Rim15 and transcription factors downstream of Ras/PKA, Tor, and Sch9. PLoS Genet 4: e13

Wei M, Fabrizio P, Madia F, Hu J, Ge H, Li LM, Longo VD (2009) Tor1/Sch9-regulated carbon source substitution is as effective as calorie restriction in life span extension. PLoS Genet 5: e1000467

Woodsmith J, Jenn RC, Sanderson CM (2012) Systematic analysis of dimeric E3-RING interactions reveals increased combinatorial complexity in human ubiquitination networks. Mol Cell Proteomics 11: M111.016162

Wullschleger S, Loewith R, Hall MN (2006) TOR signaling in growth and metabolism. Cell 124: 471-484

Yorimitsu T, Zaman S, Broach JR, Klionsky DJ (2007) Protein kinase A and Sch9 cooperatively regulate induction of autophagy in Saccharomyces cerevisiae. Mol Biol Cell 18: 4180-4189

Zaborske JM, Wu X, Wek RC, Pan T (2010) Selective control of amino acid metabolism by the GCN2 eIF2 kinase pathway in Saccharomyces cerevisiae. BMC Biochem 11: 29

Addendum

Materials and Methods

25. Media

Throughout this project, different types of media were used to grow yeast cells. In general, growth medium was always autoclaved before use. For the carbon sources for yeast growth medium, sterile glucose (dextrose), galactose and lactate stock solutions (40% w/v) were prepared separately, and added to the growth medium, to the appropriate final concentration, after autoclavation. Ethanol was added after autoclavation from a 100% pure stock solution. Glycerol was added to the medium before autoclavation. Unless stated otherwise, 2% dextrose was as the carbon source for yeast media, and % indicates w/v throughout the materials and methods section.
Solid medium was obtained by adding 1.4% agar to the solutions before autoclaving.

25.1. YP medium

Yeast extract peptone (YP) medium was prepared by dissolving 1% yeast extract and 2% peptone in distilled H_20. For some experiments, YP medium was buffered at a certain pH and/or specific components were added. The used components and their concentrations are listed in the table below (Table 4). For buffering, the media was dissolved in 50mM HEPES and 50mM MOPS, after which the pH was adjusted using 1 M HCl or 4 M KOH.

Table 4: Table of components added to YP, with their corresponding concentrations.

Component	concentration
Glucose (D, dextrose)	2%
Galactose (Gal)	3%
Glycerol (Gly)	3%
EtOH	2%
lactate	0.3% 3%
$CaCl_2$	60 mM 150 mM
NaCl	1 M
KCl	1 M
Rapamycin geneticine clonNAT	50 nM 150 $\mu g.\mu L^{-1}$ 100 $\mu g.\mu L^{-1}$
Hygromycin	200 $\mu g.mL^{-1}$
Ampiciline	100 mg.mL

25.2. Sporulation medium

Sporulation medium was generated by dissolving 1% KAc and 0.1% $KHCO_3$, and adjusting the pH to 6.5 with 1 M HCl.

25.3. Synthetic (S) medium

In addition to rich (YP) medium, yeast cells can be grown on synthetic defined medium, for which specific components can be omitted if desired. The basis of synthetic medium is made up by adding 0.19% yeast nitrogen base (YNB) without amino acids, nucleotides and $(NH_4)_2SO_4$ to 0.5% $(NH_4)_2SO_4$. For complete growth medium (used in longevity experiments), a complete supplement mixture (CSM) is added, containing a full complement of amino acids and nucleotides. Strains containing plasmids carrying auxotrophic markers are grown on specific drop-out medium, lacking the specific component which is complemented by the auxotrophic marker on the plasmid. Additional compounds were omitted in the Y2H experiment, in which an additional lack of histidine or adenine is used to test for physical interaction between proteins (see section Yeast two-hybrid (Y2H)). A summary of the different drop-out media used, and the CSM formulas used for their preparation is listed in Table 5. The carbon source used in these experiments was 2% glucose (dextrose, D), hence the annotations SD-x.

Table 5: Selective drop-out media used during the experiments.

MEDIA (SD –x)	CSM and additional supplements used
SD -Trp	0.74 g/L CSM -Trp
SD -Leu	0.69 g/L CSM-Leu
SD -Trp-Leu	0.59 g/L CSM -Ade-His-Leu-Trp-Ura + 50 mg/L Ura + 100 mg/L His + 50mg/L Ade
SD -Trp-Leu-His	0.59 g/L CSM -Ade-His-Leu-Trp-Ura + 50 mg/L Ura + 50mg/L Ade
SD -Trp-Leu-Ade	0.59 g/L CSM -Ade-His-Leu-Trp-Ura + 50 mg/L Ura + 100 mg/L His
SD-Ura	0.77 g/L CSM -Ura
SD complete	0.74 g/L CSM –Trp + 100mg/L Trp

25.3.1. LB medium

E. coli was cultivated in LB medium, which is prepared by dissolving the following components in MilliQ H_2O: 10 $g.L^{-1}$ tryptone, 5 $g.L^{-1}$ yeast extract, 10 $g.L^{-1}$ NaCl. Before autoclaving the pH was adjusted to 7,5.

26. Tetrad analysis

This experiment was carried out in *S. cerevisiae* yeast cells derived from the BY4741 background with the genotypes summarized in Table 1.

26.1. Crossing

In order to develop diploids, single colonies of the haploid *sch9*Δ (Mat**α**) and *vma*Δ (Mat**a**) strains listed above (Table 1) were inoculated in YPD medium and incubated overnight at 30 °C, shaking at 200 rpm. The *sch9*Δ (Mat**α**) strain was crossed with the *vma*Δ (Mat**a**) strains by adding 200µL of the *sch9*Δ strain to 200µL of each *vma*Δ strain in fresh 3 mL YPD. Subsequently, these mixtures were incubated for eight hours at 30 °C, shaking at 200 rpm. To select diploids, 10 µL of each mixture was spread on YPD plates containing geneticin and clonNAT. The plates were incubated for 3 days at 30 °C.

26.2. Sporulation

Single colonies of the generated diploids were inoculated in YPD medium and incubated at 30 °C, shaking at 200 rpm. After eight hours, the cells were harvested by centrifugation at 3000 rpm for 4 minutes (min), at room temperature (RT). The supernatant was discarded and 20 µL of the pellet was spotted onto sporulation plates. The cells were incubated for 3 to 6 days at RT. Ascospore formation was confirmed with the light microscope and tetrad analysis was performed.

26.3. Separation of tetrads

Cells were dissolved in 45 µL of sterile Milli-Q water. After adding 5 µl of a 2 $\mu g.\mu L^{-1}$ solution of lyticase, the samples were incubated for 7 min and 30 seconds (s) at RT, and then 15 µL of each solution was spread over a straight line on a YPD plate. Finally the tetrads were separated with a micromanipulator and incubated for 2 to 4 days at 30 °C.

26.4. Genotyping

To investigate the genotype of the tetrads, a small amount of each colony was spread out on two types of YPD plates, one type containing geneticin and the other one with clonNAT. The YPD plates were incubated for 3 days, at 30 °C.

27. Gap repair cloning of Yeast two-hybrid (Y2H) vectors

After confirming the genetic interaction between *SCH9* and the *VMA* genes, Y2H was performed to screen the Vma proteins for physical interaction with the Sch9 protein. The used protocol is based on the protocol described by Woodsmith *et al.*(Woodsmith et al, 2012).

27.1. Generating the Y2H-*VMA* vectors

The Y2H-*VMA* vectors were constructed via the *in vivo* Gap repair method. In order to perform *in vivo* Gap repair, the 'destination' vectors (pGBAE-B and pACTBE-B) are linearized and co-transformated into yeast with inserts, comprising of the *VMA* coding sequences, flanked by the *att*B1 and *att*B2 recombination sites (Fig. 29). The Y2H vectors containing *SCH9* and *PKH1* were already present in the lab.

27.1.1. Plasmid purification

E. coli cells transformed pGBAE-B and pACTBE-B vectors (containing the ampicillin resistance marker) were grown overnight in 3 mL LB medium containing ampicillin at 37 °C, shaking at 200 rpm. The next day, the vectors were purified with the Fast Plasmid™ Mini Kit-5 Prime. The *E. coli* cultures were pelleted (13 000 rpm, 1 min, RT) and the supernatant removed. 400 µL of ice-cold complete lysis solution was added to the pellet and the samples were mixed thoroughly by constant vortexing at the highest setting for 30 s. Subsequently, the lysate was incubated for 3 min at RT and transferred to a spin column assembly for centrifugation (maximal speed, 1 min, RT). 400 µL of the diluted wash buffer was added to the spin column assembly and the latter was centrifuged (maximal speed, 1 min, RT). Thereafter, the filtrate was discarded from the waste tube and the spin column was placed back into the waste tube. To dry the spin column, another centrifugation step (maximal speed, 1 min, RT) was performed. Finally, the spin column, on which the vectors were bound, was transferred to a collection tube and 50 µL of elution buffer was added to the center of the spin column. The plasmid DNA was eluted from the spin column via centrifugation (maximal speed, 1 min, RT) and the concentration was measured with a spectrophotometer (Eppendorf Bio Photometer).

27.1.2. Linearization of vectors

The plasmids were linearized by adding 2 µg of plasmid DNA to 1 µL of 10x BamHI buffer, 2 µL of restriction enzyme BamHI and topping the mix up to 10 µL with H_2O. These samples were incubated for 1 hour at 37 °C. To isolate the cut DNA, the samples were loaded on a gel containing 1% low-melting point agarose in 0.5x TAE (stock 10x TAE, Table S1). The samples, mixed with 1x loading buffer (stock 6x loading buffer, Table S1), were transferred into the wells of the gel, as well as a smart ladder. Electrophoresis was done at 100 V.

27.1.3. DNA purification from agarose gel

Two microcentrifuge tubes were weighed, the DNA bands cut out of the gel and placed into the tubes. These tubes were weighed again to determine the net weight and subsequently, 1/10 volumes of 1x β-agarase buffer (New England Biolabs) was added. The gel was melted by incubating the samples for 15 min at 70 °C and cooled down by placing the samples for 15 min at 45 °C. To breakdown agarose, 2 units of β-Agarase (New England Biolabs) per

200 µL was added to the mixture and incubated for 1 hour at 45 °C. The DNA concentration was measured with a spectrophotometer (Eppendorf Bio Photometer).

27.1.4. Construction of inserts

To be able to insert the genes coding for the Vma prey proteins into the vectors, the *VMA* coding sequences have to be flanked by the *att*B1 and *att*B2 recombination sites, in order for recombination ("Gap repair") to take place in the yeast cell. Therefore, primers were designed to contain both the desired *att*B1/2 sequences, as well as the sequences required to clone the coding VMA sequence by PCR, using genomic DNA as a template. The designed primers are presented in Table S2. PCR was performed by using the mixtures and program specified in Table S3. To verify whether the PCR succeeded, agarose gel electrophoresis was performed (protocol see section 27.1.2 except normal agarose was used).

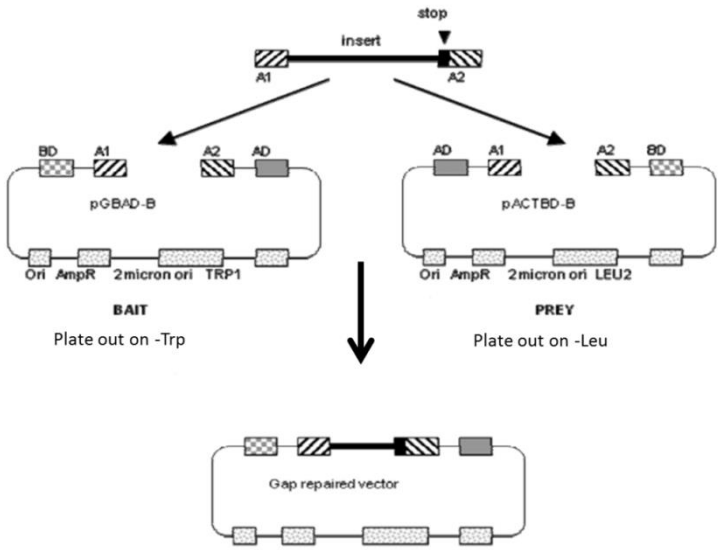

Figure 29: Schematic representation of the gap repair reaction which happens in the yeast strains transformed with the inserts and linearized vectors.

27.1.5. Gap repair reaction

To anneal the *VMA* inserts to the linearized pGBAE-B and pACTBE-B vectors, yeast cells were transformed with the above generated linearized vector and PCR products.

PJ69-4a and PJ69-4α yeast cells were inoculated in 3 mL YPD and grown overnight at 30 °C, shaking at 200 rpm. The next day, the precultures were diluted in 50mL YPD to OD_{600} 0.5 and incubated for 5 hours at 30 °C. To harvest the cells the cultures were transferred in a sterile 50 mL Falcon tube and centrifuged (2300 rpm, 5 min, RT). After removing the supernatant, the cells were dissolved in 1 mL fresh 0.1 M LiAc and transferred in

microcentrifuge tubes. The cultures were washed twice by precipitating the cells, resolving them in 1 mL 0.1 M LiAc and repeating these steps. After the final wash, the supernatant was removed and the cells were resuspended in the following master mix: 460 µL 50% PEG 3350, 70 µL 1 M LiAc, 90 µL distilled H_2O, 20 µL 10,5 $mg.mL^{-1}$ ssDNA (heat denatured for 5 min at 95 °C) and 2 µL of the BamHI linearized DNA. This mix provides sufficient master mix for 20 reactions. The master mixes were vortexed thoroughly and 32 µL was transferred into sterile PCR tubes. 4 µL of each *VMA* insert PCR product was added to a different tube and the solution was mixed by aspiration with a pipette (Table 6). As a control, also 4 µL of H_2O was added to one tube with the master mix. The samples were incubated in a PCR machine for 30 min at 30 °C, for 25 min at 42 °C and for 1 min at 30 °C. Finally, the cells were plated out on selective SD medium (see Table5) and incubated 3 to 5 days at 30 °C.

Table 6: Representation of the insert PCR products and linearized vectors that were transformed into a specific strain. These were plated out on the specified selective media

Strain	Insert product	Vector	SD medium
PJ69-4a	*VMA1*, *VMA2*, *VMA3*, *VMA4*, *VMA5*, *VMA6*, *VMA7*, *VMA8*, *VMA10*, *VMA13*, *VMA16*, *VPH1* and *STV1*	pGBAE-B	SD-Trp
PJ69-4α	*VMA1*, *VMA2*, *VMA3*, *VMA4*, *VMA5*, *VMA6*, *VMA7*, *VMA8*, *VMA10*, *VMA13*, *VMA16*, *VPH1* and *STV1*	pACTBE-B	SD-Leu

27.1.6. Colony PCR to confirm insert size

With a pipette tip, a small amount of a colony was dipped into 3 µL of 0.02 M NaOH in PCR tubes. This was done for 2 colonies per transformation. The PCR mixture described in Table S3 was added to the PCR tubes and the PCR reaction was performed using the program also elaborated in Table S3. Subsequently, agarose gel electrophoresis was performed to visualize the PCR product (protocol see section 27.1.2).

28. Genomic tagging of *VMA* genes and Western blot

28.1. Creating chromosomal VMA-Myc fusions

The primers to create the PCR product, necessary to tag the genes encoding the V_1 subunits and *VMA6* with the 9Myc epitope at their C-terminus, were designed via the method explained in Janke *et al*. (Janke et al, 2004) and are listed in Table S4. As a template for the PCR reaction, a plasmid was used containing the coding regions for both the 9Myc epitope as well as a hygromycin marker. The PCR mix and reaction conditions are shown in Table S3. Agarose gel electrophoresis was carried out to determine whether the PCR reaction had succeeded (protocol see section 27.1.2).

28.2. Genomic transformation

The DNA fragments, generated by PCR, were transformed into the *SCH9*/*sch9*Δ heterozygous diploid strain. For this, a preculture of the diploid strain was diluted to OD_{600} 0.5 in 50 mL YPD and left to grow for 4 hours at 30 °C, shaking at 200 rpm. Subsequently, the culture was centrifuged (3000 rpm, 5 min, RT) and the pellet was resuspended in 1 mL of fresh 0.1 M LiAc. The cells were transferred into a microcentrifuge tube, precipitated (2000 rpm, 2 min, RT) and after resuspending them in 500 µL of 0.1 M LiAc, they were incubated for 10 min at RT. Meanwhile single strand salmon sperm DNA (ssDNA) (10 $mg.mL^{-1}$) was boiled for 5 min at 95 °C and kept on ice. After the ten minutes, 300 µL of PLi solution (1 mL of 1M LiAc, 1 mL sterile H_2O, 8 mL 3350 PEG 50%), 5 µL of ss DNA, 50 µl of the PCR product and 50 µl of cells were brought together in a fresh microcentrifuge tube. This solution was vortexed for 10 seconds and incubated for 20 to 30 min at 42 °C to heat shock the cells. Subsequently, the microcentrifuge tubes were centrifuged (3000 rpm, 3 minutes, RT) and a recovery step was performed as follows: The cells were resolved in 1mL YPD and incubated for 4 hours at 30°C, shaking at 200 rpm. Finally, the cells were precipitated (3000 rpm, 3 minutes, RT) and resuspended in 100 µL sterile H_20. The cells were then plated out on YPD plates containing hygromycin and incubated for 3 to 5 days at 30°C.

28.3. Determination of successful genomic transformation

Control PCRs were performed by dissolving the cells in 3 µL of NaOH (0.02 M) and adding the PCR mix displayed in Table S3 and following the corresponding program. These PCRs verified whether the Myc-tags were inserted correctly at the C-terminus of the *VMA*s. The first control PCR identified the presence of VMA-S3 at the C-terminal end of the *VMA*-gene, while the second control PCR determined the presence of VMA-S2 before the *VMA*-gene terminator (Fig. 30).

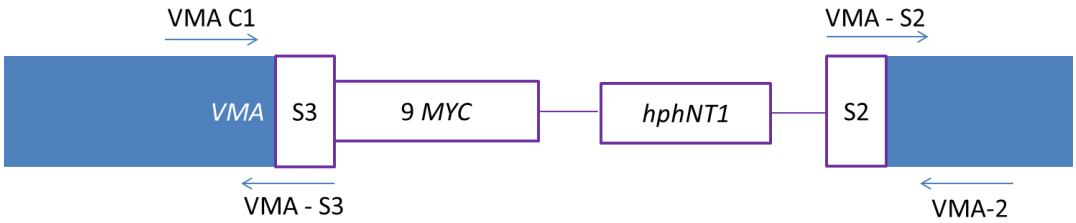

Figure 30: Schematic representation of the two performed control PCRs to check correct integration of the Myc tag at the C-terminal end of the VMA *genes. Control PCR1 is performed by combining the primers VMA C1 with VMA-S3, while the second control PCR uses the VMA-S2 and VMA-2 primers.*

After the correct integration of the Myc-tags was confirmed, the Myc-tagged diploid cells were sporulated (protocol see section 26.2) and the ascospores were separated via the tetrad analysis technique (protocol see section 26.3). To identify the tagged *VMA* genes in WT and *sch9*Δ cells, a small amount of each haploid spore was spread out on YPD plates containing

hygromycin (presence of tagged *VMA* gene) or YPD plates supplemented with ClonNat (presence of deletion of *SCH9*). The plates were incubated for 3 days at 30°C.

28.4. Protein extraction

Precultures of WT and *sch9*Δ cells expressing Vma-Myc proteins, and as control a WT strain (without Myc-tagged proteins), were were diluted to OD_{600} 0.5 in 20 mL YPD, and grown to OD_{600} 2 at 30 °C, shaking at 200 rpm. To investigate the effect of glucose deprivation on phosphorylation of the Vma proteins, 10mL of the OD_{600} 2 cultures was precipitated (3000 rpm, 3 min, RT), resuspended in 10 mL YP (no C-source) and incubated for 30 min at 30°C, shaking at 200 rpm. The following steps were performed on ice: The resulting cultures were centrifuged (3000 rpm, 3 min, 4 °C) and the pellet was dissolved in 1 mL 20% trichloroacetic acid (TCA). Subsequently, the solutions were transferred to FastPrep tubes and the cells were pelleted (3000 rpm, 3 min, 4 °C) again. The pellet was resuspended in 250 µL 20% TCA and vortexed. Glass beads were added and after 5 min, the cells were lysed using the MP FastPrep®-24 machine, for 20s at speed 6. The lysate was transferred to clean microcentrifuge tubes and the beads were washed twice by adding 500 µL of 5% TCA and vigorous vortexing. The total lysate was centrifuged for 15 minutes at maximal speed. The resulting pellet was washed twice with 750 µL cold acetone. Finally, the pellet (containing the cellular proteins) was air-dried and resuspended in 100 µL 1 M Tris buffer pH 8.

28.5. Protein quantification

The concentrations of the extracted proteins were quantified via the Bradford assay. To start, the Bradford Reagent was diluted 5x in H_2O and a standard series of known BSA concentrations was prepared by adding 1 µL of 1, 2, 3, 4, 6 and 8 $mg.mL^{-1}$ BSA in 1 mL the diluted Bradford reagent. Subsequently, 2 µL of each protein extract was transferred to a microcentrifuge tube containing 1 mL of the diluted Bradford reagent. All the samples were vortexed vigorously and the absorbance at 595 nm was measured with a spectrophotometer (Eppendorf Bio Photometer) after the sample with 8 $mg.mL^{-1}$ BSA turned bright blue. The absorbance values of the standard series were used to establish a standard curve, which is used to calculate the concentrations of the protein extracts.

28.6. Western blotting

All the protein extracts were diluted in 1 M Tris buffer pH8 and 1x sample buffer (stock 5x loading buffer, Table S1), so that the same amount of each protein extract (10 µg) would be loaded on the gels.

28.6.1. Western blot with normal gels

The running gel was prepared as indicated in Table 7, APS and TEMED were added just before pouring the gels between two cleaned glass plates. In order to obtain an smooth surface, a small amount of isopropanol was put on the top of the gel. Once the running gel was set, the isopropanol was washed away with water and the stacking gel was added on the top of the running gel. A comb was immediately inserted in the stacking gel and left to solidify.

Table 7: Protocol for the preparation of gels for Western blot. These quantities are for the preparation of two gels.

Product	**7,5% Running gel for normal gels**	**7,5% Running gel for phostag gels**	**10% Stacking gel**
30% Acrylamide	2,5 mL	2,5 mL	0,75 mL
1 M Tris-HCl (pH 8,8)	3,75 mL	3,5 mL	
0,25 M Tris-HCl (pH 6,8)			2,5 mL
10% SDS	100 µL	100 µL	50 µL
H_2O	3,6 mL	3,6 mL	1,5 mL
5 mM Phostag		50 µL	
10 mM $MnCl_2$		50 µL	
APS	100 µL	140 µL	30 µL
TEMED	15 µL	20 µL	10 µL

To perform the gel electrophoresis, the combs were removed and the gels were brought in running boxes filled with 1x running buffer (Table S1). The protein samples were boiled for 5 min at 95 °C and 10 µL was loaded in the wells. A Precision Plus Protein™ Standards ladder (BIO-RAD) was also loaded on each gel, so the molecular weight of the detected proteins could be determined. The gels were run at 25 mA/gel and the applied running time was dependent on the molecular weight (MW) of the protein.

Subsequently, the proteins were transferred from the gel to a Millipore Immobilon- P transfer (PVDF) membrane. For each protein transfer, 2 sponges and 2 Whatman papers (6,5 x 9,5 cm) were immersed in 1x blotting buffer (Table S1) and a PVDF membrane (6 x 9 cm) (activated by soaking in 100% MeOH). The blotting cassette was prepared as follow: On the white side an immersed sponged was placed, followed by respectively a Whatman paper, PDVF membrane, the gel, again a Whatman paper and finally a sponge. The blotting cassette was brought into a transfer box filled with 1x blotting buffer. To prevent overheating during the transfer, a small box filled with ice was placed next to the cassette. The transfer was performed for 90 min at a constant amperage of 300 mA.

After the transfer, the membranes were immersed in 5% milk powder dissolved in 1x TBST-buffer for 1 hour. Subsequently, the membranes were incubated with the primary antibody (Table S1) overnight at 4 °C. The following day, the membranes were washed 4 times for 5

minutes in 1x TBST- buffer and thereafter incubated for 1 hour at RT with the secondary antibody (Table S1) diluted in 1x TBST- buffer. Finally, the membrane was washed 4 times for 5 minutes in 1x TBST- buffer and the signal was detected with the pico-kit (Thermo Scientific) by mixing 2 mL stable peroxide and 2 mL lumonil/Enhancer solution and immersing the membrane in this mixture. The signal was detected with the multi-spectral imaging system machine (Biospectrum Imaging System, UVP).

28.6.2. Western blot with phostag gels

The running gel was prepared as indicated in Table 6 on ice, APS and TEMED were added just before pouring the gels between two cleaned glass plates. The next steps of gel preparation and gel electrophoresis are similar to the protocol of regular gels (see 5.6.2), only here, the gels were at 20 mA/gel and the applied running time was dependent on the molecular weight (MW) of the protein

To activate the PVDF membrane (6 x 9 cm), the latter was immersed respectively 15 s in MeOH, 2 min in H_2O and 15 min in 1x transfer buffer. After gel electrophoresis, the gels were incubated respectively 2 times 10 min in 1x transfer buffer containing 1 mM EDTA and 10 min 1x transfer buffer. Per gel, 2 sponges and 2 Whatman papers (6,5 x 9,5 cm) were immersed in 1x transfer buffer. The composition of the blotting cassette and the following steps were done as described in 5.6.1.

29. Co-immunoprecipitation (Co-IP)

To confirm the physical interaction between Vma6 and Sch9, a Co-IP experiment was performed. To be able to immunoprecipitate the potential binding partners, the Vma6-Myc protein is required, as well as an immunotagged version of Sch9. For the latter, we made use of a plasmid encoding a HA-tagged version of Sch9, which allows us to detect or precipitate this protein with the anti-HA antibody. Preparation of the buffers used in this specific experiment are described in Table 8.

Table 8: Content of buffers used during Co-IP.

Product	**Lysis buffer**	**Wash buffer**
Triton X-100	1%	0,1%
NaCl	120 mM	120 mM
Tris-HCl (pH 7,4)	50 mM	50 mM
EDTA	2 mM	2 mM
Glycerol	10%	
Protease inhibitors: • Complete (Roche) • PMSF	 1 tablet /10 mL 1 mM	

29.1. Yeast transformation with plamids

The plasmid encoding the HA-Sch9 protein was transformed into the *sch9*Δ *VMA6*-Myc strain. As a negative control, the empty vector was transformed into the *sch9*Δ *VMA6*-Myc strain and the HA-Sch9 plasmid into *sch9*Δ strain.

For the transformation, precultures of the required strains diluted to OD_{600} 0.5 in 50 mL YPD and left to grow for 4 hours at 30 °C, shaking at 200 rpm. Subsequently, the cultures were centrifuged (3000 rpm, 5 min, RT) and the pellet was resuspended in 1 mL of fresh 0.1 M LiAc. The cells were transferred into a microcentrifuge tube, precipitated (2000 rpm, 2 min, RT) and after resuspending them in 500 µL, they were incubated for 10 min at RT. Meanwhile single strand salmon sperm DNA (ssDNA) (10 $mg.mL^{-1}$) was boiled for 5 min at 95 °C and kept on ice. Next, 300 µL of PLi solution (1 mL of 1M LiAc, 1 mL sterile H_2O, 8 mL 3350 PEG 50%), 5 µL of ss DNA, 2µg of plasmid and 50 µl of cells were brought together in a fresh microcentrifuge tube. This solution was vortexed for 10 seconds and incubated for 20 to 30 min at 42 °C to heat shock the cells. Subsequently, the microcentrifuge tubes were centrifuged (3000 rpm, 3 minutes, RT) and the cells were resuspended in 100 µL sterile H_20. The samples were plated out on the corresponding selective media and incubated for 3 to 5 days at 30°C (Table 9). Note that Table 8 also displays the transformations used in the fluorescence studies.

Table 9: Scheme of the strains, plasmids and selective media used for transformation.

Strains	Plasmids	Selective media
WT VMA6-Myc	pRS416-HA-Sch9	SD-Ura
*sch9*Δ VMA6-Myc	pRS416-HA-Sch9	SD-Ura
*sch9*Δ VMA6-Myc	pRS416	SD-Ura
*sch9*Δ	pRS416-HA-Sch9	SD-Ura
WT, *sch9*Δ, *vma2*Δ, *vma3*Δ, *vma5*Δ *and vma6*Δ	Vph1-GFP	SD-Leu
WT, *sch9*Δ, *vma2*Δ, *vma3*Δ, *vma5*Δ *and vma6*Δ	GFP-Sch9	SD-Ura

29.2. Preparation of yeast protein extracts for Co-IP

Precultures of the generated strains were diluted to OD_{600} 0.5 in fresh SD-Ura media and incubated at 30 °C, shaking at 200 rpm. Once the cells had grown to OD_{600} 2, they were harvested via centrifugation (3500 rpm, 5 min, 4 °C). The cells were resolved in ice-cold 1M PBS buffer pH 7.4 and transferred into a microcentrifuge tube. The metabolism of the cultures was stopped by performing all the following steps on ice and keeping all solutions on ice. To wash the cells two times, they were resuspended in 500 µL ice cold 1 M PBS buffer pH 7.4, vortexed and precipitated (3500 rpm, 5 min, 4 °C). Subsequently, the pelleted cells were resuspended in 250 µL of lysis buffer Table 8 and transferred to a Fastprep tube

containing glass beads. The cells were shaken vigorously 4 times with MP FastPrep®-24 machine for 30s at speed 6 and with intervals of 1 minute on ice. The Fastprep tubes were centrifuged (3500 rpm, 5 min, 4 °C) and the supernatant transferred to a microcentrifuge tube. A second centrifugation step (13 000 rpm, 30 min, 4 °C) was performed, and the supernatant (protein extract) was transferred into a new microcentrifuge tube.

29.3. Protein quantification

The concentrations of the proteins were measured via the Bradford method (protocol see section 28.5.) and the protein extracts were diluted to 1 mg.

29.4. Immunoprecipitation

For immunoprecipitation, anti-HA or anti-Myc antibodies (Table S1) were added to 500 µL of the diluted extract and incubated for 4 hours at 4°C, with rotation. Meanwhile, Protein G Dynabeads® (Invitrogen) were prepared as follows: for each sample, 50 µL of the magnetic beads were washed 5 times with ice-cold 500 µL wash buffer and after 500 µL lysis buffer. Washing was done via separating the beads from buffer with a magnetic particle separator, discarding the buffer and adding fresh buffer. It is recommended to cut off the top of the tip while dissolving the beads to minimize disruption of the beads. Subsequently, the beads were added to each protein extract sample and these solutions were incubated overnight at 4 °C. The beads were collected and washed twice with 500 µL lysis buffer and twice with wash buffer, the same way as above. After the last wash, the beads were resuspended in 50 µL of 1x sample buffer (stock 5x sample buffer, Table S1), mixed gently and boiled for 10 min at 95 °C. The magnetic beads and the immunoprecipitated protein samples were separated with the magnetic particle separator and the samples were kept on ice.

29.5. Western blot

To detect the proteins (Vma6-Myc and HA-Sch9) present after immunoprecipitation, Western blot using regular gels was performed. Both set of samples, one in which the pull-down was performed with the anti-HA antibody, as well as the second in which the pull-down was performed with the anti-Myc antibody, were blotted with anti-Myc and anti-HA antibody (protocol see section 28.6.1.).

30. Fluorescence study

To investigate the vacuolar morphology and localization of Sch9, the WT, *sch9*Δ, *vma2*Δ, *vma3*Δ, *vma5*Δ and *vma6*Δ strains cells were transformed with Vph1-GFP and GFP-Sch9 plasmids and studied under the microscope.

30.1. Generating strains with Vph1-GFP and GFP-Sch9 plasmids

The transformation of Vph1-GFP and GFP-Sch9 plasmids into WT, *sch9*Δ, *vma2*Δ, *vma3*Δ, *vma5*Δ and *vma6*Δ strains was executed as described in section 29.1. (see also Table 9).

30.2. FM4-64 staining

The transformed cells were inoculated in the associated SD medium (Table 9) and grown to stationary phase at 30°C, shaking at 200 rpm. Thereafter, the precultures were diluted to OD_{600} 0.5 in fresh SD medium and incubated at 30°C, shaking at 200 rpm, until the cells were grown to OD_{600} 2.0.

To stain the cells with N-(3-triethylammoniumpropyl)-4-(ρ-diethylaminophenylhexatrienyl)-pyridinium dibromide (FM4-64), 50µL of the cultures was transferred into a microcentrifuge tube and 2 µl of FM4-64 was added. After an incubation period of 30 min in the dark at RT, the cells were pelleted (3000 rpm, 4 min, RT) and washed with 100 µL of the corresponding SD medium. Finally, the cells were resupsended in 50 µl of SD media and visualized with the fluorescence microscope.

31. Longevity

In order to investigate whether the genetic interaction between *vma*Δ and *sch9*Δ strains has an effect on yeast life span, *vma2*Δ, *vma2*Δ*sch9*Δ, *vma6*Δ and *vma6*Δ*sch9*Δ strains were selected and their superoxide levels were measured. In addition, the CLS of these strains was determined by measuring the survival during the stationary phase. The WT and *sch9*Δ were also included in this experiment, as control.

31.1. Cultivation of the cells

Four single colonies of each strain were inoculated in SD complete medium and grown to stationary phase at 30 °C, shaking at 200 rpm. To dilute the precultures so that they would reach the exponential phase simultaneously the following day, WT, *sch9*Δ, *vma*Δ and *vma6*Δ*sch9*Δ strains were diluted respectively to OD_{600} 0,005; 0,05; 0,05 and 0,1 in SD complete medium. We determined the first day in stationary phase as the day following the day in which the cells were growing exponentially.

31.2. DHE measurements

Superoxide levels were quantified through by measuring the fluorescence intensity of Dihydroethidium (DHE), a fluorescent probe which is thought to be specifically activated through reaction with superoxide molecules. To quantify the superoxide levels with a micro plate reader, the OD_{600} of the cells was measured with a spectrophotometer (Eppendorf Bio Photometer). This value was used to calculate the volume needed for an amount of 5×10^6 cells. For each culture, the calculated volume was transferred into 2 microcentrifuge tubes

and centrifuged (10 000 rpm, 2 min, RT). The supernatant was removed and in the first microcentrifuge tube 250 µL of 5 $\mu g.\mu L^{-1}$ DHE (stock 2.5 $mg.mL^{-1}$, Table S1), dissolved in PBS buffer (pH 7.0) was added, and in the second tube 250 µL of PBS, as blank. The dye were incubated for 30 min at 30 °C in a dark environment. Next, the cells were precipitated (10 000 rpm, 2 min, RT) and washed with 250 µL PBS. The cells were resuspended in 250 µL PBS and 200 µL of each sample was transferred into a black microtiter plate with a clear bottom. A micro plate reader (DXT 880 Multimode Detector, Beckman) was used to measure the fluorescence at excitation/emission wavelengths of 535/595 nm. Finally, the OD was also determined by measuring the absorbance at 595 nm. Once the cells had reached stationary phase, the procedure was performed with 100 µL of cells, instead of calculating the volume needed for 5 x 10^6 cells. The DHE measurements were repeated the 1^{st}, 3^{rd}, 6^{th} and 9^{th} day of stationary phase.

Except the dilution factor, the same steps of sample preparation were followed for DHE measurements with a flow cytometer (Guava easyCyte™ Flow Cytometer). For this assay, the final dilution of cells is an OD of 0.04 in PBS, of which the red fluorescence was determined. Data were analyzed using the FlowJo software to determine the percentage of DHE positive cells.

31.3. Survival – Colony formation units (CFUs)

To study the survival of the strains, colony forming units (CFUs) were determined on the first day the strains reached the stationary phase (designated as day 0). this was done as follows: The cultures were diluted to OD_{600} 1, after which three times a 20 fold serial dilution was made in microcentrifuge tubes, yielding a final OD of 0.000125 in sterile H_2O. Subsequently, 400 µL of the latter suspensions were plated out on YPD plates. The plates were incubated for 4 days at 30 °C and the colony formation unit (CFU) was determined by counting the amount of colonies on the plates. This procedure was repeated on the 1^{st}, 3^{rd}, 6^{th} and 9^{th} day after the cells reached the stationary phase. The CFU count of cultures at day 0 were set to 100% for each culture and subsequent CFU counts were expressed as percentages of this value.

Supplementary tables

Table S1: description of the solutions used throughout this project.

Component	Description
10x TAE	24.2% Tris-HCl 5.71% acetic acid 3.72% EDTA, pH 8.0
6x Loading buffer	62,5 mM Tris-HCl (pH 6,8) 2% SDS 10% glycerol 0,01% bromophenol Blue
5x sample buffer	250 mM Tris pH 8,0 10% SDS 0.5% bromophenol blue 50% glycerol 50 mM β-mercaptoethanol
5x running buffer	15,1 g Trizma 94 g glycine 5 g SDS dissolved 1 L H_2O
Blotting buffer for normal gels	200 mL running buffer (5x) 200 mL 100% methanol 600 mL H_2O
PBS buffer pH 7,4	137 mM NaCl 2,7 mM KCl 10 mM $Na_2HPO_4.2H_20$ 2.0 mM KH_2PO_4
10x TBS	1.5 M NaCl 0.25 M Tris, pH 8
1x TBST	1x TBS 0.05% Tween 20
Rabbit Anti-Adh2	1/ 10 000 dilution in 5% milk powder (TBST)
Mouse Anti-Myc	1/ 1000 dilution in 5% milk powder (TBST)
Goat anti-mouse peroxidase (GAMPO)	1/ 10 000 in 5% milk powder (TBST)
Goat anti-rabbit peroxidase	1/ 1000 in 5% milk powder (TBST)
CoIP Rabbit Anti-HA antibody	1/1000 in lysate
CoIP Mouse Anti-Myc antibody	1/40 in lysate
10x transfer buffer for phostag gels	30.295 g Trizma 144.13 g glycine dissolved 1 L H_2O
DHE	2.5 $mg.mL^{-1}$ in EtOH

Table S2: Primers used for construction and verification of Y2H-VMA vectors.

Name	Gene	Sequence	Used for
vma1 Fw	*VMA1*	**GGGGACAAGTTTGTACAAAAAAGCAGGCTCC** ATGGCTGGTGCAATTGAAAACG	Construction of pGBAE-B-VMA1/ pACTBE-B-VMA1
vma1 rv stop	*VMA1*	**GGGGACCACTTTGTACAAGAAAGCTGGGTC** TTAATCGGTAGATTCAGCAAATC	
VMA1 C1	*VMA1*	CTTGCAACAAAATGGTTACTCC	
vma2 Fw	*VMA2*	**GGGGACAAGTTTGTACAAAAAAGCAGGCTCC** ATGGTTTTGTCTGATAAGGAGTTG	Construction of pGBAE-B-VMA2/ pACTBE-B-VMA2
vma2 rv stop	*VMA2*	**GGGGACCACTTTGTACAAGAAAGCTGGGTC** TTAGATTAGAGATTCTTCTTGGC	
vma2 C1	*VMA2*	ATCGGTAAGGACGCTGCTGC	
vma3 Fw	*VMA3*	**GGGGACAAGTTTGTACAAAAAAGCAGGCTCC** ATGACTGAATTGTGTCCTGTCTA	Construction of pGBAE-B-VMA3/ pACTBE-B-VMA3
vma3 rv stop	*VMA3*	**GGGGACCACTTTGTACAAGAAAGCTGGGTC** TTAACAGACAACATCTTGAGTAG	
vma3 C1	*VMA3*	TATTCGTTGGGTCAAAAGCAAGC	
vma4 Fw	*VMA4*	**GGGGACAAGTTTGTACAAAAAAGCAGGCTCC** ATGTCCTCCGCTATTACTGCTT	Construction of pGBAE-B-VMA4/ pACTBE-B-VMA4
vma4 rv stop	*VMA4*	**GGGGACCACTTTGTACAAGAAAGCTGGGTC** TCAATCAAAGAACTTTCTTGTCTTG	
vma4 C1	*VMA4*	GGGAAAAGGCCCAGCGCGC	
vma5 Fw	*VMA5*	**GGGGACAAGTTTGTACAAAAAAGCAGGCTCC** ATGGCTACTGCGTTATATACTGC	Construction of pGBAE-B-VMA5/ pACTBE-B-VMA5
vma5 rv stop	*VMA5*	**GGGGACCACTTTGTACAAGAAAGCTGGGTC** TTATAAATTGATTATATACATCACAAATG	
vma5 C1	*VMA5*	CTTGAGAGTTTACGTGGAATCTG	
vma6 Fw	*VMA6*	**GGGGACAAGTTTGTACAAAAAAGCAGGCTCC** ATGGAAGGCGTGTATTTCAATATT	Construction of pGBAE-B-VMA6/ pACTBE-B-VMA6
vma6 rv stop	*VMA6*	**GGGGACCACTTTGTACAAGAAAGCTGGGTC** TCAATAAACGGAAATATAATTGTTG	
vma6 C1	*VMA6*	CAAGATTTCGAAGGAGTTAGAGC	
vma7 Fw	*VMA7*	**GGGGACAAGTTTGTACAAAAAAGCAGGCTCC** ATGGCTGAGAAACGTACTCTTATA	Construction of pGBAE-B-VMA7/ pACTBE-B-VMA7
vma7 rv stop	*VMA7*	**GGGGACCACTTTGTACAAGAAAGCTGGGTC** TTACTCACCGAACAACTTTCTGA	
vma7 C1	*VMA7*	GTAAGACTACTAAGGAGGAAATC	
vma8 Fw	*VMA8*	**GGGGACAAGTTTGTACAAAAAAGCAGGCTCC** ATGTCTGGTAATAGAGAGCAAGT	Construction of pGBAE-B-VMA8/ pACTBE-B-VMA8
vma8 rv stop	*VMA8*	**GGGGACCACTTTGTACAAGAAAGCTGGGTC** TCAGAATATAACATCGTCTTCTTG	
vma8 C1	*VMA8*	GTTGAAACTTTAGTTGAATTAGCC	
vma10 Fw	*VMA10*	**GGGGACAAGTTTGTACAAAAAAGCAGGCTCC**A TGGTATGTGCCATTACATTACG	Construction of pGBAE-B-VMA10/ pACTBE-B-VMA10
vma10 rv stop	*VMA10*	**GGGGACCACTTTGTACAAGAAAGCTGGGTC** TTACAAGGCATTGATATGGACTTC	
vma10 C1	*VMA10*	AGCCAAGGAAATCGACTCATAC	
vma11 Fw	*VMA11*	**GGGGACAAGTTTGTACAAAAAAGCAGGCTCC** ATGTCAACGCAACTCGCAAGTAA	Construction of pGBAE-B-VMA11/ pACTBE-B-VMA11
vma11 rv stop	*VMA11*	**GGGGACCACTTTGTACAAGAAAGCTGGGTC** TCATTCAGAGCCTCTAGTGTTC	
vma11 C1	*VMA11*	TTGTGGCCGTTTTAATTGCAGG	
vma13 Fw	*VMA13*	**GGGGACAAGTTTGTACAAAAAAGCAGGCTCC** ATGGGCGCAACCAAAATTTTAATG	Construction of pGBAE-B-VMA13/ pACTBE-B-VMA13
vma13 rv stop	*VMA13*	**GGGGACCACTTTGTACAAGAAAGCTGGGTC** TTATTTGAAGGTATATGGAATGATTG	
vma13 C1	*VMA13*	TACAAGATCTTTAGACAATTGATCG	
vma16 Fw	*VMA16*	**GGGGACAAGTTTGTACAAAAAAGCAGGCTCC** ATGAACAAGGAATCTAAAGATGATG	Construction of pGBAE-B-VMA16/
vma16 rv stop	*VMA16*	**GGGGACCACTTTGTACAAGAAAGCTGGGTC**	

		TTACTGAAATTCAGAAGCTTTACC	pACTBE-B-VMA16
vma16 C1	*VMA16*	CGAAATCAAACCTGTACACTGG	
vph1 Fw	*VPH1*	**GGGGACAAGTTTGTACAAAAAAGCAGGCTCC** ATGGCAGAGAAGGAGGAAGCG	Construction of pGBAE-B-VPH1/ pACTBE-B-VPH1
vph1 rv stop	*VPH1*	**GGGGACCACTTTGTACAAGAAAGCTGGGTC** TTAGCTTGAAGCGGAAGAGCTT	
vph1 C1	*VPH1*	GGGTGTGTTTATGACGGTTGC	
stv1 Fw	*STV1*	**GGGGACAAGTTTGTACAAAAAAGCAGGCTCC** ATGAATCAAGAAGAGGCTATATTC	Construction of pGBAE-B-STV1/ pACTBE-B-STV1
stv1 rv stop	*STV1*	**GGGGACCACTTTGTACAAGAAAGCTGGGTC** TTATTCTATTATTGCACGAAATGAAAA	
stv1 C1	*STV1*	TGGGATATGACAATTTCAAACGC	

Table S3: List of PCR mixtures and the corresponding programs used during this study.

Objective of PCR	PCR mix (per sample)	Program
Cloning of *VMA* genes to with simultaneous incorporation of attB1 and attB2 recombination sites (construction of Y2H vectors)	1 µL Forward primer (vma Fw) 1 µL Reverse primer (vma rv stop) 4 µL 5x Phusion HF buffer 2 µL dNTP (10x) 1 µL genomic DNA 0,5 µL Phusion polymerase 11,5 µL H_20	Step 1: 300 s at 95 °C Step 2: 45 s at 95 °C Step 3: 30 s at 56 °C Step 4: x s at 72 °C Step 5: return to step 2 (9x) Step 6: 300 s at 72 °C Step 9: forever at 10 °C
Control PCR: prey insert size	1 µL Forward primer (VMA C1) 1 µL Reverse primer: • pGBAE-B_{rv} • pACTBE-B_{rv} 2 µL KAPA Taq buffer 2 µL dNTP (10x) 0,2 µL KAPA Taq polymerase 11,8 µL H20	Step 1: 300 s at 95 °C Step 2: 60 s at 95 °C Step 3: 60 s at 56 °C Step 4: 60 s at 72 °C Step 5: return to step 2 (39x) Step 6: 300 s at 72 °C Step 9: forever at 15 °C
Annealing primers to Myc-tag and hygromycin marker	2 µL Forward primer (VMA - S3) 2 µL Reverse primer (VMA - S2) 10 µL 5x Phusion HF buffer 2 µL dNTP (10x) 0,5 µL 9Myc-hphNT1 plasmid 0,5 µL Phusion polymerase 33 µL H_20	Step 1: 180 s at 98 °C Step 2: 15 s at 98 °C Step 3: 20 s at 58 °C Step 4: 90 s at 72 °C Step 5: return to step 2 (9x) Step 6: 15 s at 98 °C Step 7: 90 s at 72 °C Step 8: return to step 6 (24x) Step 9: forever at 10 °C
Control PCR 1: verification of presence of VMA-S3 at the C-terminal end of the *VMA*-gene	1 µL Forward primer (VMA C1) 1 µL Reverse primer (VMA - S3) 2 µL 10x KAPA Taq buffer 1 µL dNTP (10x) 0,1 µL KAPA Taq polymerase 11,9 µL H_20	Step 1: 300 s at 95 °C Step 2: 30 s at 95 °C Step 3: 30 s at 56 °C Step 4: 25 s at 72 °C Step 5: return to step 2 (34x) Step 6: 5 s at 72 °C Step 7: 90 s at 72 °C Step 9: forever at 10 °C
Control PCR 2: verification of the presence of VMA-S2 before the *VMA*-gene downstream DNA	1 µL Forward primer (VMA - S2) 1 µL Reverse primer (VMA-2) 2 µL 10x KAPA Taq buffer 1 µL dNTP (10x) 0,1 µL KAPA Taq polymerase 11,9 µL H_20	Step 1: 300 s at 95 °C Step 2: 30 s at 95 °C Step 3: 30 s at 52 °C Step 4: 25 s at 72 °C Step 5: return to step 2 (34x) Step 6: 5 s at 72 °C Step 7: 90 s at 72 °C Step 9: forever at 10 °C

Table S4: Primers used for creating VMA-Myc fusions and their verification.

Name	Gene	Sequence	Used for
VMA1 - S2	*VMA1*	GAAATACGAAGAAAAGACATCTAACAAATATACCAGAAGATAAATGCTACATATATCTTAATCGATGAATTCGAGCTCG	Construction of Vma1-Myc
VMA1 - S3	*VMA1*	CATGGCGAATTCGAAAAATTGTTGAGCACTATGCAAGAAAGATTTGCTGAATCTACCGATCGTACGCTGCAGGTCGAC	
VMA1-2	*VMA1*	CTACCTCATAATGGATCTAAATTGC	Control insertion
VMA1 C1	*VMA1*	CTTGCAACAAAATGGTTACTCC	Control insertion
VMA2 - S2	*VMA2*	TTTACAAAAAAAAAACGGACAAAATAAAAAAAGCCTTTTTCTTCAGCAACCGTCCTCTTAATCGATGAATTCGAGCTCG	Construction of Vma2-Myc
VMA2 - S3	*VMA2*	GATCCCGACACAAGAAGCTCCGGTAAGAAGAAGGACGCCAGCCAAGAAGAATCTCTAATCCGTACGCTGCAGGTCGAC	
VMA2-2	*VMA2*	CGTTGCGGGCGTGGTGCTG	Control insertion
VMA2 C1	*VMA2*	ATCGGTAAGGACGCTGCTGC	Control insertion
VMA4 - S2	*VMA4*	AAAAAAATCTGTTAGGAGTGTATATGTAAGTATGTAGGTATACAAGCTGCTGGTCGATCAATCGATGAATTCGAGCTCG	Construction of Vma4-Myc
VMA4 - S3	*VMA4*	GCATTGCCCGCCATCAGATTGGAATTGTATGGTCCTTCCAAGACAAGAAAGTTCTTTGATCGTACGCTGCAGGTCGAC	
VMA4-2	*VMA4*	GAAATGGCGTGTTTGGTCTTCC	control insertion
VMA4 C1	*VMA4*	GGGAAAAGGCCCAGCGCGC	control insertion
VMA5 - S2	*VMA5*	AAAATTCTAAAAAAAAAACAGAAATATATATTAATCTAAGTTAGTATTATAAATCGATTAATCGATGAATTCGAGCTCG	Construction of Vma5-Myc
VMA5 - S3	*VMA5*	CAATATGCTTCTCTTGTCGACACAGAGTATGAACCATTTGTGATGTATATAATCAATTTACGTACGCTGCAGGTCGAC	
VMA5-2	*VMA5*	CCTACTAGTGCTAAATCCTGTAG	Control insertion
VMA5 C1	*VMA5*	CTTGAGAGTTTACGTGGAATCTG	Control insertion
VMA6 - S2	*VMA6*	ACCATATAGGTAACAATTTCTCTTAGTGACATAAAAGAAGAAGGAACGATAACTTTTTCAATCGATGAATTCGAGCTCG	Construction of Vma6-Myc
VMA6 - S3	*VMA6*	ATTGCAGAATGTATCGCACAAAACCAAAGAGAAAGAATCAACAATTATATTTCCGTTTATCGTACGCTGCAGGTCGAC	
VMA6-2	*VMA6*	CTTCTCGATCTATTTTTATTATTCCC	Control insertion
VMA6 C1	*VMA6*	CAAGATTTCGAAGGAGTTAGAGC	Control insertion
VMA7 - S2	*VMA7*	CCGCCTGCTACTAGTAATCTACCAGTAATTGTGTTTGTTTTGGGAAAGATCGTTCGCTTAATCGATGAATTCGAGCTCG	Construction Vma7-Myc
VMA7 - S3	*VMA7*	CATCCCTACGACCCTGAAAAGGACTCTGTATTGAAGAGAGTCAGAAAGTTGTTCGGTGAGCGTACGCTGCAGGTCGAC	
VMA7-2	*VMA7*	CGAGGCCGTGTCACGTTCCC	Control insertion
VMA7 C1	*VMA7*	GTAAGACTACTAAGGAGGAAATC	Control insertion
VMA8 - S2	*VMA8*	CTTTTTTTTAATAATGGCTTACATATTTTTGAAAAGGGTCTTGTTCTGCCTGAAACTTCAATCGATGAATTCGAGCTCG	Construction Vma8-Myc
VMA8 - S3	*VMA8*	GCTGATGAGGAACCTCAAGGTGAAACATTGGTTGCTGATCAAGAAGACGATGTTATATTCCGTACGCTGCAGGTCGAC	
VMA8-2	*VMA8*	CAATATTTACATTTTGATACTGTCC	Control insertion
VMA8 C1	*VMA8*	GTTGAAACTTTAGTTGAATTAGCC	Control insertion
VMA10 - S2	*VMA10*	TATTGGTATTATATTATAAAAAGATATATGATTAGAAAACTAGAATGTAATGCAATATTAATCGATGAATTCGAGCTCG	Construction Vma10-Myc
VMA10 - S3	*VMA10*	GTCAAAATTTTGATCGAGACTGTCATCAAGCCTTCTGCTGAAGTCCATATCAATGCCTTGCGTACGCTGCAGGTCGAC	
VMA10-2	*VMA10*	GTGAAAAGAATTCTACTATTCTGC	Control insertion
VMA10 C1	*VMA10*	AGCCAAGGAAATCGACTCATAC	Control insertion
VMA13 - S2	*VMA13*	TACAAAACTACTTATTTAGGCTTCAAACCCACTACTACTTTACGGTCTTCTATATCTTTAATCGATGAATTCGAGCTCG	Construction Vma13-Myc
VMA13 - S3	*VMA13*	TCTAGGGTGAAATACGAGGCCCTCAAGGCCACGCAGGCAATCATTGGATATACCTTCAAACGTACGCTGCAGGTCGAC	
VMA13-2	*VMA13*	CGGCAGGCGGTTCCCGGAC	Control insertion
VMA13 C1	*VMA13*	TACAAGATCTTTAGACAATTGATCG	Control insertion

Table S5: R-x-x-S/T phosphorylation motifs present in the Vma proteins.

Protein	Position	Sequence	pS matched motif ?
Vma1			
	225	PRPVTEKLS	RPVT
	458	VRKATYQTY	RKAT
	376	VRRLSRTIK	RRLS
	433	YRKASNKAY	RKAS
	448	ARDLSLLGS	RDLS
	517	SRDTSLMER	RDTS
	787	AREASIYTG	REAS
	823	LREISGRLG	REIS
	864	DRTGSVSIV	RTGS
Vma2			
	255	ERIITPRLA	RIIT
	292	LREVSAARE	REVS
	328	GRNGSITQI	RNGS
Vma3			
		no match with R-x-x-T	
	120	VRGSSQQPR	RGSS
Vma4			
	55	VRNETNNID	RNET
	95	AREQSLDGI	REQS
Vma5			
	167	ERKKTGDLS	RKKT
		No match with R-x-x-S	
Vma6			
	324	VRNITWIAE	RNIT
	87	IRDQSSGST	RDQS
Vma7			
		No match with R-x-x-T	
	83	ARVDSFTNA	RVDS
Vma8			
	47	FRDITKRID	RDIT
		No match with R-x-x-S	
Vma10			
		No match with R-x-x-T	
		No match with R-x-x-S	
Vma11			
		No match with R-x-x-T	
		No match with R-x-x-S	
Vma13			
		No match with R-x-x-T	
	24	IRSRSVAWD	RSRS
	331	ERKYSDEEL	RKYS

Vma16			
	98	PRITTKNLI	RITT
		No match with R-x-x-S	
Vph1			
		No match with R-x-x-T	
	115	VRNASYLEE	RNAS
Stv1			
	29	IREVTFLLG	REVT
	223	TRNQSVEDL	RNQS

Risk-analysis

In the laboratory of functional biology we work with agents which require biosafety level 1. The necessary precautions were taken to minimize the risks to health and safety. To this end, all laboratory members applied the standard rules of ‘Good Laboratory Practice’. When entering the lab, a lab coat was worn and during experiments gloves were put on. Before leaving the laboratory, the gloves and lab coat were removed and hands were washed.

During this study, experiments were performed with *S*. *cerevisiae* and *E*. *coli* strains that are non-infectious and cannot survive outside laboratory environment. When manipulating these organisms, we worked underneath a flow to protect ourselves and also the cultures from contamination. To keep the working environment sterile we used 70% ethanol.

Handlings with hazardous products were performed under the fume hood. Ethidium bromide is a carcinogenic product (R25, R36/37/38, R46; S22, S24/25, S26, S36/37/39, S45, S53), operations with this products were completed in an accustomed room. An extra pair of gloves was worn during the experiment, which were removed before leaving the room.

A thorough analysis and preparation was carried out before starting an experiment, wherefore the necessary precautions were taken for potential hazards.

SECTION OF MOLECULAR PHYSIOLOGY OF PLANTS AND MICRO-ORGANISMS
Kasteel Arenberg 31 bus 2433
3001 LEUVEN, BELGIË
tel. + 32 16 32 15 16
fax + 32 16 32 19 67
joris.winderickx@bio.kuleuven.be
www.kuleuven.be